QUANTITATIVE REMOTE SENSING OF FOREST LEAF FUNCTIONAL TRAITS: LEAF DRY MATTER CONTENT AND SPECIFIC LEAF AREA

Abebe Mohammed Ali

Graduation committee:

Prof.dr. F.D. van der Meer	University of Twente
Prof.dr.ing. W. Verhoef	University of Twente
Prof.dr. M. Herold	Wageningen University
Dr. W.D. Kissling	University of Amsterdam
Dr. M. Heurich	Bavarian Forest National Park, Germany

ITC dissertation number 289
ITC, P.O. Box 217, 7500 AA Enschede, The Netherlands

ISBN 978-90-365-4209-8
DOI 10.3990/1.9789036542098

Cover designed by Benno Masselink
Printed by ITC Printing Department

Photo cover page is taken from Bavarian Forest National Park Internet page

UNIVERSITY OF TWENTE.

FACULTY OF GEO-INFORMATION SCIENCE AND EARTH OBSERVATION

QUANTITATIVE REMOTE SENSING OF FOREST LEAF FUNCTIONAL TRAITS: LEAF DRY MATTER CONTENT AND SPECIFIC LEAF AREA

DISSERTATION

to obtain
the degree of doctor at the University of Twente,
on the authority of the rector magnificus,
prof.dr. H. Brinksma,
on account of the decision of the graduation committee,
to be publicly defended
on Thursday 06 October 2016 at 12:45 hrs

by

Abebe Mohammed Ali

born on 23 February 1973

in Wollo, Ethiopia

This thesis is approved by

Prof.dr. A.K. Skidmore, promoter
Dr. R. Darvishzadeh Varchehi, co-promoter

To my late parents
Mrs Beyenech Abegaz
Mr Muahmud Ali

Acknowledgments

This work would have not been in its present form without the tremendous support, dedication and contribution of different individuals and organizations that I would like to sincerely thank and acknowledge.

First, I would like to acknowledge the Netherland fellowship program (NFP) administered by the Netherlands organization for international cooperation in higher education (NUFFIC) for the financial support to pursue this study. Without this financial support my dream would not have been accomplished. My appreciation and gratitude go to Wollo University, Ethiopia, for offering me permission and financial support to conduct PhD study.

I extend my sincere gratitude to my promoter, Prof. Andrew K. Skidmore, without whom this thesis would not have existed. I feel very fortunate and honoured to have worked with him. He was always there to motivate, support and guide me with his wisdom throughout my PhD. I will always remember the first day I was in his office, he encouraged me to think more about the 'why questions' at the beginning of a scientific research project. This suggestion was ringing in my mind as the years passed and as time and hard work slowly turned me into a scientific worker.

I am also greatly indebted to the excellent supervision and advisory of Dr. Roshanak Darvishzadeh, who has become my supervisor after one year of the PhD journey. I am very grateful for the many inspiring scientific discussions we shared. Her comments were always to the point that had the power to sharpen this work. Above all she is sincere, friendly and a very easy person to communicate with. Many thanks go to my other supervisor Dr. Iris van Duren for her valuable and timely feedback and wonderful support.

The proposal development and field data collection phase of this work would have not been possible without the precious support of Dr. Tiejun Wang. His guidance and suggestions during the proposal development were pivotal to wipe out the early stage confusions I encountered. My stay in Bavaria was so grateful because of his studious coordination.

I acknowledge the German Remote Sensing Data Centre (DLR) for provision of the pre-processed hyperspectral data needed for this study. In particular, I sincerely appreciate the generous efforts made by Dr. Uta Heiden, Dr. Stefanie Holzwarth and Dr. Nicole Pinnel in organizing the HySpex overflight, test site selection and on time provision of the pre-processed hyperspectral data. I also thank Hooman Latifi in the Institute of Geography and Geology, University of Würzburg in selecting the test site, and facilitating the field campaign. Thanks also go to the Bavarian Forest National Park particularly to Dr Marco Heurich,

Dr. Joerg Mueller and Wilhelm Breit for approving access to the study area, providing the crossbow with its accessories, and other field and logistical facilities.

I would like to thank the NRs department staffs, ITC student affairs, Geoscience laboratory team, ITC library, ICT help desk, travel unit and finance department staffs who helped me during my stay at ITC. I am grateful to Willem Nieuwenhuis for helping me with programing. My special thanks go to Loes Colenbrander, Esther Hondebrink, Marga Koelen, Carla Gerritsen, Theresa van den Boogaard, Marion Pierik and Roelof Schoppers for their excellent services. I am very thankful to Dr Joy Burrough-Boenisch whose excellent English editing helped me to publish papers.

My deep gratitude goes to the PhD community at ITC. Special thanks go to Zhihui Wang for her collaboration in field data collection, unreserved help in data processing and on time replies for my endless inquiries throughout my PhD journey. Cordial thanks to my office mate Mitra Shariati Najafabadi, Linlin Li for their invaluable support and encouragement throughout my stay. Thanks go to my friends in ITC, in particular Getachew Feleke, Saad Khan, Jesper Katomero, Norhakim Yusof, Dr. Tagel G/hiwot, Habtom Tsega, Adugna Mullissa, Rhemat Ullah and Dr. Saleem Ullah who gave me wonderful company during my PhD. I always remember the warm discussions we had on politics, culture, economy and other topics during tea break.

Special thanks go to my relatives and friends back home and abroad for their relentless support and encouragement. Few of them are: Endris Abay and his family, Dr. Ali Yasin and his family, Yimam Mohammed, Getachew Tasew and his family, Demeke Mulugeta and his family, Nuredin Jemal, Arega Mekonen, Alemayehu Asefa, Birhan Asmame, Mekonen Asfaw and Dr. Zenebe Adimasu. My gratitude also goes to all members of geography and environmental studies department of Wollo University. I cannot mention each of you here separately.

Most of all I would like to thank all my family who, as always, has given me endless love and support throughout my PhD journey. I extend my gratitude to my sisters and brothers in general for their encouragement and assistance. In particular I would like to thank my wife Jemilla Tadesse for her love, understanding and inspiration. To my daughters Zebiba, Shemsiya and Feriha, I am full of apologies for being away from all of you.

Table of Contents

List of figures

List of tables

List of abbreviations and acronyms

Acronym	*Meaning*
1D	One Dimensional
3D	Three Dimensional
ALA	Average Leaf Angle
ANOVA	ANalysis Of VAriance
ASD	Analytical Spectral Device
ATCOR	Atmospheric / Topographic CORrection for airborne imagery
BNP	Bavarian National Park
C	Current year needles
C^{+}	Two growing periods old needles
C^{++}	Three growing periods old needles
Cab	Chlorophyll a+b concentration
CAI	Cellulose Absorption Index
CC	Canopy Closure
CD	Crown Diameter
CHRIS	Compact High Resolution Imaging Spectrometer
CI	Chlorophyll Index
C_m	Leaf dry matter content per area
C_w	Leaf water content per area
CWA	Continuous Wavelet Analysis
DART	Discrete Anisotropic Radiative Transfer (model)
DLR	Deutsches Zentrum für Luft- und Raumfahrt
DRRI	Difference of Reflectance Ratio Index
DVI	Difference Vegetation Idex
EnMAP	Hyperspectral sensor for Environmental Mapping and Analysis
EVI	Enhanced Vegetation Index
FOV	Field Of View
GDVI	Generalized Difference Vegetation index
GF	Gap Fraction
GeoSAIL	Geometric and Scattering from Arbitrarily Inclined Leaves hybrid model
GVMI	Global Vegetation Moisture Index
HERO	Hyperspectral Environment and Resource Observer
HySpex	High resolution, high speed hyperspectral camera
IFOV	Instantaneous Field Of View
INFORM	INvertible FOrest Reflectance Model
L_SAVI	Litter-Soil-Adjusted Vegetation Index
LAD	Leaf Angle Distribution
LAI	Leaf Area Index
LAI_s	Leaf Area Index of Single tree
LCAI	Ligno-Cellulose Absorption Index
LDMC	Leaf Dry Matter Content
LIBERTY	Leaf Incorporating Biochemistry Exhibiting Reflectance and Transmittance Yields (model)
LMA	Leaf Mass per Area
LSD	Least Significant Difference

LT	Leaf thickness
LUT	Look-Up Table
MAVI	Moisture-Adjusted Vegetation Index
MCARI	Modified Chlorophyll Absorption in Reflectance Index
MERIS	Medium Resolution Imaging Spectrometer
MISR	Multiangle Imaging SpectroRadiometer
MLH	Maximum LikeliHood (classification)
mND	modified Normalized Difference vegetation index
MNLI	Modified Non-Linear vegetation Index
mSR	Modified Simple Ratio vegetation index
mSR2	modified Simple Ratio vegetation index2
mSR3	Modified Simple Ratio vegetation index3
MTCI	MERIS Terrestrial Chlorophyll Index
N	Leaf structural parameter
NDLI	Normalized Difference Lignin Index
NDVI	Normalized Difference Vegetation Index
NEO	Norsk Elektro Optikk
NIR	Near Infra-Red (part of the electromagnetic spectrum)
NLI	Non-Linear vegetation Index
NMDI	Normalized Multi-band Drought Index
nMSE	normalized Mean Square Error
OLI	Operational Land Imager
OSAVI	Optimized Soil-Adjusted Vegetation Index
PROSPECT	Leaf optical PROperties SPECTra model
PVI	Perpendicular Vegetation Index
R	Reflectance
R^2	Coefficient of determination
RDVI	Re-normalized Difference Vegetation Index
RMSE	Root Mean Square Error
RTM	Radiative Transfer Model
SAILH	Scattering by Arbitrarily Inclined Leaves, with implemented Hot spot (model)
SAVI	Soil-Adjusted Vegetation Index
SAVI2	Soil-Adjusted Vegetation Index2
SD	Stem Density
Sentinel-2	Superspectral imaging mission for terrestrial applications
SH	Stand Height
SLA	Specific Leaf Area
SLAVI	Specific Leaf Area Vegetation Index
SR	Simple Ratio vegetation index
SWIR	ShortWave InfraRed
TCARI	Transformed Chlorophyll Absorption in Reflectance Index
TSAVI	Transformed Soil- Adjusted Vegetation Index
TVI	Transformed Vegetation Index
UTM	Universal Transverse Mercator (geographic projection)
VARI	Visible Atmospherically Resistant Index
VIS	VISible (part of the electromagnetic spectrum)
WDRVI	Wide Dynamic Range Vegetation Index
WDVI	Weighted Difference Vegetation Index

Chapter 1

General introduction

1.1 Remote sensing of biodiversity

Biodiversity studies require the quantification and monitoring of values and ranges of functional traits such as plant height, leaf dry matter content, specific leaf area and seed mass that influence an ecosystem functioning (Tilman 2001, Cornelissen *et al.* 2003). A trait is any measurable morphological, physiological or phenological feature of an organism (Violle *et al.* 2007). In plants, a trait is called a functional trait when it affects plant fitness indirectly via its impacts on plant growth, reproduction, and survival (Lavorel *et al.* 2007, Violle *et al.* 2007, Bernhardt-Römermann *et al.* 2008). Estimates of the leaf functional traits such as leaf dry matter content (LDMC) and specific leaf area (SLA) provide us with information on ecosystem productivity, stability and resource dynamics (Tilman 2001). LDMC and SLA are key traits in understanding carbon assimilation, resource capture, usage and availability (Wilson *et al.* 1999). They are important variables in large-scale ecosystem models and provide us with spatial variation of photosynthetic capacity, leaf nitrogen content (Pierce *et al.* 1994) and are indicative of plant physiological processes such as the light capture, growth rates and life strategies of plants.

Traditional approaches to assess such biodiversity variables provide useful, yet spatially constrained information. The task of identifying and monitoring elements of biodiversity at large regional or national scales, using traditional surveying techniques, remains logistically difficult and/or financially expensive to achieve (Duro *et al.* 2007).

Fortunately, remote sensing offers the opportunity for biodiversity characterizations in a systematic, repeatable, spatially exhaustive and cost-effective manner at local, regional and global scales. The launch of many new satellite systems over the past few decades and the development of new technologies have given us an unprecedented number of remote sensing tools with which to address many of the fundamental questions regarding biodiversity (Duro *et al.* 2007, Wang *et al.* 2010, He *et al.* 2012). Recent advances in imaging spectroscopy and laser scanning have opened up new opportunities to map canopy functional traits and species diversity which were assumed to be beyond the reach of remote sensing (Turner *et al.* 2003, Carlson *et al.* 2007, Papeş *et al.* 2010). Studies utilizing remote sensing as a means of mapping, monitoring or modeling biodiversity are becoming more prevalent and are being conducted at various scales of inquiry. A number of studies have tried to estimate biodiversity (simply as the number of species) using airborne and spaceborne hyperspectral images (Lauver 1997, Gould 2000, Saatchi *et al.* 2008, Papeş *et al.* 2010, Féret and Asner 2011a, Ruiliang 2011). However, directly mapping individual species from remote sensing becomes very difficult at larger scales (regional and global) and when ecosystems have high species variability. Hence, plant functional traits, particularly those found in tree crown

leaves, can be estimated from remote sensing and can be used for assessing and monitoring biodiversity as an alternative approach to species mapping (Carlson *et al.* 2007, Gregory 2008). Thus, besides their role in functional diversity, plant functional traits estimated from remote sensing can be used to predict the most commonly used measure of biodiversity (i.e. species richness). While traditional methods of inventorying and assessing biodiversity will still be required, remotely sensed data can augment such efforts.

1.2 Hyperspectral remote sensing sensors for quantifying leaf functional traits

Hyperspectral remote sensing, also known as imaging spectroscopy technology, is an advanced tool that provides high spatial/spectral resolution data for a given target from a distance. Hyperspectral sensors detect reflected radiation across a continuous spectrum (Meer *et al.* 2002), often including 200 or more contiguous spectral bands across the electromagnetic spectral regions, such as the visible, near infrared and shortwave infrared regions. In tandem with increases in spatial resolution, gains in spectral resolution offer new possibilities for the remote sensing of targets based on spectral behaviour (mainly spectral absorption features) of the material in question (Turner *et al.* 2003). This added spectral resolving power is useful in sorting out subtle variations in vegetation characteristics (traits) that are difficult to measure using the conventional multispectral sensors (Ustin *et al.* 2009, Asner *et al.* 2011a, Ollinger 2011). The spectral absorbance properties of plant leaf traits are mostly manifested in the reflectance spectra of leaves and this offers the opportunity of using measurements of reflected radiation as a non-destructive method for quantifying plant traits (He *et al.* 2012, Féret and Asner 2014).

Hyperspectral technologies are well accepted in remote sensing as a tool for many applications, such as in geology, ecology, geomorphology, limnology, pedology, and atmospheric and forensic sciences, especially for cases in which other remote sensing means have failed or are incapable of obtaining additional information. With the advent of imaging spectrometers that are airborne [e.g. AVIRIS, HyMap, AISA-Eagle, AISA-Hawk and HySpex], which operate in the VIS, NIR and SWIR spectral regions, and those that are spaceborne [e.g. CHRIS and Hyperion], with high spectral and radiometric resolutions and signal to noise ratios, there have been opportunities to acquire vegetation reflectance spectra and test methods for estimating plant traits (Blackburn 2007a). The forthcoming generation of operational spaceborne imaging spectrometer missions [e.g. Hyperspectral Environment and Resource Observer (HERO) and Environmental Mapping and Analysis Program (EnMAP)] will facilitate the development of a greater range of practical applications (Blackburn 2007a, Staenz *et al.* 2013). At the same time as airborne and spaceborne technologies are developing, there is growing interest in the development of field-based

instruments that can be used to obtain plant spectra. The maturation of sensor technology and growing operational deployment of ground-based, airborne and spaceborne instruments will greatly enhance the capabilities for routinely acquiring hyperspectral data and, potentially, for quantifying plant functional traits over a wide range of spatial scales, repeatedly (Blackburn 2007a).

1.3 Analytical approaches for quantifying leaf functional traits from remote sensing data

Alongside developments in hyperspectral data acquisition there has been an increasing intensity of research focused on developing techniques for analysing plant spectra in order to quantify vegetation characteristics. The rich information provided by hyperspectral sensors over a number of wavelengths brings both opportunities and challenges to remote sensing based studies (Fu *et al.* 2007). They provide fine spectral resolution data which have tremendous significance for distinguishing subtle spectral variation due to alteration of the vegetation variable under study. However, a large number of adjacent narrow wavebands can produce spectral autocorrelation (Blackburn 2007b). The autocorrelation causes redundancy within hyperspectral data sets. Therefore, it is necessary to employ appropriate techniques to characterize the main sources of spectral variability and to identify sensitive bands that offer maximum informational content before attempting to quantify vegetation parameters from remote sensing data. There are a wide range of techniques to identify sensitive bands to a given vegetation variable, such as continuum removal, continuous wavelet analysis, unimodal segmentation and fingerprint (e.g. Shi *et al.* 2006, Fu *et al.* 2007, Ramoelo *et al.* 2011, Zhang *et al.* 2012a). They decompose the leaf reflectance spectra into a number of components and identify the most sensitive spectral bands for the given trait under study. In many quantitative remote sensing studies, continuous wavelet analysis was demonstrated as a powerful tool that provides an effective way to examine absorption features in leaf reflectance at various scales (Cheng *et al.* 2011, Cheng *et al.* 2012, Ullah *et al.* 2012). It allows each scale component to be compared directly with the input reflectance spectrum and provides pertinent information about the shape and position of spectral features in objects' reflectance spectra (Cheng *et al.* 2011). Therefore, in this study we have employed continuous wavelet analysis to identify the most sensitive spectral bands for retrieval of leaf functional traits such as leaf dry matter content and specific leaf area.

Once the spectral features sensitive to a given variable under study are identified, diverse models can be applied to quantify variables from remotely sensed data. They can be characterized as inductive and deductive on the basis of their logic, or as deterministic and stochastic on the basis of their processing method (Skidmore 2002). The methods applied to retrieve parameters from

remote sensing data can be grouped into statistical and physical (Darvishzadeh *et al.* 2008c, le Maire *et al.* 2008): statistical techniques are inductive or empirical approaches which are used to find a relation between the plant trait measured in situ and its spectral reflectance or some transformation of reflectance (e.g., a vegetation index). They include simple linear regression, multiple linear regression, stepwise linear regression analysis, and partial least squares regression. Vegetation indices are widely used in this approach. When hyperspectral data are utilized, it is possible to select the most informative narrow spectrum features from the entire electromagnetic spectrum domain and use them for simple and fast assessment of vegetation properties (Broge and Mortensen 2002). However, statistical models such as vegetation indices are known to be site-specific and lack generalization.

An alternative is to use a deductive or physical model approach (Radiative Transfer Model (RTM) inversion), which is based on physical laws. RTMs can be run in the forward or inverse modes. Running an RTM in its direct or forward mode enables the creation of a simulated training database covering a wide range of situations and configurations. Such forward RTM simulations allow for sensitivity studies of parameters and development of vegetation indices. This makes RTM inversion approaches more powerful than statistical methods. However, the retrieval of variables through RTM inversion could be ill-posed, since different combinations of the input parameters may produce the same spectral signature. These models are also computationally demanding and require a large number of leaf and canopy variables, which require extra effort to acquire. However, neither of these approaches has been widely investigated for the estimation of plant functional traits such as LDMC and SLA in structurally different vegetation types and heterogeneous forests. Therefore, this study aimed at testing how accurate and precise estimation of LDMC and SLA can be achieved from field, airborne and spaceborne data by applying empirical and radiative transfer model inversion techniques.

1.4 Research objectives

The main objectives of this study were to:

i) Investigate the potential of leaf reflectance and transmittance for indirectly estimating two leaf functional traits (i.e., LDMC and SLA) at leaf level through the inversion of leaf radiative transfer model.
ii) Evaluate the effect of canopy structural variables such as stem density, leaf area index, crown diameter, stand height and leaf angle distribution on spectral variation associated with LDMC and SLA using a canopy radiative transfer model.
iii) Identify the most sensitive spectral features for quantifying forest leaf LDMC and SLA from airborne hyperspectral data by applying continuous wavelet transformation and retrieving the two leaf functional traits at

canopy level through inversion of a radiative transfer model via an optimized predictive model constructed from the most sensitive spectral features.

iv) Calibrate and validate narrow-band vegetation indices for fast and accurate estimation of leaf functional traits at leaf and canopy levels.

v) Investigate and test the potential of new generation satellite images such as the multispectral Landsat-8 surface reflectance data for estimation of leaf functional traits at landscape scale.

1.5 The test site

The test site for this study was the mixed mountain forest of the Bavarian Forest National Park. The park is located in south-eastern Germany along the border with the Czech Republic (490 3' 19" N, 130 12' 9" E). Elevation of the test site varies from 600 m to 1,473 m above sea level. The climate of the region is temperate, with high annual precipitation (1,200 mm to 1,800 mm) and low average annual temperature (30 to 60 Celsius). Heavy snow cover is characteristic of the area in winter. Brown soils are the predominant soil type at lower altitude (below 900 m a.s.l) whereas at high altitude (above 900 m a.s.l) brown soils and brown podzolic soil predominate. The soils in the area are naturally acidic and low in nutrient content (Heurich *et al.* 2010).

The natural forest ecosystems of the Bavarian Forest National Park vary with altitude: there are alluvial spruce forests in the valleys, mixed mountain forests on the hillsides and mountain spruce forests in the high areas. The dominant tree species include European beech (*Fagus sylvatica*), Norway spruce (*Picea abies*) and Fir (*Abies alba*). In the mixed mountain forests Sycamore maple (*Acer pseudoplatanus L*), Mountain ash (*Sorbus aucuparia L*) and Goat willow (*Salix caprea*) are also found (Heurich and Neufanger 2005). Due to heavy disturbance by bark beetles and wind storms in recent decades, the forest structure in the park is very heterogeneous (Lehnert *et al.* 2013).

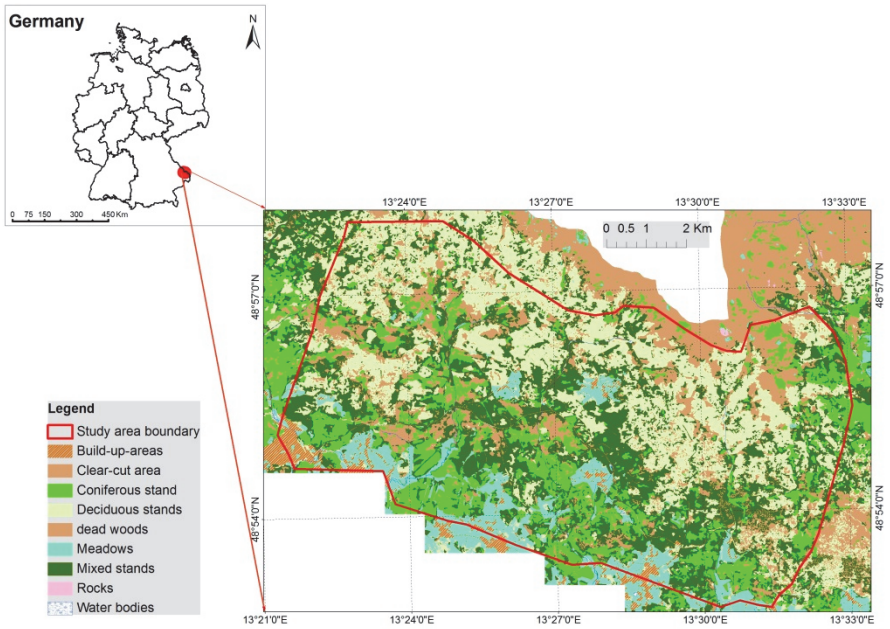

Figure 1.1: Location of the study area in Bavarian Forest National Park and its landcover types.

1.6 Thesis outline

This thesis has seven chapters, five of which are standalone papers. Two of them have been already published in peer-review ISI journals, two are under review and the remaining one is in preparation for journal submission. The structure of the chapters is as follows.

Chapter 2 is about examining alternative approaches to retrieve LDMC and SLA at laboratory level (leaf scale) through inversion of leaf reflectance and transmittance simulated by the leaf radiative transfer model PROSPECT (PROpriétés SPECTrales). In this chapter look-up tables of leaf reflectance and transmittance are generated using the PROSPECT model and inverted with and without prior information by applying a merit function. The merit function searches for the best matches of the laboratory level measured spectra of each sample from the PROSPECT look-up table.

Chapter 3 deals with the effects of canopy structural variables in upscaling the retrieval of LDMC and SLA variables to canopy level. It presents the influence of the canopy structural variables and sensor configuration on canopy reflectance. The influence of different canopy situations and sensor configurations on the relationship between the two traits and canopy reflectance is demonstrated.

In chapter 4 the role of continuous wavelet transformation in the retrieval of the two traits through inversion of INFORM (invertible forest canopy radiative transfer model) is addressed. Results for the most sensitive spectral features for retrieving LDMC and SLA are reported. The identified optimal spectral features of the simulated spectra were used to develop predictive models, and their performance in retrieving the two leaf traits from hyperspectral data is validated and explained.

The findings concerning calibrating and validating narrow-band indices for fast and accurate estimation of SLA both at leaf and canopy level are described in chapter 5. Numerous vegetation index forms ranging from reflectance in a single band (wavelength) to indices that are based on multiple wavelengths were calibrated on HySpex hyperspectral bands, and the findings discussed. The transferability of the recalibrated indices was evaluated by using ground measurements and RTM simulations, and results are presented in detail.

Chapter 6 demonstrates outputs from the Landsat-8 Operational Land Imager (OLI) data capability assessment for SLA estimation at landscape level. The performance of different bands and several indices in predicting SLA from Landsat-8 data is assessed and predictive models developed using wavelet transformed spectra and RTM inversion are described

Finally, chapter 7 focuses on synthesizing the overall major findings of the thesis. The contributions of the research undertaken in this study in the realm of biodiversity assessment through remotely sensed data are discussed. Future research directions and recommendations are also proposed.

Chapter 2

Estimating leaf functional traits by inversion of PROSPECT: assessing leaf dry matter content and specific leaf area in mixed mountainous forest[1]

[1] This chapter is based on:
Ali, A. M., R. Darvishzadeh, A. K. Skidmore, I. v. Duren, U. Heiden and M. Heurich, 2016b. Estimating leaf functional traits by inversion of PROSPECT: Assessing leaf dry matter content and specific leaf area in mixed mountainous forest*, International Journal of Applied Earth Observation and Geoinformation* 45, Part A: 66-76.

Ali, A. M., R. Darvishzadeh, A. K. Skidmore, I. Van Duren, U. Heiden and M. Heurich, 2015. PROSPECT inversion for indirect estimation of leaf dry matter content and specific leaf area. International Archives of the Photogrammetry, Remote Sensing and Spatial Information Sciences - ISPRS Archives.

Abstract

Assessments of ecosystem functioning rely heavily on quantification of vegetation properties. The search is on for methods that produce reliable and accurate baseline information on plant functional traits. In this study, the inversion of the PROSPECT radiative transfer model was used to estimate two functional leaf traits: leaf dry matter content (LDMC) and specific leaf area (SLA). Inversion of PROSPECT usually aims at quantifying its direct input parameters. This is the first time the technique has been used to indirectly model LDMC and SLA. Biophysical parameters of 137 leaf samples were measured in July 2013 in the Bavarian Forest National Park, Germany. Spectra of the leaf samples were measured using an ASD FieldSpec3 equipped with an integrating sphere. PROSPECT was inverted using a look-up table (LUT) approach. The LUTs were generated with and without using prior information. The effect of incorporating prior information on the retrieval accuracy was studied before and after stratifying the samples into broadleaf and conifer categories. The estimated values were evaluated using R^2 and normalized root mean square error (nRMSE).

Among the retrieved variables the lowest nRMSE (0.0899) was observed for LDMC. For both traits higher R^2 values (0.83 for LDMC and 0.89 for SLA) were discovered in the pooled samples. The use of prior information improved accuracy of the retrieved traits. The strong correlation between the estimated traits and the NIR/SWIR region of the electromagnetic spectrum suggests that these leaf traits could be assessed at canopy level by using remotely sensed data.

2.1 Introduction

Components of biodiversity that influence ecosystem dynamics, stability, productivity, nutrient balance and other aspects of ecosystem functioning are collectively referred as functional diversity (e.g. Tilman *et al.* 1997, Tilman 2001). Most ecologists now agree that a major determinant of ecosystem functioning is functional diversity, rather than number of species per se (Díaz and Cabido 2001). By quantifying functional diversity in natural communities, researchers gain additional understanding of the spatial and temporal distribution of biodiversity, ecosystem services and plant community productivity (Cadotte *et al*. 2009, Lavorel *et al*. 2011). It is believed that better conservation and restoration decisions can be made by measuring and understanding functional diversity (Cadotte *et al*. 2011). This realization has underpinned the shift in focus of biodiversity research from species diversity to functional diversity (Tilman 2001).

Like species diversity, functional diversity is quantified on the basis of trait values of organisms (Petchey and Gaston 2006, Zhang *et al*. 2012b). A trait is any measurable morphological, physiological or phenological feature of an organism (Violle *et al*. 2007). In plants, a trait is called a functional trait (e.g. specific leaf area) when it affects plant fitness indirectly via its impacts on plant growth, reproduction, and survival (Violle *et al*. 2007). It is the combination of plant functional traits that determines how plants respond to environmental factors; affect other trophic levels, and influence ecosystem processes and services (Zhang *et al*. 2012b). For instance, plants growing in a resource-rich environment will have a relatively high specific leaf area and low dry matter content, whereas for plants growing in a resource-poor environment the opposite is true (Wilson *et al*. 1999). Traits also provide a link between ecosystem functional diversity and species richness (Carlson *et al.* 2007, Gregory 2008). The functional traits are increasingly used to investigate community structure and ecosystem functioning, as well as to classify species into functional types (Smith *et al.* 1997) or for to validate global vegetation models (Albert *et al*. 2010).

In general, plant traits can be categorized into four groups (Cornelissen *et al*. 2003): whole-plant traits (e.g. growth form and height), stem and belowground traits (e.g. stem specific density and specific root length), regenerative traits (e.g. seed mass and dispersal mode) and leaf functional traits. Two fundamental leaf functional traits that are of central interest for researchers are Leaf Dry Matter Content (LDMC) and Specific Leaf Area (SLA) (Wilson *et al*. 1999, Asner *et al*. 2011b). The LDMC, sometimes referred to as tissue density, is the dry mass of a leaf divided by its fresh mass, commonly expressed in mg/g (Cornelissen *et al*. 2003). It reflects plant growth rate and carbon assimilation and is a better predictor of location on an axis of resource

capture, usage and availability (Wilson *et al*. 1999). The SLA is defined as the leaf area per unit of dry leaf mass usually expressed in m^2/kg (Cornelissen *et al*. 2003). It is referred to as leaf mass per unit area, as specific leaf mass, as well as leaf specific mass. SLA links plant carbon and water cycles, and provides information on the spatial variation of photosynthetic capacity and leaf nitrogen content (Pierce *et al*. 1994). According to the latter, "SLA is indicative of plant physiological processes such as light capture, growth rates and life strategies of plants". A worldwide foliar dataset indicates that 82% of all variation in photosynthetic capacity can be explained by SLA and nitrogen (Wright *et al*. 2004). SLA is species-specific, but significant plasticity exists within and between individual plants of the same species (Pierce *et al*. 1994, Asner *et al*. 2011b).

Besides their independent role as important ecological indicators, LDMC and SLA could be used to estimate leaf thickness (LT). The estimation of LT from the two traits has been investigated in detail by Vile *et al*. (2005). This implies SLA is a compound trait which is inversely proportional to the product of LDMC and LT. A study by Hodgson *et al*. (2011) found that LDMC × LT accounted for nearly three quarters of the observed variation in SLA and those very different combinations of LT and LDMC regularly generate similar values of SLA. However, there are misconceptions in the definition of the stated traits. In many publications, leaf mass per area (LMA or C_m), which is the inverse of SLA, is defined as LDMC.

Several trait data bases have been established worldwide through field measurements (e.g. Kleyer *et al*. 2008, Kattge *et al*. 2011). However, acquiring information on such traits purely on the basis of field measurements is labour-intensive and time-consuming, and thus expensive. Remotely sensed data can play a critical role in acquiring such data at broad spatial scales. Hyperspectral remote sensing has the advantage of providing detailed and continuous spectral information, which can potentially be used for measuring these traits. Previous studies have focused on using hyperspectral data to quantify biochemical and biophysical variables of vegetation, such as chlorophyll content, nitrogen and leaf area index (Darvishzadeh *et al*. 2008a, Vohland and Jarmer 2008, Asner and Martin 2009, Knox *et al*. 2010, Skidmore *et al*. 2010, Asner *et al*. 2011b, Laurent *et al*. 2011, Ramoelo *et al*. 2011, Asner and Martin 2012, Ramoelo *et al*. 2012). Hyperspectral remote sensing has also been used to map canopy functional and species diversity (Carlson *et al*. 2007, Papeş *et al*. 2010) and to estimate biodiversity (even simply as the number of species) (Lauver 1997, Gould 2000, Saatchi *et al*. 2008, Papeş *et al*. 2010, Féret and Asner 2011, Ruiliang 2011, Féret and Asner 2014). However, directly mapping individual species from remote sensing becomes difficult at larger scales and in ecosystems with very high species variability. An alternative approach to mapping species is to estimate plant functional traits, particularly those found

in tree crown leaves, and to use these for assessing and monitoring biodiversity (Carlson *et al*. 2007, Gregory 2008).

The methods applied to retrieve plant traits from remote sensing data can be grouped into statistical and physical (Darvishzadeh *et al*. 2008b, le Maire *et al*. 2008): statistical techniques are used to find a relation between the plant trait measured in situ and its spectral reflectance or some transformation of reflectance. Vegetation indices are widely used in this approach. When hyperspectral data are utilized, it is possible to select the most informative narrow spectrum features from the entire electromagnetic spectrum domain and use them for simple and fast assessment of vegetation properties (Broge and Mortensen 2002). However, statistical methods are known to be site-specific and lack generalization. An alternative is to use a deductive or physical model approach (Radiative Transfer Model (RTM)) inversion, which is based on physical laws. Running an RTM enables the creation of a simulated training database covering a wide range of situations and configurations. Such forward RTM simulations allow for sensitivity studies of parameters and development of vegetation indices. This makes RTM inversion approaches more powerful than statistical methods. However, the retrieval of variables through RTMs inversion is ill-posed, since different combination of the input parameters may produce the same spectral signature. To overcome the effect of the ill-posed problem, Combal *et al*. (2003) recommended the use of prior information. Several studies have reported significant improvement to the accuracy of parameter retrieval after using prior information (e.g. Malenovsky *et al*. 2006, Dasgupta *et al*. 2009); others (Feret *et al*. 2011, Romero *et al*. 2012) have tried to exclude unrealistic combinations of input parameters by applying a linear regression equation derived from correlating the input parameters.

Leaf RTMs simulate leaf reflectance and transmittance by using certain input parameters derived from leaves. There are a number of leaf RTMs and each one requires a different number of input parameters. One such leaf radiative transfer model is the LIBERTY (Leaf Incorporating Biochemistry Exhibiting Reflectance and Transmittance Yields) model (Dawson *et al*. 1998) for conifer needles. However, it requires many input parameters which need to be obtained by intensive fieldwork and laboratory analysis (Malenovsky *et al*. 2006, Morsdorf *et al*. 2009). Another widely applied leaf radiative transfer model is PROSPECT (Jacquemoud and Baret 1990). PROSPECT, which stands for PROpriétés SPECTrales (French for Spectral Properties). It simulates leaf reflectance and transmittance and is the most popular leaf optical properties model of all those published since 1990 (Jacquemoud *et al*. 2009).

Although much work has been done on estimating plant traits from remote sensing, the estimation of LDMC and SLA at all scales (i.e. leaf, canopy and landscape) is rare. To our knowledge, the use of remote sensing techniques to

estimate LDMC has not yet been tested at any scale. Compared to other biophysical variables, studies conducted on SLA are also limited and have mainly been conducted using statistical methods at a canopy scale. Lymburner *et al*. (2000) tested several existing vegetation indices in order to estimate SLA from Landsat TM imagery and found a strong correlation between average canopy SLA and green, red, NIR and MIR reflectance of Landsat TM data. A strong correlation between leaf mass per area and reflectance in the 750 nm to 2,500 nm wavelength range has been also reported for tropical rainforest leaf samples (Asner and Martin 2008, Asner *et al*. 2011). Normalized indices for leaf mass per area at leaf and canopy scales have been developed only recently, by le Maire *et al*. (2008) and Feret *et al*. (2011). However, these indices need to be tested on other images, sites and canopies (le Maire *et al*. 2008). Physical models, which are supposed to be much more robust than statistical approaches, have not been tested for LDMC and SLA estimations. Our study therefore aimed to investigate how accurately and precisely the LDMC and SLA can be estimated in heterogeneous forests at leaf level by using radiative transfer models, so that the application can be extended to canopy and landscape scales.

2.2 Data and Methods

2.2.1 Study area and field data collection

The area chosen for this study was the mixed mountain forest of the Bavarian Forest National Park, which is more heterogeneous in tree species than similar areas in the region. It is located in south-eastern Germany along the border with the Czech Republic (49^0 3’ 19” N, 13^0 12’ 9” E). Elevation varies from 600 m to 1473 m above sea level. The climate of the region is temperate, with high annual precipitation (1200 mm to 1800 mm) and low average annual temperature (3 to 6 ^{0}C). Heavy snow cover is characteristic of the area in winter. Brown soils are the predominant soil type at lower altitude (below 900 meters a.s.l) whereas at high altitude (above 900 meters a.s.l) brown soils and brown podzolic soil predominate. The soils in the area are naturally acidic and low in nutrient content (Heurich *et al*. 2010).

The natural forest ecosystems of the Bavarian Forest National Park vary with altitude: there are alluvial spruce forests in the valleys, mixed mountain forests on the hillsides and mountain spruce forests in the high areas. The dominant tree species include European beech (*Fagus sylvatica*), Norway spruce (*Picea abies*) and Fir (*Abies alba*). In the mixed mountain forests Sycamore maple (*Acer pseudoplatanus L*.), Mountain ash (*Sorbus aucuparia L.*) and Goat willow (*Salix caprea*) are also found (Heurich and Neufanger 2005).

Table 2.1: Distribution of collected samples, by species.

Category	species	No of samples
Broadleaf trees	1. European beech	44
	2. Sycamore maple	4
	3. Mountain ash	3
	4. Goat willow	2
	Subtotal	**53**
*Conifers	1. Fir	21
	2. Norway spruce	7
	Subtotal	**84**
Total No. of samples		137

*equal number of samples were taken from the current growing period (C), second growing period (C^{+}) and three and more growing periods (C^{++}) needle age class (i.e. the numbers of samples per age class were 21 for Norway spruce and 7 for fir species)

A field campaign was conducted between 11 July and 23 August 2013. The study area was stratified into broadleaf, conifers and mixed forest categories. Considering the nature of the forest heterogeneity, time and cost constraints, 26 plots (8 in broadleaf, 7 in conifer and 12 in mixed stands) were randomly selected within each forest category. Each plot was 30 by 30 meters, so that the samples could subsequently be used to estimate variables from medium resolution remote sensing data. Leaf samples were then collected from each tree species found in the plot (Table 2.1). As the two traits of interest (SLA and LDMC) tend to vary as one moves downward from the top of the tree, all the samples were taken from mature sunlit leaves at the top of the canopy. A crossbow was used to shoot an arrow attached to a fishing line at a branch with sunlit leaves. Once the fishing line had passed around the targeted branch, the fishing line was used to feed a rope over the branch and then the branch was pulled down gently until it broke off. Leaves/shoots were immediately removed from the branch and SPAD chlorophyll measurements were made for the broadleaf samples. The shoots of the conifer needles were classified into three needle age classes: current growing period (C), second growing period (C^{+}) and three and more growing periods (C^{++}). The samples were then placed in a zip-locked plastic bag together with wet pulp paper and transported to the laboratory in a portable cooler with frozen icepacks. In the laboratory, the leaf samples were stored in a cold dark room and processed within the day of collection.

2.2.2 Laboratory measurements

a) Physical variable measurements

The biophysical characteristics of the samples such as fresh and dry weight and hemispherical surface area were acquired simultaneously with the spectra measurements. The fresh weight of each sample was determined (before the spectral measurements) by using a digital scale of high precision. Leaf area of broadleaf samples was measured using the LI-3000C portable leaf area meter (Li-Cor, Inc, Lincoln, NE, USA). In the case of the conifer needles, the surface of the sample needles was scanned using an HP double lamp desktop scanner at a resolution of 1200 dpi; the needle projections were computed from the greyscale images using ImageJ image processing software (which is freely available online). Norway spruce needles are cylindrical and therefore their total surface was first computed as a projected area multiplied by a universal conversion factor of 2.57 derived experimentally for Norway spruce needles (Waring 1983). Then, the total needle surface area was divided by two to acquire the hemispherical-surface projection of sampled spruce needles. Finally, the samples were oven-dried at 65 ^{0}C for 48 hours and their dry biomass was weighed. The leaf traits were then computed using the sample leaves or needles area, fresh weight and dry weight. The summary statistics of all the measured variables are presented in Table 2.2.

Table 2.2: Summary statistics of the measured variables in 137 leaf samples. The calculated variables were leaf dry matter content (LDMC), leaf mass per area (C_m), Specific leaf area (SLA) and leaf water content (C_w).

Category	Basic statistics	C_m (g/cm^2)	C_w (g/cm^2)	LDMC (mg/g)	SLA (cm^2/g)
Broadleaf	Minimum value	0.0034	0.0063	337.3	73.48
	Maximum value	0.0136	0.0156	541.3	294.09
	Mean value	0.0079	0.0092	460.6	135.38
	St. deviation	0.0021	0.0021	42.70	38.25
Conifers	Minimum value	0.0110	0.0116	361.5	34.36
	Maximum value	0.0291	0.0337	598.4	90.74
	Mean value	0.0202	0.0247	449.7	51.52
	St. deviation	0.0039	0.0043	43.20	10.92

b) Spectral measurements

Hemispherical reflectance and transmittance from 350-2500 nm with 1 nm spectral resolution were measured using a FieldSpec ®3 portable spectroradiometer equipped with an integrating sphere manufactured by Analytical Spectral Devices, Inc (ASD), USA. The spectral measurement for each sample was obtained by averaging the spectra on 10 randomly selected leaves in the case of broadleaf species and on 12-16 needles for conifers. Care was taken to avoid large primary and secondary veins during the spectral measurement. In order to minimize the effect of signal variance, two hundred scans were averaged in every spectra measurement to a single spectrum. A

calibrated reference standard (with approximately 99% reflectance) was used to convert raw radiance to reflectance.

Whereas the spectral measurement of broadleaf material is straightforward, the spectral measurement of conifer needles is not. This is because the conifer needles are very small and do not cover the sample port of the integrating sphere, which has a port diameter of 15 mm for reflectance and 13.5 mm for transmittance. Therefore, the technique first developed by Daughtry *et al*. (1989) and later revised by (Mesarch *et al*. 1999) was applied to measure the spectral property of the conifer needles. A universal sample holder that could accommodate all lengths of conifer needles was designed, following Malenovsky *et al*. (2006). Needles were detached from each sample shoot, placed on the sample holder, secured with scotch tape and leaving a space of approximately one needle's width between needles to avoid multiple reflectance from adjacent needles (Daughtry *et al*. 1989). The sample holder was carefully placed at the sample port of the integrating sphere, and reflectance and transmittance spectra were acquired following the port configuration procedures of the ASD integrating sphere.

A black painted paper mask with a 15 mm diameter circular aperture was precisely superimposed on the samples and photographs were taken using a 16.1 mega pixel Panasonic DCM-TZ35 camera. Then the gap fraction (GF) between illuminated needles was calculated based on the illuminated area of the sample port, which was 9 mm diameter for both reflectance and transmittance. The illuminated areas of the samples were clipped by drawing a circle of 9 mm diameter at the centre of each picture. The proportion of pixels with gaps between needles was then determined by dividing the number of pixels with gaps into the total number of pixels found in the 9 mm circular aperture area using ImageJ software. Then, the following equations (Eq.1 and 2) were adapted from Mesarch *et al*. (1999) for the Field spec ASD spectrometer, to compute the hemispherical reflectance and transmittance of the sampled needles.

$$Reflectance = \frac{\frac{\rho - \mathrm{Rd}}{1 - \mathrm{Rd}}.\mathrm{Rr}}{1 - \mathrm{GF}} \tag{2.1}$$

$$Transmittance = \left[\left(\frac{\tau - \mathrm{Rd}}{1 - \mathrm{Rd}}\right) - (\mathrm{PwGF})\right]\frac{1}{1 - \mathrm{GF}}\mathrm{Rr} \tag{2.2}$$

where ρ and τ are measured sample reflectance and transmittance, Rd is stray light (measured in reflectance mode), Rr is reference of sample reflectance, GF is the gap fraction of the sample, and Pw is the reflectance of the integrating sphere wall. Stray light (ambient light) inside the integrating sphere was measured as a radiation flux of the empty illuminated sample port in reflectance mode. The reflectance of the integrating sphere wall was

determined by: PW = $\frac{\mathrm{Ftn}}{1-\mathrm{Fn}}\mathrm{Rr}$ where Ftn and Fn are radiance measurements in transmittance and reflectance modes with no sample (Daughtry *et al*. 1989).

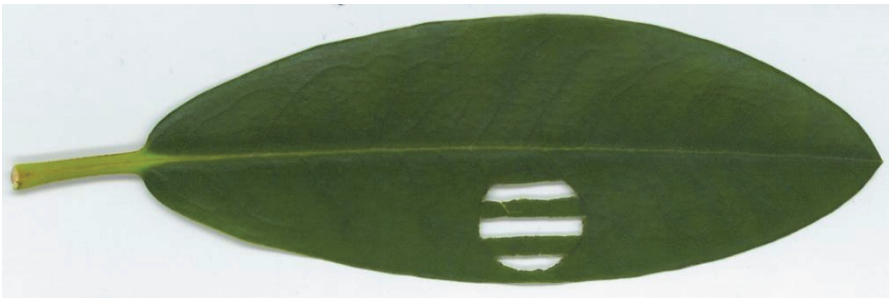

Figure 2.1: The holes cut into a broadleaf sample to mimic conifer needle samples set up on the integrating sphere sample port

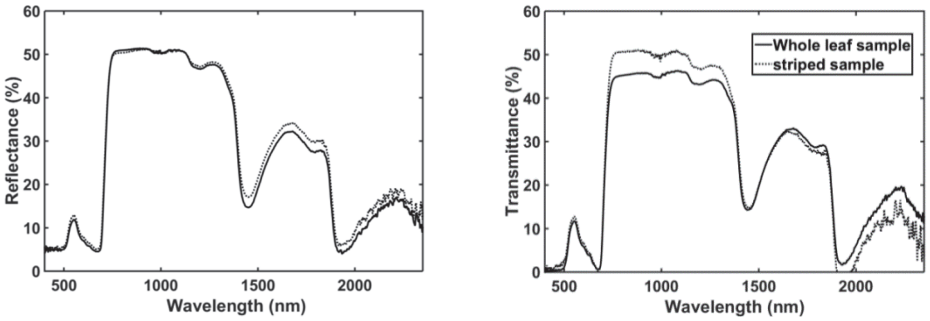

Figure 2.2: Comparison of reflectance (left) and Transmittance (right) spectra of a whole leaf sample and striped leaf sample taken from a broadleaf tree.

To check the reliability of the method, we conducted some preliminary experiments before measuring the conifer needles. The test entailed using a broadleaf sample that covered the entire port of the integrating sphere. First we measured the reflectance and transmittance while the entire port of the integrating sphere was covered by the selected leaf sample. In the exact circular area of the leaf that covered the port we then cut holes (Figure 2.1) to mimic the arrangement of the conifer needles on the sample port; we henceforth refer to the sample treated this way as the striped sample. We repositioned the cut circular area of the striped sample over the port and repeated the spectral measurements. We then adjusted the striped sample's reflectance and transmittance so that we could evaluate the gap fraction effects on the measured spectra of conifer needles. This reliability test yielded RMSE=0.08 for transmittance and RMSE = 0.023 for reflectance. Larger errors, particularly for transmittance, were observed in the wavelength ranges 750-1300nm and 1900-2500nm (Figure 2.2).

Through visual inspection, spectral measurements in the ranges of 350-400 and 2351-2500 were found to be noisy and were removed from all spectral datasets. The Savitzky–Golay smoothing filter (Savitzky and Golay 1964) with a second order polynomial function and bandwidth of 15 nm was applied, to eliminate random noise within the reflectance and transmittance spectral signatures.

2.2.3 PROSPECT model simulation

Testing the accuracy and robustness of physical (i.e. deductive) models, demand a large volume of data. Obtaining this data by measuring real leaves would be very laborious. A solution is to use radiative transfer models (RTM) to generate a large spectral dataset incorporating a wide range of parameters and variability. Leaf RTMs simulate leaf reflectance and transmittance properties by using specific input parameters derived from leaves. The most popular RTM for leaf parameters is the PROSPECT leaf optical properties model (Jacquemoud *et al*. 2009). It idealizes a leaf as a stack of plates composed of absorbing and diffusing constituents. It simulates leaf optical properties (i.e. reflectance and transmittance) parameterized by the following inputs: chlorophyll content (Cab) in µg/cm^2, leaf dry mass per unit area (C_m) in mg/cm^2, leaf water mass per unit area (C_w) in mg/cm^2, and effective number of leaf layers (N) (Jacquemoud and Baret 1990). The model has been widely applied to broadleaf vegetation to estimate chlorophyll content (Zhang *et al*. 2008, Ma *et al*. 2012, Rivera *et al*. 2013). It has also been successfully recalibrated and used to simulate the optical properties of coniferous needles (Malenovský *et al*. 2008, Morsdorf *et al*. 2009).The model was revised by Feret *et al*. (2008) to improve its performance and applicability.

Both PROSPECT-4 and PROSPECT-5 were released at the same time. The difference between them is that in PROSPECT-5 leaf pigments are separated into total chlorophylls and total carotenoids, which improves the chlorophyll retrieval (Feret *et al*. 2008). Since we were not interested in pigment retrieval, in this study, PROSPECT-4 was used to simulate leaf reflectance and transmittance. SLA (cm^2/mg) was computed as $1/C_m$. Since LDMC is the amount of leaf dry weight per unit of fresh leaf mass, this parameter was derived from C_m and C_w. Equations (2.3)–(2.6) show the derivation of LDMC from C_m and C_w:

$$LDMC = \frac{W_d}{W_f} \tag{2.3}$$

$$C_w = \frac{W_f - W_d}{A} \tag{2.4}$$

$$C_m = \frac{W_d}{A} \tag{2.5}$$

By reformulating Eq.2.4 and Eq. 2.5 for W_d and W_f

$$LDMC = \frac{C_m}{C_m + C_w} \quad (2.6)$$

where LDMC is leaf dry matter content in mg/g, C_w is leaf water mass per area in mg/cm^2, C_m is leaf dry mass per area in cm^2/mg, W_d and W_f are leaf dry and fresh weights in mg and g respectively and A is leaf area in cm^2.
Many studies have confirmed that wavelengths in the visible and near infrared region (400-800 nm) are highly sensitive to leaf pigments such as chlorophylls and carotenoids, while the shortwave infrared region is the most sensitive region for retrieving parameters related to dry matter (Jacquemoud *et al*. 1996, Asner *et al*. 2009, Asner *et al*. 2011b, Romero *et al*. 2012). Therefore, the spectral region from 800 to 2350 nm was used to retrieve LDMC and SLA. This range avoids the need to measure leaf pigments for model calibration and validation, since they have no impact on the selected range spectral signature (Romero *et al*. 2012). The latter was also confirmed by sensitivity analysis for the chlorophyll, by running the model in forward mode.

i) Generation of look-up tables

Various inversion algorithms can be used to retrieve a given parameter through RTMs. One of the most popular and efficient is the Look-Up Table (LUT) approach (Dasgupta *et al*. 2009). It involves performing repeated simulations of spectra by using the model with all combinations of the input parameters constrained by reasonable ranges of the input variables. The LUT is then inverted during retrievals.

We followed the general procedures set by Feret *et al*. (2008) in the LUT generation and inversion. The first step was to determine the structural input parameter N of the 137 leaf samples, which could neither be collected in the field nor measured in the laboratory. The wavelength-independent parameter N was retrieved for each sample by inverting the model by using simulation at three wavelengths corresponding to maximum reflectance, maximum transmittance and minimum absorption of the measured spectra (Jacquemoud and Baret 1990, Feret *et al*. 2008). Although leaf structure parameter N corresponds to the number of leaf layers and is most plausible as a whole number, to take account of the subtle variations in leaf structure, N can be considered as a real number with continuous values (Jacquemoud *et al*. 1996). To start the simulation the maximum and minimum values found in the literature were used for the range of N. Therefore, N was set between 0.5 and 3.0 (Combal *et al*. 2003, Malenovsky *et al*. 2006, Féret and Asner 2011). A mini LUT (251N X 137=34387) was generated from all possible combinations of the field measured values of C_m and C_w (137 pairs) with that of N values set at a step of 0.01 within the stated range (251 N values). The structural parameter N was then retrieved (here after considered as measured value of N) using the simulated spectra which best fit the measured spectra of each sample. The search for best simulation was determined by calculating and

finding the lowest root mean square error of an unconstrained non-linear multivariate function (Coleman and Li 1996):

$$M_N = \sqrt{\frac{\sum_\lambda[(\rho mes\text{-}\rho sim)^2+(\tau mes\text{-}\tau sim)^2]}{n}} \quad (2.7)$$

where n is the number of wavelengths selected (three in this case), ρmes and τmes are measured values of reflectance and transmittance, and ρsim and τsim are simulated values of the three wavelengths (λ).

Before using the PROSPECT model for simulation, it may be necessary to calibrate physical and optical constants such as the refractive index and absorption coefficients of leaf material with experimental data (Feret *et al*. 2008). Thus, forward simulations were first conducted using the retrieved N values and input parameters corresponding to 38 broadleaf and 56 conifer needle samples randomly selected from the total sample. The suitability of the original PROSPECT model had been verified by calculating the RMSE between measured and simulated spectra of the selected samples. The RMSE was within the range of RMSEs documented in the literature (Feret *et al*. 2008). As a result, PROSPECT-4 was applied directly, without calibration, to simulate the spectra of the different types of sample leaves and needles.

To generate the LUTs, the PROSPECT model was run in the forward mode under two scenarios. In the first scenario, the model input parameters (C_m, C_w and N) were generated using a uniform distribution based on a maximum range available in the literature (Table 2.3) (Combal *et al*. 2003, Malenovsky *et al*. 2006, Féret and Asner 2011). In the second scenario, the maximum and minimum values of the input parameters were set based on samples statistics as prior information. The values of C_m and C_w were set based on the maximum and minimum values of the samples collected in the field (Table 2.2). For structural parameter N, we used the retrieved range presented in Table 2.4 in the Results section. During all simulations, chlorophyll content was arbitrarily set to 40µg/cm^2. All possible combinations of the input variables were systematically used to generate LUT records.

There was high variation in the spectral properties between broadleaf and conifer needle samples. In order to observe the effect of sample heterogeneity on accuracy (i.e., R^2 and RMSE) we ran the model with and without stratifying the samples into broadleaves and conifer needles. Running the model in forward mode generated a LUT for conifer needle and broadleaf samples separately, as well as for the samples pooled when constrained approach was applied. The unconstrained method yielded 156,978 LUT records (51N x 54C_m x 57C_w). When the maximum and minimum limits of the input parameters were constrained by prior information, there was a large reduction in the total number of LUT records: to 7,182 (18N x 21C_m x 19C_w) for broadleaf, 43,290

(26N x 37C_m x 45C_w) for conifer needles and 74,360 (26N x 52C_m x 55C_w) for the pooled samples. The computation time for generating the LUT varied according to the volume of the LUT.

Table 2.3: Leaf variables used to build the spectra LUT with and without prior information for the 137 leaf and conifer needle samples by using the maximum and minimum limits from the literature and field observation.

Method	Category		Input variables			
			C_{cab} (µg/cm^2)	C_m (g/cm^2)	C_w (g/cm^2)	N
Unconstrained approach (Without prior information)	All the three strata	Min	40	0.0030	0.0060	0.50
		Max	40	0.0295	0.0340	3.00
		Step	-	0.0005	0.0005	0.05
Constrained approach (with prior information)	Broadleaf samples	Min	40	0.0034	0.0063	1.0
		Max	40	0.0136	0.0156	1.85
		Step	-	0.0005	0.0005	0.05
	Conifer needles	Min	40	0.0110	0.0116	1.0
		Max	40	0.0291	0.0337	2.25
		Step	-	0.0005	0.0005	0.05
	Pooled samples	Min	40	0.0034	0.0063	1.0
		Max	40	0.0291	0.0337	2.25
		Step	-	0.0005	0.0005	0.05

ii) Model inversion and validation

The PROSPECT input parameters (N, C_m and C_w) and the two leaf functional traits (LDMC and SLA) were simultaneously retrieved by searching the best matches to the measured spectra in the generated LUT. During inversion, LDMC was represented by $C_m/(C_m+C_w)$ as shown on Eq.(6) and SLA as inverse of C_m. This is to minimize effects of measurement errors of C_m and C_w on LDMC and SLA estimates when inversion with prior information was used. Otherwise the two leaf traits are totally dependent on C_m and C_w and can be computed from the estimated values of these model input parameters.

Two searching algorithms were used in the inversion process. For the LUT generated without prior information we used an unconstrained approach which depended solely on comparing the similarity between simulated and measured spectra. This was done by computing the RMSE and finding its lowest value, using the merit function (MN) in Eq. (2.7). However, different sets of input variables and simulated spectra could result in to the same RMSE when compared with the measured data. Therefore, when (spectral) RMSE is the criterion to search the best match, multiple solutions may exist in the LUT. To overcome this limitation, the LUTs generated with prior information were inverted by using mean and variance of the measured input parameters as a constraint in addition to measuring the similarities between the observed and simulated spectra (Eq. 2.8) (Combal *et al*. 2003, Malenovsky *et al*. 2006,

Lauvernet *et al*. 2008, Jacquemoud *et al*. 2009). The estimations of all the variables were made using all available wavelengths in the NIR and SWIR (801-2350nm).

$$M_N = \sum_\lambda \frac{(\rho mes - \rho sim)^2}{\sigma^2_{\rho mes}} + \sum_\lambda \frac{(\tau mes - \tau sim)^2}{\sigma^2_{\tau mes}} + \sum_j \frac{(V_j - V_j^{prior})^2}{\sigma^2_{V_j mes}} \quad (2.8)$$

where V_j is the estimated value of the simultaneously retrieved variables such as C_m, C_w, LDMC, SLA and N, V_j^{prior} is the measured prior value of the variable j (i.e., means of C_m, C_W, LDMC and SLA in Table 2.2 and mean of N in Table 2.4), $\sigma^2_{\rho mes}$ and $\sigma^2_{\tau mes}$ are variances of the measured reflectance and transmittance respectively and $\sigma^2_{V_j mes}$ is the variance of the measured input variable j. The estimated parameters were then plotted against the measured leaf trait concentrations and evaluated by means of root mean square error (RMSE); normalized RMSE (nRMSE) was calculated as RMSE divided by the mean of the given variable and coefficient of determination (R^2).

2.3 Results

2.3.1 Determination of the structural parameter N and model suitability

The retrieved values of N range from 1 to 2.25. The maximum N value was recorded for the C^{++} age class of fir tree, while the minimum values were observed in Norway spruce C age class needles and European beech leaves. The average N values were 1.74 for Fir and 1.5 for Norway spruce. Among the broadleaf species, a higher mean value of N (1.7) was observed in Mountain ash (Table 2.4).

Table 2.4: Descriptive statistics of the structural parameter N values for sampled trees as retrieved by inversion of the PROSPECT-4 model at three selected wavelengths in the infrared region.

	Beech	Maple	Mountain ash	Fir			Norway Spruce		
				C	C^+	C^{++}	C	C^+	C^{++}
Mean	1.42	1.43	1.70	1.63	1.69	1.89	1.47	1.50	1.56
Minimum	1.00	1.20	1.60	1.35	1.45	1.50	1.00	1.15	1.20
Maximum	1.80	1.60	1.85	2.05	2.00	2.25	2.20	2.10	2.20
St. deviation	0.16	0.17	0.13	0.23	0.20	0.25	0.28	0.23	0.27

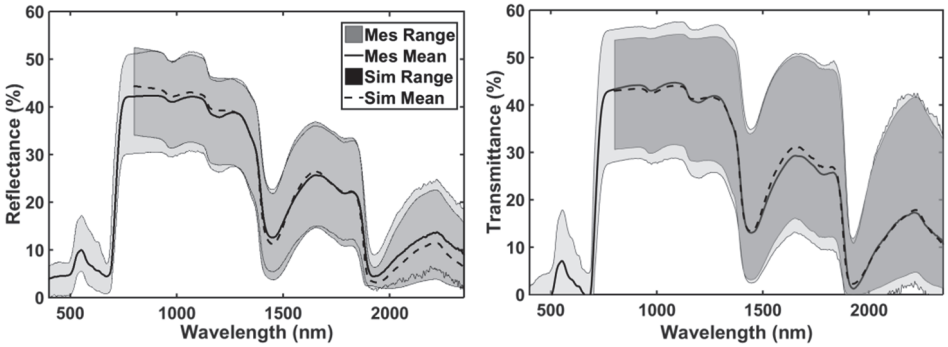

Figure 2.3: Comparison of minimum, mean and maximum leaf reflectance (left) and transmittance (right) of measured (Mes) and PROSPECT simulated (Sim) spectra for all 137 samples collected in the mixed mountain forests of the Bavarian Forest National Park.

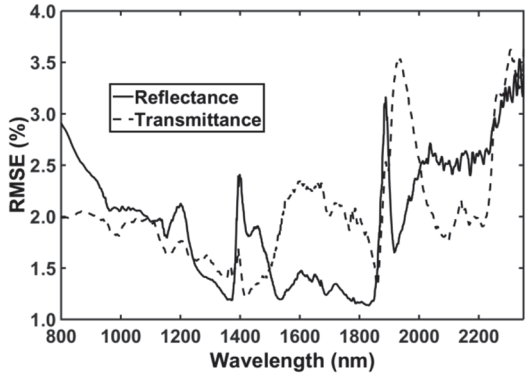

Figure 2.4: Root Mean Square Errors (RMSE) computed between the measured and PROSPECT simulated reflectance and transmittance for the 137 leaf and needle samples.

In order to evaluate the suitability of the leaf model, we calculated R^2 and the RMSE between measured spectra and the corresponding simulated spectra. The hemispherical reflectance and transmittance measured in laboratory and simulated using the PROSPECT-4 leaf model are illustrated in Figure 2.3. Both the reflectance and transmittance signatures showed good matching throughout the NIR-SWIR region (R^2 value of 0.99 and 0.97 for reflectance and transmittance respectively). Greater disagreement (RMSE close to 3.5%) was observed in the wavelength range from 1900 to 2350 nm (Figure 2.4) for both reflectance and transmittance. The mean RMSE for both reflectance and transmittance was near 2%. Mean spectral values also showed the resemblance of the simulated spectra to the measured spectral information. Nevertheless, more deviations between the measured and simulated mean values were observed for reflectance than for transmittance.

2.3.2 Retrieval of traits by inversion and evaluation

The LUTs were used to search for the matches of all the input variables and the two traits (i.e. LDMC and SLA) using equations 2.7 and 2.8. The variations between the measured values with values retrieved with or without constraining information are presented in Table 2.5. The retrieval ability of the unconstrained search algorithm ranges from an nRMSE value of 0.8291 (for SLA of broadleaf samples) to 0.2046 (for the LDMC of pooled samples). In most cases, the lowest nRMSE was observed for LDMC.

Table 2.5: Root mean square error (RMSE) normalized RMSE (nRMSE) and regression equations between observed and estimated values of leaf dry mass per area (Cm), leaf water content per area (Cw), SLA and LDMC with or without prior information from inversion of the PROSPECT model for broadleaf leaf and conifer needle samples.

Method	Category	Variable	RMSE	nRMSE	Regression Equation
Inversion without prior information	Broadleaf samples	C_m	0.0037	0.47	Y=0.52x+0.00059
		C_w	0.0024	0.26	Y=0.62x+0.0019
		SLA	112.25	0.83	Y=1.9x-5.2
		LDMC	100.7	0.22	Y=0.58x+110
	Conifer samples	C_m	0.0086	0.43	Y=0.36x+0.0054
		C_w	0.0053	0.21	Y=0.73x+0.0039
		SLA	35.36	0.69	Y=0.68x+48
		LDMC	92.2	0.20	Y=0.86x-18
	Pooled samples	C_m	0.0066	0.43	Y=0.97x-0.00076
		C_w	0.0044	0.24	Y=1.2x+0.00075
		SLA	63.88	0.76	Y=1.2x+17
		LDMC	119.9	0.26	Y=0.81x+21
Inversion with prior information	Broadleaf samples	C_m	0.0018	0.23	y = 0.41x + 0.004
		C_w	0.0019	0.21	y = 0.55x + 0.004
		SLA	26.7	0.20	y = 1.1x -2.8
		LDMC	0.376	0.09	y = 0.74x + 110
	Conifer samples	C_m	0.0032	0.16	y = 0.24x + 0.016
		C_w	0.0033	0.13	y = 0.37x + 0.016
		SLA	9.28	0.18	y = 0.22x + 38
		LDMC	41.3	0.09	y = 0.33x + 150
	Pooled samples	C_m	0.0033	0.21	y = 0.63x + 0.005
		C_w	0.0036	0.19	y = 0.72x + 0.004
		SLA	21.73	0.26	y = 0.77x + 16
		LDMC	40.8	0.09	y = 0.65x + 130

The retrieval of SLA showed poor performance for most of the unconstrained inversion cases, ranging for nRMSE between 0.6903-0.8291. In all cases, the application of prior information enormously improved the accuracy of the retrieved values, as expected. For instance, in broadleaf samples, when prior information was used the nRMSE between the measured and estimated values dropped from 0.4683 to 0.2278 for C_m, from 0.2909 to 0.2065 for Cw and from 0.2186 to 0.0925 for LDMC. Despite over estimation of lower and

underestimation of higher values in some cases, the retrieved values with prior information were also showed a better relationship with the measured values in the scatter plots (Figure 2.5). The nRMSE values for many of the retrieved variables with prior information are lower when the variables were retrieved for broadleaf and conifer samples separately than when retrieving the variables for the pooled samples. The lowest nRMSE was observed in all samples for LDMC. High R^2 values for the PROSPECT input parameters and the two leaf traits were detected in the pooled samples. In most cases, the correlation coefficient between retrieved and measures SLA was higher than LDMC, but the forecast precision of LDMC was better than that of SLA.

2.4 Discussion and Conclusions

This study quantifies and estimates two important leaf functional traits: SLA and LDMC. These traits, which are not widely addressed in the field of remote sensing, can be accurately derived from the input parameters of the PROSPECT radiative transfer model. The model's performance was evaluated for samples from mixed forest. The results indicate that the PROSPECT_4 leaf model accurately simulates spectral information of samples from mixed mountain forests and can be used to retrieve the biochemical content of leaves/needles directly and indirectly through inversion. In some cases, we found higher accuracies for the indirect estimated variable (LDMC) than for the direct input variables of the model, which further supports the reliability of the indirect retrieval approach.

The values of the structural parameter N in fir tree needles of three seasons or older were high compared to the N values of the younger needles. This can be attributed to the lower water content in the older leaves and confirms earlier findings by Jacquemoud *et al*. (1996), who stated that for the same species, N estimated on dry leaves is higher than the N estimated for fresh leaves, due to an increase of multiple scattering resulting from the loss of water. Our estimated values of the structural parameter N fit well within the known range (1.0-2.5) for a wide variety of species (Jacquemoud and Baret 1990). However, Malenovsky *et al*. (2006) found higher values (1.72-2.63) of N for Norway spruce; this might be because of site-specific nature of the parameter or the bias in spruce needle samples spectra measurement

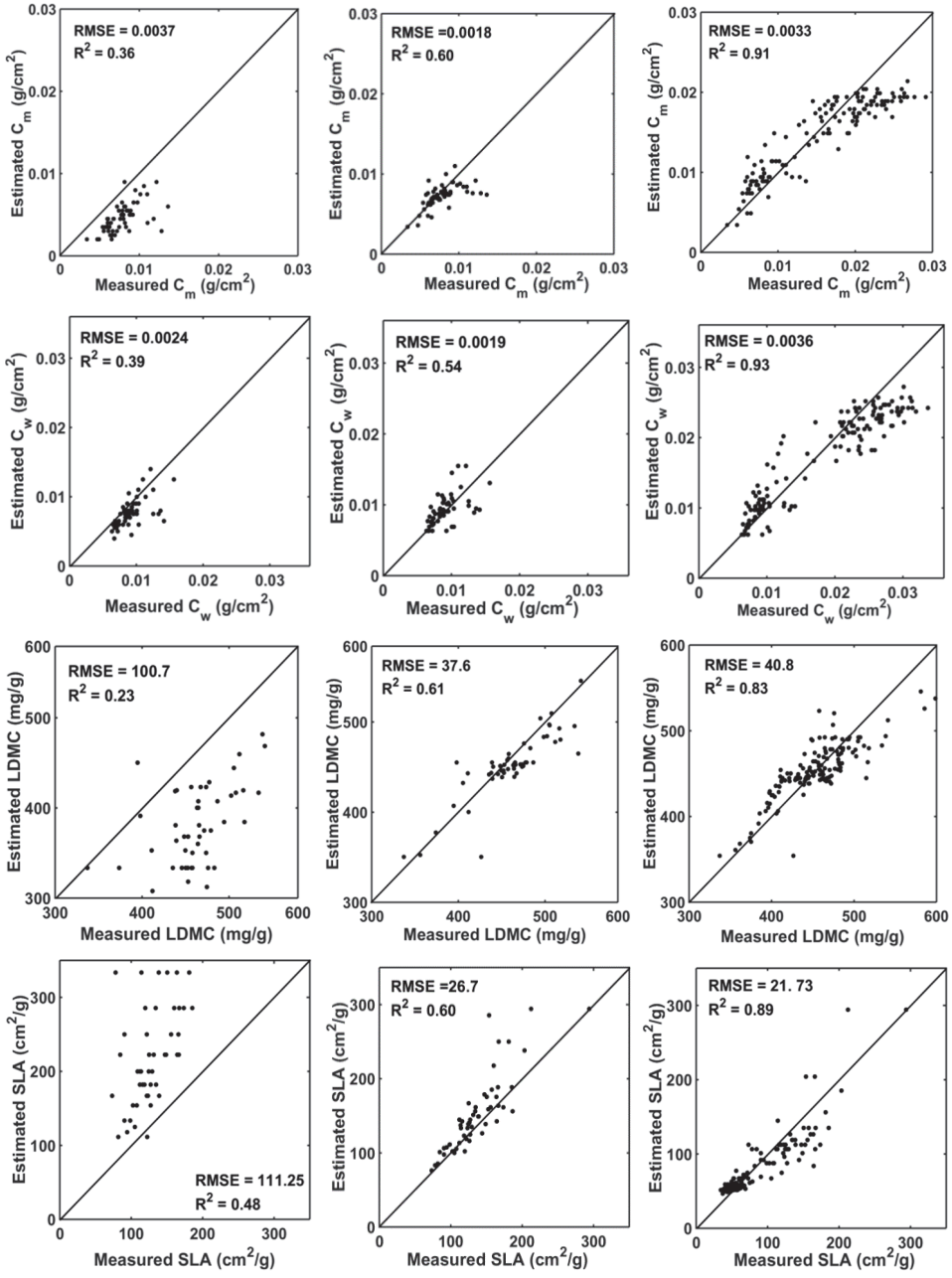

Figure 2.5: Actual vs retrieved leaf mass per area (C_m), leaf water content (C_w), SLA and LDMC without prior information (left), broadleaf samples, using prior information (middle) and pooled samples, using prior information (right). The solid line shows the1:1 relation.

(Particularly transmittance) (Figure 2.2) could have negatively affected the retrieved N values. The mean value of 1.42 for beech trees agrees with the results of Demarez *et al*. (1999), who studied the seasonal variation of N for selected broadleaf tree species.

PROSPECT inversion with a priori information for broadleaf samples yielded an RMSE = 0.0018g/cm^2 for C_m, which confirms the results of Romero *et al*. (2012), who estimated C_m of 11 selected species leaf samples by inversion of the model after removing unrealistic combinations between the input parameters from the LUT. The RMSE and range values for C_m for both broadleaf and conifer samples as well as for the pooled data were within the range reported by Asner *et al*. (2011b), who estimated the C_m for 2871 samples collected from heterogeneous humid tropical rain forests. However, our estimation of C_m and C_w yielded a relatively less accurate result (RMSE = 0.0032 and 0.0033) for conifer needles than the estimates obtained by Malenovsky *et al*. (2006), who studied Norway spruce needle samples by using the spectral range of 450-110 nm. This is probably because the latter study was on mono species while in our samples there are a couple of conifer species. The high RMSE between the measured and simulated spectra in the SWIR range (Figure 2.3) might be also the other cause.

Overall, the leaf trait LDMC was more accurately estimated than the other variables investigated in this study. One possible reason for such accurate estimate of LDMC could be the relatively smaller errors introduced during LDMC field measurement. It seems to be more challenging to measure C_m, C_w and SLA reliably in the field, partly due to errors related to measuring the area of samples.

The results of the model inversion highlight the reliability and feasibility of using remote sensing data for estimation of leaf traits. The comparison of the spectral-based results of this study with field measurements indicates the potential of remote sensing data to estimate leaf traits over a range of vegetation types. This leaf-level result indicates that leaf traits, especially SLA and LDMC, are quantitatively represented by leaf spectra. Previous studies focused on the estimation of some or all of the direct input variables of PROSPECT model by using few bands of the visible and near infrared regions. Here we have shown that model inversion from a wide spectral range can provide indirect and direct estimates of multiple leaf traits for mixed mountain forests. Most importantly, this leaf-level analysis offers a basis to test the possible gains and losses incurred in scaling up to the canopy and landscape scale.

In this study we have demonstrated the inversion results from the wavelength range from 801-2350 nm. Inversion based on selected spectral bands (not

shown here) does not improve the retrieval accuracy. This is because of the informative nature of the whole shortwave spectral region for estimating variables related to leaf dry matter and thickness. Similar results have been reported in the tropical rain forest when using the soil leaf canopy model (Asner *et al*. 2009).

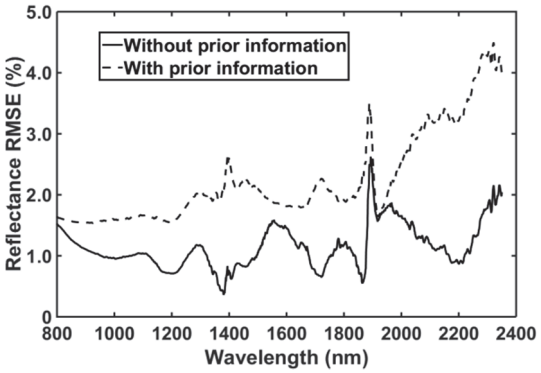

Figure 2.6: Root Mean Square Errors (RMSE) computed between the measured and PROSPECT simulated reflectance for the 53 broadleaf samples with and without using prior information.

The evaluation results of the inversion presented in Figure 2.5 and Table 2.5 demonstrated the inherent capacity of using prior information in improving the accuracy of the estimated variables using RTM inversion. This is in agreement with several previous studies (e.g. Malenovsky *et al*. 2006, Dasgupta *et al*. 2009). Besides limiting the upper and lower boundaries of the model input parameters, we used a modified cost function in the LUT search, which takes into account the uncertainty of the prior information on the variables to be estimated. However, the minimum distance between the measured and modelled spectra could probably be compromised for the uncertainty analysis, which is why we found a much lower RMSE between measured and simulated spectra during the inversion without prior information than during the inversion with prior information (Figure 2.6).

It was observed that the RMSE between measured and observed spectra was higher for longer wavelengths than for shorter wavelengths (Figure 2.4). This could be associated with several factors. One possible reason could be error associated with the equipment used for the spectral measurement. Our preliminary reliability test for adjusting gap fraction (GF) effect showed error inclusion during GF correction for conifer samples. This agrees with Yanez-Rausell *et al*. (2014), who tried to address the effect of gaps between samples and other factors affecting spectral measurement of conifer needles by using the integrating sphere. The GF effect is generally higher in the shortwave region than in the visible and near infrared region. Although the error was systematic and occurred across all samples, it probably contributed to the

higher RMSE between the measured and PROSPECT simulated spectra shown in Figure 2.4. This emphasizes the need for future studies to develop more accurate spectral measurement techniques.

The determination of SLA, C_m and C_w requires accurate measurements of leaf area. But the calculation of areas of irregular shape, particularly conifer needles, is prone to error. Errors are introduced – particularly when calculating the area of conifer needle samples – by the shadow effect while scanning samples, while classifying the scanned images to binary format, while rounding off pixels, by the correction factor used and by other procedures. Studies showed that the shape of the Norway spruce needles vary for different age classes and need different conversion factors (Homolova *et al*. 2013). But we simply used a universal conversion factor from literature which could be source of error. Although it is not possible to avoid all these errors, in future studies efforts should be made to develop simple and fast techniques for computing needle area and for optical property measurement of narrow leaf samples by using the integrating sphere.

In general, our results have confirmed that two important leaf functional traits are measurable with spectral information. This in turn highlights the potential to extend the study to canopy and landscape scales by using advanced hyperspectral airborne and spaceborne sensors. However, it is worth mentioning that when the observational scale moves from leaf to canopy and landscape scales, the relationship between reflected radiation and leaf traits may change (Ustin *et al*. 2009). The spectral properties caused by leaf traits are then affected by soil, non-photosynthetic vegetation, stem characteristics, canopy structure, shadows, illumination and view angles (Roberts *et al*. 2004, Ollinger *et al*. 2008). Retrieval methods that have been designed at leaf scale are likely to suffer from these structural and external factors when used at canopy scale (Asner *et al*. 1998). Therefore, further study is needed to understand the impact of canopy structural and external factors (such as sun zenith and azimuth angles) other than the leaf functional traits on canopy reflectance in order to accurately estimate the two functional traits from remote-sensing data at canopy or landscape scale.

Chapter 3

Effects of Canopy Structural Variables on Retrieval of Leaf Dry Matter Content and Specific Leaf Area from Remotely Sensed Data[2]

[2] This chapter is based on:

Ali, A. M., R. Darvishzadeh, A. K. Skidmore and I. V. Duren, 2016. Effects of Canopy Structural Variables on Retrieval of Leaf Dry Matter Content and Specific Leaf Area from Remotely Sensed Data, *IEEE Journal of Selected Topics in Applied Earth Observations and Remote Sensing* 9(2): 898-909.

Abstract

Leaf dry matter content (LDMC) and specific leaf area (SLA) are two important traits in measuring biodiversity. To use remote sensing for the estimation of these traits it is essential to understand the underlying factors that influence their relationships with canopy reflectance. The effect of canopy structures – particularly stem density (SD), leaf area index (LAI), stand height (SH), crown diameter (CD) and average leaf angle (ALA) on the relationship between LDMC and SLA with the canopy reflectance were investigated using a canopy reflectance dataset simulated by the INFORM radiative transfer model. The parameterization of the model was based on the range of the field parameters collected in the Bavarian National Park in July 2013 and the configuration of the HYSpex hyperspectral sensor.

Strong correlations were observed between the two leaf traits and indices derived from simulated canopy spectra in the NIR and SWIR region (R^2 values of 0.87 for LDMC and 0.85 for SLA). Among the tested HYSpex wavelengths, the bands most sensitive to variation were 2298.69 nm for LDMC and 2280.71 nm for SLA. The effects of the stated structural variables on the relationships were best controlled by the modified normalized difference vegetation index: ([R2275-R1920]/ [R2275+R1920-2*R1520]). The structural variables that most affected the relationship were forest stem density and crown diameter. The modelling results suggest that the spectral variation due to changes in LDMC and SLA is best captured for stands with SD>400 trees/ha and CD≥5m. The influence of LAI and stand height on the relationships can be greatly reduced using vegetation indices. We conclude that LDMC and SLA can be accurately estimated from canopy reflectance, irrespective of the heterogeneity of structural variables, provided that canopy cover exceeds 50%.

3.1 Introduction

Leaf dry matter content (LDMC) and specific leaf area (SLA) are two fundamental functional traits in biodiversity. LDMC is the ratio of the dry mass of a leaf to its fresh mass expressed in mg/g. It reflects plant growth rate (Vile *et al*. 2006), carbon assimilation and resource usage and availability (Wilson *et al*. 1999), whereas SLA is the ratio of leaf area to leaf dry mass, usually expressed in cm^2/g (Cornelissen *et al*. 2003). SLA links plant carbon and water cycles, and provides information on the spatial variation of photosynthetic capacity and leaf nitrogen content (e.g. Pierce *et al*. 1994, Feng *et al*. 2008, Benomar *et al*. 2011). SLA is also indicative of plant physiological processes such as light capture, growth rates and life strategies of plants (Pierce *et al*. 1994). Leaf traits are generally correlated with each other (Wright *et al*. 2004, Dominguez *et al*. 2012, Osnas *et al*. 2013). As a result, LDMC and SLA are interdependent, and have been used to estimate (or predict other ecological indicators, such as leaf thickness (Shipley 2002, Vile *et al*. 2005, Marenco *et al*. 2009), relative growth rate (Shipley 2006) and soil fertility (Hodgson *et al*. 2011). They are increasingly used to investigate community structure and ecosystem functioning (Lavorel *et al*. 2008, Duru *et al*. 2009, Albert *et al*. 2010, Mouchet *et al*. 2010, Lavorel *et al*. 2011). Since the focus of biodiversity research is shifting from species diversity to functional diversity (Tilman 2001), accurately measuring these traits is therefore of prime importance.

Plant functional traits can be retrieved from remotely sensed data using either statistical (inductive) approaches or physically-based models (deductive approaches) (Skidmore 2002). The statistical approaches investigate the relationship between vegetation variables and their spectral reflectance or some derivative of reflectance. Vegetation indices (VIs) are the most common statistical methods utilized, due to their simplicity. An alternative is to use radiative transfer models (RTM) or so-called physical models, which mimic the transfer and interaction of solar radiation inside the canopy and simulate the reflectance of a given canopy (specific situation). They offer an explicit connection between the vegetation variables and traits and the canopy reflectance (Houborg *et al*. 2007). Although remote sensing is a fast and cost-effective alternative, acquiring information on functional traits is still mainly restricted to field observation, which is labour-intensive and time-consuming. In particular, hyperspectral remote sensing (often called imaging spectroscopy) has the advantage of providing detailed and continuous spectral information which can be potentially used for measuring plant functional traits (e.g. Kokaly *et al*. 2009, Kampe *et al*. 2010, Asner *et al*. 2011a, Asner *et al*. 2011b, Féret and Asner 2014).

Over the last four decades, several statistical methods and RTMs have been developed to estimate biochemical and biophysical variables at leaf and canopy

levels, using hyperspectral data (e.g. Tucker 1980, Jacquemoud and Baret 1990, Yoder and Waring 1994, Schlerf and Atzberger 2006). Both approaches have been applied to estimate vegetation biophysical and biochemical variables from remotely sensed data (e.g. Darvishzadeh *et al*. 2008b, Darvishzadeh *et al*. 2012, Wang *et al*. 2014) and they have also been compared in terms of their efficacy in estimating vegetation variables in grasslands from hyperspectral imagery (Darvishzadeh *et al*. 2011).

However, when the observational scale moves from leaf to canopy scale, the relationship between reflected radiation and leaf traits tends to weaken (Ustin *et al*. 2009). The scattering and absorption properties caused by leaf traits are then confounded by soil, non-photosynthetic vegetation (litter, bark, and branches), stem characteristics, canopy structure and shadows (Roberts *et al*. 2004, Wolf *et al*. 2010, Ollinger 2011). Indices that have originally been designed at leaf scale are particularly likely to suffer from these additional heterogeneity factors when used at canopy (i.e., larger) scale (Asner *et al*. 1998, Ustin *et al*. 2009, Ollinger 2011). Therefore, understanding the impact of these factors on canopy reflectance is a crucial first step toward accurately estimating the desired vegetation variables using remote sensing approaches. Sensitivity analysis enables the investigation of the influence of the targeted variable and the confounding factors on canopy reflectance. This in turn gives information on the potential to successfully retrieve variables by using statistical or RTM inversion methods from remotely sensed data (Morris *et al*. 2008).

Several studies have attempted to examine the sensitivity of RTMs and VIs in quantifying biochemical variables. The effect of soil types and soil properties on canopy reflectance is well documented in the literature (Vygodskaya and Gorshkova 1986, Ross *et al*. 1990, Riou and Seyler 1995, Bach and Verhoef 2003, Darvishzadeh *et al*. 2008a). Asner (1998) revealed LAI and leaf angle distribution as the dominant determinants of canopy reflectance if canopy closure and soil effect are controlled. A study by Barton and North (2001) has concluded that the positive correlation between photochemical reflectance index and photosynthetic light use efficiency is influenced by solar zenith, leaf area index (LAI), leaf angle distributions and soil types when using photochemical models. Bowyer *et al*. (2003) compared the performance of local and global sensitivity analysis methods in determining the sensitivity of reflectance data to the input parameters of the PROSPECT and GeoSAIL RTMs. Bannari *et al*. (2006) analysed the sensitivity of chlorophyll indices to soil optical properties and demonstrated that chlorophyll indices are less sensitive to changes in soil optical properties and can be used for a better estimation of chlorophyll content in a sparse crop cover environment. The influences of non-photosynthetic vegetation and canopy closure on chlorophyll (Verrelst *et al*. 2010) and LAI retrieval (Malenovský *et al*. 2008) have also been investigated

for various canopy situations using single bands and VIs on an RTM simulated dataset. A recent study by Xiao *et al*. (2014) using Prospect_5 and 4SAIL RTM at different levels reported the sensitivity of reflectance to the variation in vegetation variables such as leaf chlorophyll content, leaf mass area, leaf water content, LAI and vegetation fractional cover. Review of the literature revealed that there have not been many studies involving stem density (SD) and stand height (SH). Therefore, more studies need to be conducted to examine the effect of these structural variables on canopy reflectance.

Although LDMC and SLA are keystone ecological parameters, the efforts made to estimate these parameters from remotely sensed data are rare. It is only recently that a study at leaf scale using the PROSPECT model has shown that LDMC and SLA can be accurately estimated from remotely sensed data and has recommended upscaling and extension of the inversion to the canopy scale (Ali *et al*. 2016b). To our knowledge no study has examined the impact of canopy structural variables on the estimation accuracy of LDMC and SLA from remotely sensed data. Therefore, here we investigated the influence of key canopy structural variables such as single tree LAI (LAI_s), stem density (SD), stand height (SH), crown diameter (CD) and average leaf angle (ALA) on LDMC and SLA retrieval using a radiative transfer model. Specifically, three aims were addressed: 1) It was examined whether there is a significant canopy reflectance variation due to changes in LDMC and SLA content; 2) The performance of selected wavelengths and several VIs in retrieving LDMC and SLA under various canopy situations was evaluated; 3) The stand-specific impact of LAI_s, SD and SH on the estimation of LDMC and SLA was assessed in detail.

3.2 Methodology

3.2.1 Test site and field data

The sensitivity of canopy reflectance to the desired plant functional traits and confounding structural variables was analysed based on RTM simulation of the mixed mountain forest of the Bavarian Forest National Park. The park is located in south-eastern Germany along the border with the Czech Republic (49^0 3’ 19” N, 13^0 12’ 9” E). Elevation varies from 600 m to 1,473 m above sea level. The climate of the region is temperate, with high annual precipitation (1,200 mm to 1,800 mm) and low average annual temperature (3 to 6 ^{0}C). Heavy snow cover is characteristic of the area in winter. Spodosols are the predominant soil type at lower altitude (below 900 meters a.s.l) whereas at high altitude (above 900 meters a.s.l) spodosols and brown podzolic soil predominate. The soils in the area are naturally acidic and low in nutrient content (Heurich *et al*. 2010). The natural forest ecosystems of the Bavarian Forest National Park vary with altitude: there are alluvial spruce forests in the

valleys, mixed mountain forests on the hillsides and mountain spruce forests in the high areas. The dominant tree species include European beech (*Fagus sylvatica*), Norway spruce (*Picea abies*) and Fir (*Abies alba*). In the mixed mountain forests Sycamore maple (*Acer pseudoplatanus L*), Mountain ash (*Sorbus aucuparia L*) and Goat willow (*Salix caprea*) are also found (Heurich and Neufanger 2005).

A field campaign was conducted between 11 July and 23 August 2013. The study area was stratified into broadleaf, conifer and mixed forest stands. Considering the nature of the forest heterogeneity, time and cost constraints, 26 plots (eight broadleaf, six conifer and 12 mixed stands) were randomly selected within each forest stand. Each plot was square, with sides 30 meters long. At each plot leaf samples were collected and structural variables were measured. The collected leaf samples were transported to a laboratory. For every sample LDMC, SLA, leaf mass per area (C_m) and leaf water content (C_w) were computed from samples fresh and oven-dried mass at 65^0C for 48 hours. The leaf samples' hemispherical reflectance and transmittance from 350-2,500 nm with 1 nm spectral resolution were also measured using a FieldSpec®3 portable spectroradiometer equipped with an integrating sphere manufactured by Analytical Spectral Devices, Inc. (ASD), USA. See Ali *et al*. (2016b) for details of the leaf samples' physical variables and spectral measurements.

The measured forest structural variables were LAI, SD, canopy closure (CC), CD, SH and ALA. LAI and ALA were computed from hemispherical photographs taken in each plot by using CIMES-FISHEYE software (Walter 2009). SD was recorded as number of trees per hectare, based on the number of trees in each plot. CC was estimated by averaging five observations in a plot, using a crown densiometer. CD and SH were calculated from mean crown diameter and mean height of five trees randomly selected in each plot. The crown diameter of each tree was determined by averaging two perpendicular projected distances on the ground. The total height of each tree was estimated by using a Nikon Forestry 550 laser rangefinder. The measured physical and structural variables from the field are summarized in Table 3.1. During the field campaign, the spectral reflectance characteristics of understory vegetation and ecosystem elements in the forest floor such as bark, litter, mosses and lichens were also measured by using the ASD field spectroradiometer coupled to a high intensity contact probe.

Table 3.1: Summary statistics of the measured leaf (n=137) and canopy structural variables (n=26) in Bavarian forest, leaf mass per area (c_m), leaf water content (c_w), leaf dry matter content (LDMC), specific leaf area (SLA), leaf area index (LAI), stem density (SD), canopy closure (CC), crown diameter (CD) and stand height (SH).

Statistics	Variable	Minimum	Maximum	Mean	St. dev
N = 137	C_m (g/cm^2)	0.0034	0.0291	0.014	0.003
	C_w (g/cm^2)	0.0063	0.0337	0.017	0.0032
	LDMC (mg/g)	337.3	598.4	455.2	42.95
	SLA (cm^2/g)	34.36	294.09	93.45	24.58
N = 26	LAI	2.79	6.21	4.6	0.72
	SD (n/ha)	222	1722	771	461
	CC (%)	77	91	81.5	4.6
	CD (m)	1.65	15.45	5.4	2.2
	SH (m)	8	38	23	4.6

3.2.2 Canopy radiative transfer model selection

A large variety of canopy RTMs is currently available and a recent comparison is presented by Widlowski *et al*. (2013). There are four broad categories of canopy reflectance models: i) the 1D or turbid media models (e.g., the SAIL (Verhoef 1984)); ii) geometric optical models (e.g., GOST (Fan *et al*. 2014); iii) Monte Carlo ray tracing three-dimensional (3D) models (e.g., DART model (Gastellu-Etchegorry *et al*. 2004)), which stochastically calculate photon trajectories within turbid or geometric canopies; iv) hybrid models (e.g., GEOSAIL (Huemmrich 2001)), which combine elements of the turbid medium, the geometric optical and the ray tracing models.

The canopy RTM should be adjustable to canopy compositional variability. It is crucial to select a model that is capable of accurately representing the complex forest structure with minimal input requirements to build scenes of a forest canopy. Simple turbid medium (1D) RTMs are unlikely to be able to account for changes in structural composition. Geometric optical models simulate bidirectional reflectance as a purely geometric phenomenon by considering the shape of objects, their count densities and patterns of placement as driving variables, but do not count the interaction between elements due to multiple scattering among leaves and individual canopies (Xiaowen and Strahler 1992). Ray tracing models and hybrid models that have 3D functionalities are expected to be better equipped to simulate the radiative transfer fluxes within a heterogeneous canopy, but often the amount of a priori knowledge needed to build the description of a canopy can be a limiting factor. Among the hybrid models, the Invertible Forest Reflectance model "INFORM" (Atzberger 2000, Schlerf and Atzberger 2006) seems to be particularly suitable with respect to

linking canopy variables to reflectance data while preserving simplicity in generating scenes.

INFORM is a combination of the forest light interaction model (Rosema *et al*. 1992) and SAIL (Verhoef 1984) canopy RTMs with the PROSPECT (Jacquemoud and Baret 1990) leaf RTM. INFORM is parameterized by leaf parameters such as C_m, C_w and chlorophyll content, canopy parameters such as SD, LAI_s and SH and external parameters such as sun zenith (θ_s) and sun azimuth angle (Ψ), and simulates canopy spectral reflectance of forest stands between the 400 and 2500 nm wavelengths. Unlike the 3D RTMs, the out puts of INFORM are not simulated images. It provides spectral signatures on top of a canopy under well specified conditions. In other words, the simulated spectra are independent of spatial resolution. The influence of the structural variables on LDMC and SLA retrieval was investigated on simulated data using the coupled leaf and canopy RTM-INFORM. All possible canopy structural compositions of LAI_s, SD, SH, CD and ALA that may occur in the test site were considered during the simulation.

3.2.3 INFORM parameterization and forest reflectance simulation

The structural variables (SD, LAI_s, SH, CD and ALA) addressed in this study were among the main structural components that greatly vary throughout the forest stands in the Bavarian Forest National Park. To study the effect of the confounding factors, a relationship should be established between the confounding variables with LDMC and SLA (here after referred as "the two leaf traits") for any given canopy structure or composition that could occur in the test site. Thus, INFORM was parameterized on the basis of Bavarian National Park Forest leaf and stand characteristics. The model input parameters, C_m, C_w, LAI_s, SD, SH, CD, ALA, θs and Ψ were generated using a uniform distribution based on the available range of the ground truth data (Table 3.1).

Other leaf, canopy and external input parameters were fixed to average values based on the ground truth data, sensor (HYSpex) specification, and previous studies (Ali *et al*. 2016b). In INFORM, LAI is represented by single tree leaf area index (LAI_s). Hence, the range for LAI_s was estimated by computing LAI_s from LAI and CC as LAI_s=LAI/CC. For every combination of input parameters, LDMC and SLA were indirectly calculated from C_m and C_w as LDMC = $C_m/(C_m+C_w)$ and SLA = $1/C_m$ (see Ali *et al* 2016b for details). The input parameter values used for forest canopy reflectance simulation with INFORM are presented in Table 3.2.

The simulation was done without the presence of atmosphere on top of the canopy. Bare soil occurred extremely rarely on the forest floor. Hence, the field

spectra of understorey vegetation and the forest floor elements were averaged and used as a fixed background reflectance during the simulation.

Table 3.2: Input parameters used during inform simulation based on field observation and previous studies

Input variable	Symbol	Unit	mean	Range of simulated variation		
				Min	Max	Step
Leaf dry mass per area	C_m	g/cm^2	0.014	0.0034	0.0291	0.005
Equivalent water thickness	C_w	g/cm^2	0.017	0.0063	0.0337	0.005
Leaf structural parameter*	N	NA	1.5			
Chlorophyll content*	C_{ab}	g/cm^2	40			
Single tree LAI	LAI_s	NA	4.0	2	8	0.5
Understorey LAI	LAI_u	NA	0.1			
Stem density	SD	n/hr	771	200	1800	150
Stand height	SH	M	23	8	38	5
Crown diameter	CD	M	5.4	3	11	2
Average leaf angle	ALA	degree	50	40	60	5
Sun zenith angle	θ_s	degree	32	20	80	20
Observation zenith angle	θ_0	degree	0			
Azimuth angle	Ψ	degree	153	100	200	30
Fraction of diffused radiation*	Sky1	fraction	0.1			

* fixed based on previous studies.

The shortwave-infrared region is reported as the most sensitive region for retrieving parameters related to dry matter (Jacquemoud *et al*. 1996, Asner *et al*. 2009, Asner *et al*. 2011b, Romero *et al*. 2012). This region also avoids the need to measure leaf pigments for model calibration and validation, since they have no impact on the selected range spectral signature (Romero *et al*. 2012). Therefore, the forest canopy spectral reflectance was simulated in 309 spectral wavelengths (800-2500 nm) corresponding to the near-infrared (NIR) and shortwave-infrared (SWIR) band settings of the HYSpex system developed by the Norwegian company Norsk Elektro Optikk. The HYSpex system comprises two imaging spectrometers with spectral ranges of 400–1000 nm and 1000–2500 nm and up to 416 spectral channels at high spatial resolution. The HYSpex system records radiance data in contiguous bands at a spectral resolution of 3.7 nm for 400-992 nm spectral range (sensor 1) and 6 nm for 968-2498 spectral range (sensor 2). It has a spatial resolution of 1.6 meters for sensor 1 and 3.3 meters for sensor 2. The HYSpex instrument was flown over the study site on board a Cessna 208B Grand Caravan at average altitudes of 3006.5 m above sea level on 22 July 2013 between 9:00 and 11:15 local time. The German earth observation centre has successfully tested the system

and made it available to the remote sensing community [69]. The solar zenith and azimuth angles were set close to the range of the Bavarian National Park overflights settings and the view zenith angle was set at nadir.

3.2.4 Confounding factors affecting LDMC and SLA retrieval

Table 3.3: Vegetation indices used for the sensitivity analysis of LDMC and SLA against the confounding factors (LAI_s, SD and SH). The indices are those studied in Le Maire *et al*. (2008).

Index type	Original Formula	Formula in HYSpex bands
Difference (D)	R2380-R2300	R2382.63-R2298.69
Simple Ratio (SR)	R2280/R1395	R2280.71/R1393.44
Normalized Difference (ND)	(R2280-R1395)/ (R 2280+R1395)	(R2280.71-R1393.44)/ (R 2280.71+R1393.44)
modified Normalized Difference (mND)	(R2275-R1920)/ (R2275+R1920-2*R1520)	(R2274.71-R1921.01)/ (R2274.71+R1921.01-2*R1519.34)
modified Simple Ratio (mSR)	(R2275-R1520)/ (R1920-R1520)	(R2274.71-R1519.34)/ (R1921.01-R1519.34)
Normalized Difference (ND)	(R2260-R1490)/(R2260+R1490)	(R2262.72-R1489.36)/ (R2262.72+R1489.36)

NB: All the HYSpex bands involved in the indices calculation were also individually tested for their sensitivity to the two leaf traits and confounding factors analysis.

Using the INFORM model, a total of 8,108,100 forest canopy spectra (6 C_m×6C_w×13 LAI_s×11SD×7 SH x 5CD x 5ALA x 4θs x 3Ψ) were simulated and used for the subsequent analysis of the contribution of each targeted variable to the spectral signal at stand scale. The analysis attempted to evaluate the suitability of imaging spectroscopic-based approaches for estimating LDMC and SLA. Several VIs based on a previous study by le Maire *et al*. (2008), who evaluated the performance of different types of vegetation indices for leaf mass per area retrieval in a forest canopy were used and assumed to be sensitive to LDMC and SLA. These indices and their individual wavelengths were adjusted to the HYSpex band configurations (Table 3.3).

The effects of confounding factors on LDMC and SLA were analysed by studying how the variations of the confounding factors change the relationship between the two leaf traits and the spectral bands or spectral indices. To test which of the input parameters (the two leaf traits, LAI_s, SD, SH, CD or ALA) determines most of the spectral variation in the forest canopy spectra simulations at various sun zenith and azimuth angles, we used analysis of variance (ANOVA) to decompose the total variance into terms related to the individual factors. Firstly, the sensitivity of the simulated spectra for the variation in the two leaf traits and different combinations of the confounding factors was tested for its statistical significance, using an F-test. ANOVA computes the variance as the sum of squared deviations. In our case, the sum of squares of the simulations

was partitioned into a sum of squares related to the overall mean, a sum of squares related to the treatment effects, and a residual sum of squares.

To test whether a specific band (or index) is sensitive to the two leaf traits, the F statistic for LDMC and SLA was used. To test the sensitivity for the two leaf traits relative to the factors (LAI_s, SD, SH, CD and ALA) an F statistic was calculated by dividing the mean square related to the two leaf traits by the mean square related to each of the factors. The best spectral band (index) for LDMC and/or SLA estimation is the one that has the largest calculated F value. Pairwise multiple comparison tests were then done for the spectral bands and spectral indices with a significant F-test result, using the least significant difference (LSD), which is the widely used post hoc analysis, to determine which values of a given factor differ significantly from each other. Coefficients of determination (R^2) between the two traits and each of the selected spectral bands (index) were also computed and used for evaluating the correlation strength of the HYSpex canopy reflectance (indices) to the two leaf traits.

Secondly, the LDMC and SLA effects on the spectral band or spectral index with high significance value were further analysed for each combination of confounding variables. The two traits' variations were plotted against the best performing bands and indices in the F-test, and the effect of each selected structural variable was examined individually, keeping all other variables constant. The relationship between the two leaf traits' variation and the reflectance was measured by means of local sensitivity analysis.

We chose the local sensitivity analysis method because the model simulation was run by varying the two leaf traits and the five confounding variables at variable solar zenith and azimuth angles, keeping all other parameters constant as shown in Table 3.2. In the other sensitivity analysis method (global sensitivity analysis), all the input parameters vary simultaneously (Bowyer *et al*. 2003). From the results yielded by local and global sensitivity analyses, it appears that these analyses alter the magnitude of the importance of the factors under investigation (Bowyer *et al*. 2003). Slopes of relationships between the leaf traits and the structural variables were used to measure the sensitivity of the selected index for variation in the two leaf traits. The derivative ($\partial y/\partial x$) was computed from the relationship between the two leaf traits' content (x variable) and vegetation index (y variable) for every combination of the two leaf traits' intervals and confounding variables from the INFORM generated reflectance spectra. The average slope was then calculated as the derivative averaged over all intervals for a stand-specific situation. The steeper the slope, the more accurate is the estimation of the two leaf traits. Thus, the average slope was considered as a stand-specific indicator of the two leaf traits' detectability.

Thirdly, the combined effects of the confounding factors on the two leaf traits were investigated by pairing up two factors at a time while other variables were kept constant at the observed average value in the test site. For instance, the combined effect of LAI_s and SD was evaluated by keeping SH, CD and ALA values at their averages in the test site. For simplicity, the steps were only repeated for possible combinations of LAI_s, SD and H confounding factors. Plotting the average slopes for each of these paired combinations provided three scenarios of canopies that might occur in heterogeneous forest. The sensitivity analysis was finalized by establishing a link between the modelling results and structural information measured in the Bavarian National Park mixed mountain forest canopies.

3.3 Results

3.3.1 Spectral variation due to LDMC and SLA

Before testing the strength of spectral variation caused by the two leaf traits, we checked the trend of reflectance variation when the scale moves from leaf to canopy level. Figure 3.1 shows how the mean and standard deviation (std) of the simulated reflectance shifts with upscaling. Upscaling from leaf to canopy level increased the spectral variation in the NIR region and diminished the spectral variation in the SWIR region. The overall spectral variation at canopy level (std of 12.14 %) is lower than the leaf scale (std of 15.39%). Nonetheless, strong correlations between the two traits and canopy reflectance (indices) were observed (see Tables 3.4 and 3.5).

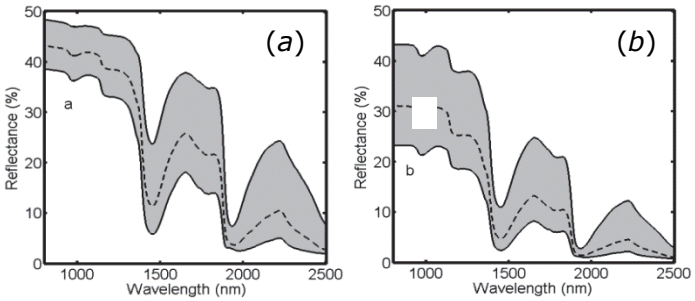

Figure 3.1: Simulated reflectance at leaf scale (a) and canopy scale (b) as simulated by INFORM using the input parameters presented in Table 3.2. The dashed lines show the mean and the shaded areas show the ranges of the simulated reflectance.

The canopy scale reflectance was further evaluated using the F-test in order to ascertain whether the spectral variation due to LDMC and SLA in the presence of canopy confounding factors is significant. The results from single band tests are summarized in Table 3.4. The larger the F-test value, the more assurance

that the band is more sensitive to LDMC and/or SLA than the other factors, meaning that the impact of the structural variables variation is much less than that of LDMC and/or SLA variation. Among the selected HYSpex wavelengths, the band at 2298.69 nm was the most sensitive band for variation in both LDMC and SLA. The band at 2280.71 nm also showed strong correlation to variation in SLA. The selected bands showed stronger correlation with LDMC than SLA. A substantial amount of influence on spectral variation originated from the structural variables SD, CD and ALA and the least disturbing effect came from LAI_s and SH. The F-test (lower values) indicated that the confounding factors are more influential at shorter than at longer wavelengths.

Table 3.4: R^2 and ANOVA F-test values calculated for testing HySpex single wavelengths (bands) sensitivity for LDMC and SLA variation against the confounding variables. The R^2 column indicates the correlation between the two leaf traits and canopy spectra at the specified wavelength. The column headed LDMC provides the variations caused by LDMC against the total variance of the confounding variables tested, whereas columns $LDMC/LAI_s$, LDMC/SD, LDMC/SH, LDMC/CD and LDMC/ALA show the calculated F-test values caused by LDMC variance against the variance caused by each factor, and the same goes for SLA.

Wavelength (nm)	R^2	LDMC	$LDMC/LAI_s$	LDMC/SD	LDMC/SH	LDMC/CD	LDMC/ALA
1393.44	0.538	0.3424^{ns}	131.548	5.368	46.875	0.674^{ns}	2.09^{ns}
1489.36	0.608	0.5926^{ns}	137.156	10.34	62.497	0.721^{ns}	2.897^{ns}
1519.34	0.557	0.371^{ns}	199.569	5.254	54.579	0.395^{ns}	2.005^{ns}
1921.01	0.522	1.108^{ns}	7.398	5.015	15.735	5.782^{ns}	1.195^{ns}
2262.72	0.676	2.217	76.246	81.387	72.645	2.024^{ns}	4.564^{ns}
2274.71	0.678	2.796	71.913	120.589	73.398	2.621^{ns}	4.687^{ns}
2280.71	0.685	2.935	70.36	142.354	73.98	3.008^{ns}	4.925^{ns}
2298.69	0.698	4.016	60.839	249.187	73.019	4.07^{ns}	4.631^{ns}
2382.63	0.659	8.073	35.159	56.569	57.371	17.176	5.294^{ns}
Wavelength (nm)	R^2	SLA	SLA/LAI_s	SLA/SD	SLA/SH	SLA/CD	SLA/ALA
1393.44	0.036	0.097^{ns}	64.055	2.186^{ns}	22.792	0.166^{ns}	1.005^{ns}
1489.36	0.053	0.238^{ns}	79.546	6.259	37.215	0.293^{ns}	1.389^{ns}
1519.34	0.076	0.297^{ns}	210.215	5.084	59.321	0.137^{ns}	1.291^{ns}
1921.01	0.005	0.057^{ns}	0.498^{ns}	0.312^{ns}	1.002^{ns}	0.369^{ns}	0.013^{ns}
2262.72	0.379	6.006	288.90	312.159	273.698	9.270^{ns}	19.004
2274.71	0.387	7.009	278.921	471.615	284.150	11.807^{ns}	20.356
2280.71	0.390	7.043	271.390	559.497	284.997	13.000^{ns}	19.918
2298.69	0.381	8.925	233.954	948.720	272.439	17.975	21.722
2382.63	0.204	7.061	75.659	116.277	121.914	36.976	11.995

R^2 and F-test evaluation results of the VIs are presented in Table 3.5. In most cases, the R^2 and the calculated F-test values of indices are much higher than the single bands. Among the tested VIs, the modified normalized difference (R2274.71-R1921.01)/ (R2274.71+R1921.01-2*R1519.34) and the modified simple ratio (R2274.71-R1519.34)/ (R1921.01-R1519.34) indices are the two

best suitable indices for both LDMC and SLA. However, like the single bands, the selected indices were also influenced by the confounding variables. The influence of CD was even higher for LDMC than for SLA. In five of the six indices tested, the variation due to LDMC was not significant (at P=0.01) over that of the variation due to CD. Along with CD, SD was the perturbing structural variable that weakens the relationship between the indices and the two leaf traits.

Table 3.5: R^2 and ANOVA F-test values calculated for testing HySpex-derived vegetation indices sensitivity for LDMC and SLA variation against the confounding variables. The R^2 column indicates the correlation between the two leaf traits and the specified indices. The column headed LDMC provides the variations caused by LDMC against the total variance of the confounding variables tested, whereas columns LDMC/LAI_s, LDMC/SD, LDMC/SH, LDMC/CD and LDMC/ALA show the calculated f-test values caused by LDMC variance against the variance caused by each factor, and the same goes for SLA.

Index	R2	LDMC	LDMC/LAIs	LDMC/SD	LDMC/SH	LDMC/CD	LDMC/ALA
D	0.73	1.052	1158.689	13.597	230.138	1.126ns	8.657ns
SR	0.68	0.519	86.010	3.382ns	1409.469	0.492ns	300.497
ND	0.72	1.086	61.679	6.364	292.000	1.398ns	130.709
mND	0.87	3.792	514.301	24.001	24610.176	4.697	154.807
mSR	0.85	2.795	373.015	18.371	15753.252	3.394ns	126.301
ND2	0.79	1.107	145.036	8.521	3622.538	1.491ns	155.092
Index	R2	SLA	SLA/LAIs	SLA/SD	SLA/SH	SLA/CD	SLA/ALA
D	0.65	6.343	7041.529	84.003	1402.279	7.831ns	53.256
SR	0.66	3.398	564.958	23.053	9351.259	4.081ns	1980.137
ND	0.70	7.728	408.769	42.017	1944.00	10.006ns	871.456
mND	0.84	25.438	3411.538	160.097	163701.879	31.095	1026.226
mSR	0.89	19.001	2480.356	123.179	104746.894	23.325	854.839
ND2	0.67	6.690	787.247	46.437	19623.513	7.007ns	841.127

^{ns} not Significant at P=0.01. The degrees of freedom were 34(LDMC), 5(SLA), 12(LAI_s), 10(SD), 6(SH), 4(CD) and 4(ALA).

3.3.2 Relationships between LDMC and SLA, with single bands and vegetation indices

In the previous section, single bands and VIs that were highly sensitive to LDMC and SLA variation were presented. Figure 3.2 presents the results from the structural variables effect on the relationship between the two leaf traits with the highly sensitive bands (2298.69 nm for LDMC and 2280.71 nm for SLA). The relationships were set up by varying one confounding variable at a time and fixing the others at an average value for the test site (LAI_s = 5.5; SD = 800 trees/ha. and SH = 23m, CD = 5.4m and ALA = 50^0).

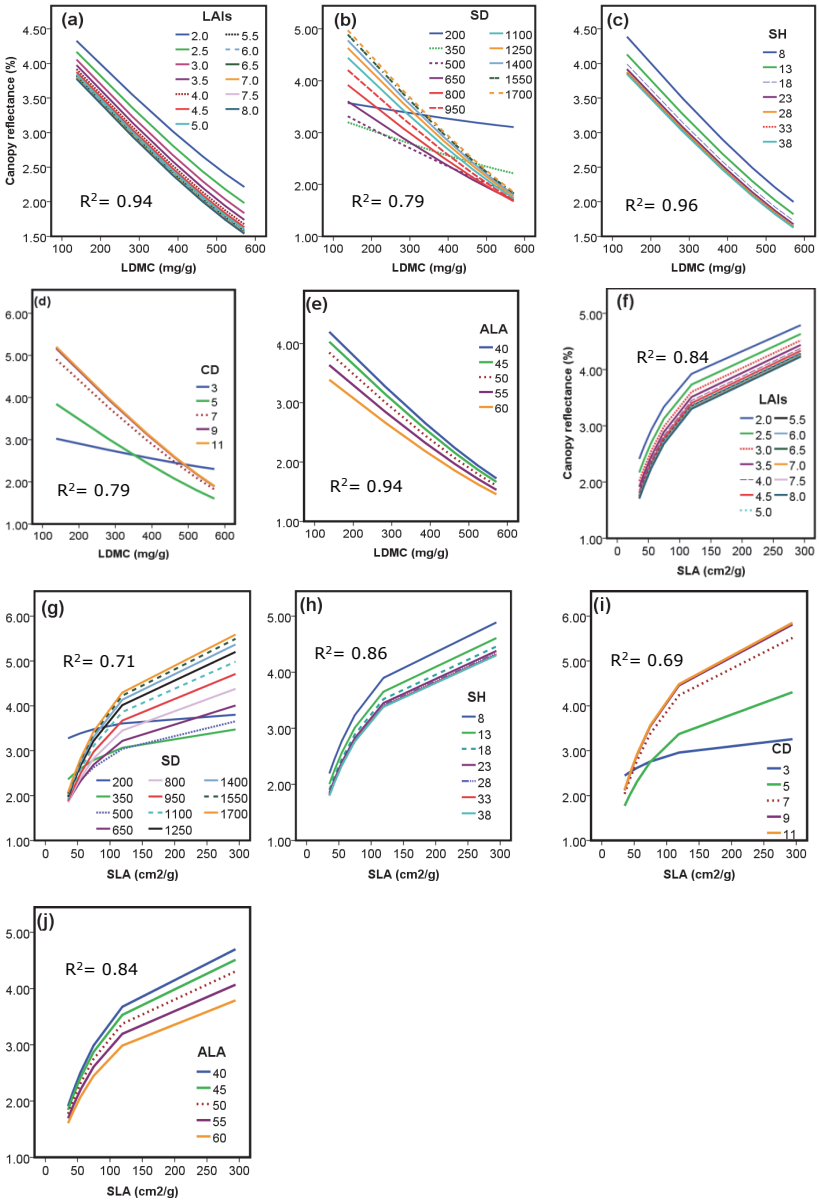

Figure 3.2: Relationship between LDMC and the 2298.69 nm band, and SLA and the 2280.71 nm band, for a range of single tree LAI (a, f), stem density (b, g), stand height (c, h), crown diameter (d, i) and average leaf angle (e, j) with fixed values set to LAI_s= 5.5; SD = 800 trees/ha, SH = 23m, CD =5.4m, ALA = 50^0, θ_s = 32^0 and Ψ =153.

The high R^2 values of Figure 3.2a, 3.2c and 3.2e reveal that the relationship between LDMC and reflectance at 2298.69 nm is little affected by variations in LAI_s, SH and ALA compared to SD and CD. An increase in SH values decreases

the reflectance linearly. Lower LAI_s (<3) and lower SH (<18m) values have greater impact than higher LAI_s (>4) and SH (>23m) on the inverse linear relationship between reflectance and LDMC. The LSD post hoc comparison (p=0.01) revealed that LAI_s ≥6.5 and SH ≥ 30 have no significant impact on the relationship of LDMC and reflectance at 2298.69 nm.

Similarly, it can be observed that LAI_s, SH and ALA variations have less effect on the relationship between SLA and reflectance at 2280.71 nm (Figure 3.2f, 3.2h, 3.2i). LAI_s ≥6 and SH ≥ 30 did not show significant impact on the relationship between SLA and reflectance at 2280.71 nm for the LSD test (p=0.01). It is evident that the greatest influence on both relationships arises from SD and CD (Figure 3.2b, 3.2e, 3.2g and 3.2i).

At lower SD (<400 trees/ha) and CD (≤ 3) values, almost all variations in reflectance originate from the confounding factors, and the bands were almost insensitive to variations in LDMC and SLA. In addition, the impact of SD, CD and ALA increases with decreasing LDMC concentration, and vice versa for SLA. In contrast, the impact of SH followed a uniform pattern for all values of the two leaf traits.

Compared to single bands, the structural variables effect on the relationships between LDMC and SLA with the mND index was greatly condensed (see Figure 3.3). The influence of LAI_s, SH and ALA variations is minimal (Figure 3.3a, 3.3c, 3.3e, 3.3f, 3.3h and 3.3j). The LSD test (p= 0.01) showed that LAI_s ≥ 5 and SH ≥ 13m have no significant effect on the relationship between LDMC and SLA and the mND index. However, for SD and CD, the slope of the relationships rapidly declined when the SD and CD values dropped below 400 trees/ha and 3m respectively (Figure 3.3b, 3.3d, 3.3g and 3.3i)

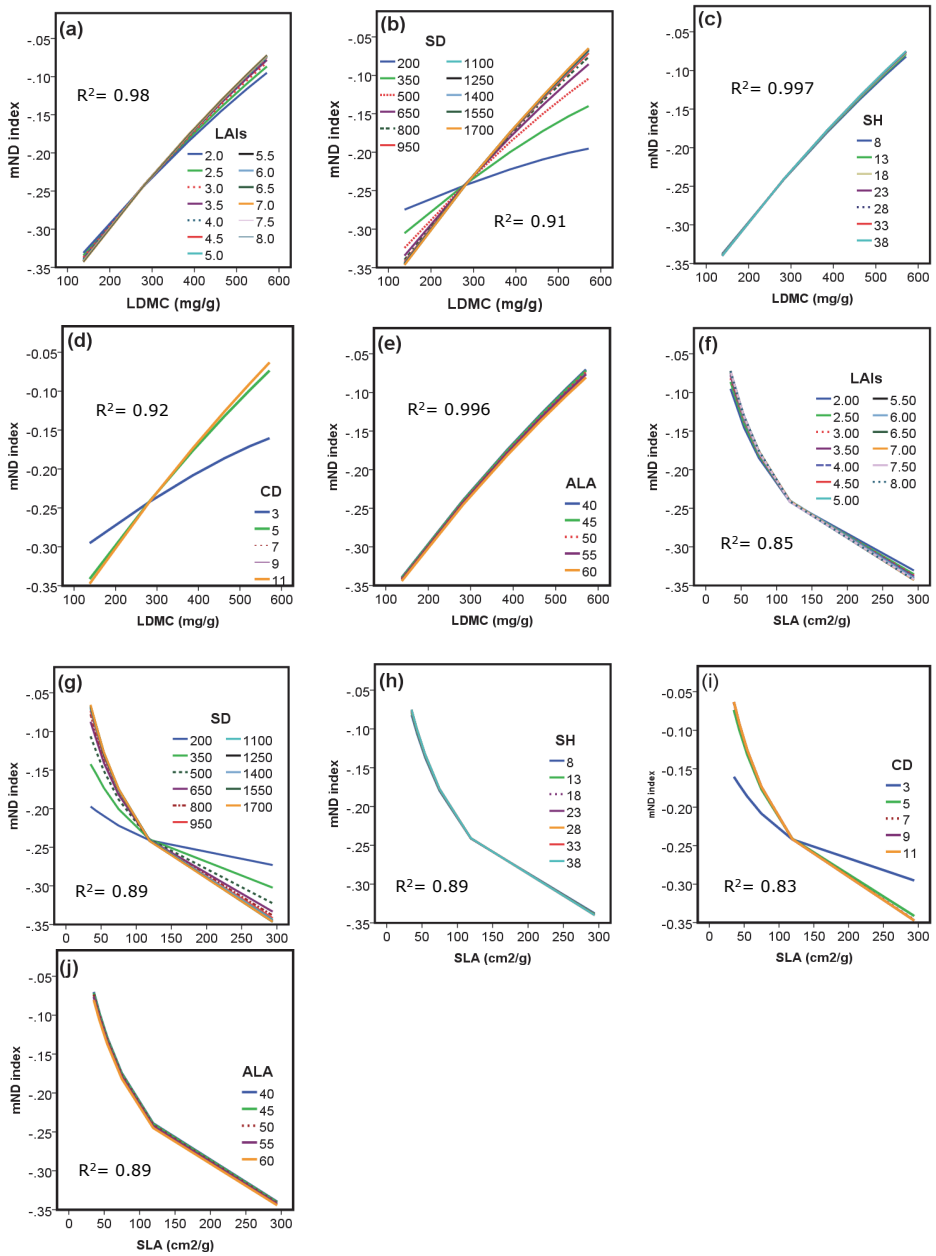

Figure 3.3: Relationship between LDMC, SLA and the modified normalized index (mND) for a range of single tree LAI (a, f), stem density (b, g) ,stand height (c, h), crown diameter (d, i) and average leaf angle (e, j) with fixed values set to LAI_s= 5.5; SD = 800 trees/ha, SH = 23m, CD =5.4m, ALA = 50^0, θ_s = 32^0 and Ψ =153.

3.3.3 Implications for the detectability of LDMC and SLA from remotely sensed data

The slope of the relationships between the leaf traits and mND index was used as a measure of detectability, to examine how varying two confounding variables at a time affects the accuracy of LDMC and SLA retrieval. The results obtained were linked to the actual stand properties of the Bavarian National Park Forest, to study for which forest stands (broadleaf, conifer or mixed) the detectability of the two leaf traits was most affected by the different combinations of the structural variables.

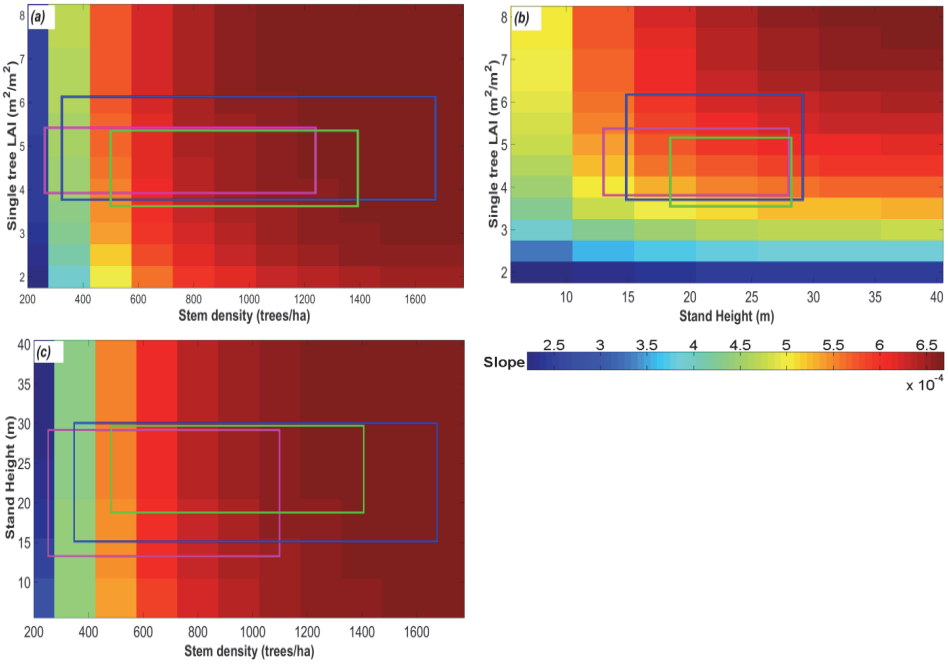

Figure 3.4: Average slopes derived from the relationship between mND index and LDMC for three specific combinations of the structural variables (a: LAI_s and SD, b: LAI_s and SH and c: SH and SD) with fixed variables set at average test site values. The three boxes in each subfigure show the structural information range of broadleaf (purple), conifer (light green), and mixed (blue) stands of the Bavarian National Park Forest.

The detectability of LDMC by using the mND index and structural information derived from the broadleaf, conifer and mixed stands of the test site is illustrated in Figure 3.4. As can be observed from the figure, the greater the slope, the higher is the detectability of the two leaf traits. In terms of LAI_s and SH, all three stand types have nearly optimal conditions for retrieving canopy LDMC and SLA. They all have LAI_s above 3.5 and SH above 13 m (Figure 3.4b). The ranges of the structural information of broadleaf (purple), conifer (light green) and mixed (blue) stands of the Bavarian National Park Forest were plotted in the form of boxes. The light green boxes in Figure 3.4 (a, b and c)

demonstrated that the conifer structural information is better for the leaf traits estimation than the other stands. By contrast, the purple and blue boxes in Figure 3.4a and 3.4c revealed that the broadleaf and mixed stands (particularly some of the broadleaf stands) have very low SD values, which could significantly weaken the relationship between the traits and spectral variation at canopy scale.

3.4 Discussion and conclusions

Variations in forest canopy structures play an important role in retrieving biochemical and biophysical variables from canopy reflectance, yet the relative importance of each structural variable on the retrieval of LDMC and SLA from canopy reflectance has not been adequately addressed. The sensitivity of canopy reflectance in the NIR and SWIR spectral range to the variation of the two leaf traits and canopy structural variables were explored in this paper using a local sensitivity method with the simulated dataset from the INFORM model. Comparison of simulated reflectance at leaf and canopy scale indicated that the spectral variation at canopy level is lower than that at leaf level, due to the structural variables effect. The canopy reflectance reacts differently in the NIR and SWIR region for structural variables variation. From Figure 3.1 it can be inferred that structural variables suppress canopy reflectance across the NIR and SWIR spectral region, but still there is a significant spectral variation that could be used to estimate the leaf traits.

Our R^2 and F-test results showed the presence of significantly strong correlations between the variation in the two leaf traits and canopy reflectance (tables 3.4 and 3.5). The F-test result also indicated the greater suitability of longer wavelengths compared to shorter wavelengths for assessing both LDMC and SLA at canopy scale. Specifically, the contribution of the two leaf traits on the variability of forest canopy reflectance in the SWIR region of the spectrum is immense. In many cases, R^2 and the calculated F statistics value is much higher in VIs (Table 3.5) than in single bands (Table 3.4), which confirms that vegetation indices (VIs) outperform single bands in correlating leaf traits to canopy reflectance. This is because more spectral information is involved (especially from different regions of the spectrum) when using VIs than when using information from a single band. This result is in agreement with Malenovský *et al*. (2008), and Verrelst *et al*. (2010), who studied the effect of woody elements on forest chlorophyll content retrieval. Several non-significant F-test values were observed when the sensitivity of the canopy reflectance was tested for the variation in the two leaf traits against the structural variables. Predominantly, SD and CD variations influenced the relation between LDMC to both single bands and VIs. Large F-test calculated values were observed in the SWIR, which point out both LDMC and SLA being more detectable in the SWIR of the spectrum than in the NIR investigated in this study (data not shown).

Le Maire *et al*. (2008), Asner *et al*. (2011b) and many others also reported the suitability of the SWIR region for the retrieval of biochemical and biophysical variables such as leaf mass per area and water content.

The five structural variables (LAI_s, SD, SH, CD and ALA) examined in this study perturbed canopy reflectance at all single bands tested, but the greatest influence was observed for SD and CD, followed by ALA (Figure 3.2). Unlike SH, the influence of LAI_s, SD, CD and ALA varies with LDMC and SLA concentrations. This may be due to the confounding variables interaction with the two leaf traits. The F-test analysis on the interaction effects of the five confounding factors against LDMC and SLA concentration variation showed significant differences for the interaction of LAI_s, SD, CD and ALA with the two traits at $\alpha = 0.01$. Comparison of results from single bands (Figure 3.2) and VIs (Figure 3.3) gives an insight into how VIs yield robust estimations of leaf traits, irrespective of the structural variables influence. The mND vegetation index was able to avoid much of the influence of all the five structural variables, except in a few cases of low SD and CD conditions. This indicates that the influence of the five structural variables on the two leaf traits' retrieval using remotely sensed data can be greatly minimized by spectral derivatives such as using VIs. The post hoc test confirmed that higher values of LAI_s (≥ 5) and SH ($\geq$ 13m) have no impact and can be ignored in parametrizing RTM. Nevertheless, the correlation between the two leaf traits and canopy reflectance (single bands or mND index) may decline or vanish as long as the forest is sparsely populated (SD<400 trees/ha) with medium or small tree crown diameter. Figure 3.2b, 3.2c, 3.2g and 3.2i noticeably demonstrate that the correlation might be weakened in sparsely populated forest stands. This suggests that high estimation accuracy of the two leaf traits is to be expected for vegetation with high SD (>400 trees/ha) or canopy closure. This finding confirms the result of a study by Okin *et al*. (2001), which suggested that for reliable retrieval of vegetation variables the canopy closure should be at least 30%.

An early study by Asner (1998), and Asner *et al*. (1998) revealed that in addition to the tremendous influence of canopy closure, LAI is a major driver of canopy reflectance. A sensitivity analysis by Xiao *et al*. [53] also showed that the sensitivity of canopy reflectance to variation in equivalent water thickness (C_w) and leaf mass per area (C_m) is obscured mainly by LAI in the NIR and SWIR region. Our study supports these findings, but also demonstrates that if single bands are used instead of VIs (Figure 3.2), SH, CD and ALA could also perturb the relationship between the variation in the two leaf traits and canopy reflectance. Therefore, for accurate estimation of LDMC and SLA, it is important to use spectral derivatives such as VIs or adopt various inversion strategies other than sensitive single wavelengths.

As depicted in Figure 3.4, except for a few extremely low values of the structural variables, the slope between LDMC and the mND index is greater than 5×10-4, and even greater slope values (>2×10-3) were observed for the relationship between SLA and mND (not shown here). This reaffirms the detectability of the two leaf traits when using mND index. From the three stand structural combination templates we may conclude that the most important structural factors determining the detectability of the two leaf traits are stem density and crown diameter.

In a nutshell, our results have demonstrated: 1) the presence of a strong relationship between the two leaf traits' variation and canopy reflectance; 2) the existence of significant canopy reflectance disturbance from SD, LAI_s SH, CD and ALA; 3) the capability of VIs to correct confounding effects of canopy structural heterogeneity originating from these structural variables; and 4) the promising detectability of the LDMC and SLA of the test site from hyperspectral data. However, it is worth mentioning that in our analysis we investigated the influence of only five structural variables (SD, LAI_s SH, CD and ALA). The background was represented by an average value for all elements in the understory. Other input parameters except solar zenith and azimuth angle were set at average values. These choices, along with our choice of wavelengths, VIs and the INFORM model for simulation, might have biased our results. For instance, in low SD stands, the background reflectance may contribute to the variation in the reflectance related to the two leaf traits if the understory is green vegetation. It can also act as an additional confounding factor if the forest floor is litter, bare soil and/or lying wood (Verrelst *et al*. 2010). The INFORM model simulates top of canopy reflectance based on certain input parameters by assuming that the forest canopy is fully occupied by green leaves. The simulated result could be biased if there is a significant amount of woody material or litter in the canopy. In this study, only specific spectral bands from the HYSpex available spectral regions were investigated. However, utilizing other spectral bands may provide useful information to distinguish subtle spectral variations due to LDMC and SLA. Therefore, further research is required to understand how structural variables (other than LAI_s, SD, SH, CD and ALA), the presence of non-photosynthetic materials in the canopy, background composition, and illumination and viewing positions affect the relationship between the leaf traits (LDMC and SLA) and canopy reflectance in the NIR–SWIR region. The present study investigated the retrieval of the two leaf traits based on the spectral features and the indices developed for leaf mass per area, but additional study is recommended to discover spectral features and VIs that are specifically sensitive to LDMC and SLA, so that these can be accurately mapped using remotely sensed data.

Chapter 4

Retrieval of Forest Leaf Functional Traits from HySpex Imagery Using Radiative Transfer Models and Continuous Wavelet Analysis[3]

[3] This chapter is based on:
Ali, A.M., A.K. Skidmore, R. Darvishzadeh, I.C. van Duren, S. Holzwarth and J. Müller, 2016. Mapping forest leaf dry matter content from hyperspectral data. In: *Proceedings* of ASPRS 2016 annual conference: IGTF 2016*: imaging & geospatial technology forum, 11-15 April 2016, Fort Worth, United States of Am*erica. 14p

Ali, A. M., A. K. Skidmore, R. Darvishzadeh, I. V. Duren, S. Holzwarth, and J. Müller (2016). Retrieval of Forest Leaf Functional Traits from HySpex Imagery Using Radiative Transfer Models and Continuous Wavelet Analysis, *ISPRS, Journal of photogrammetry and remote sensing*. (***In review after second revision***)

Abstract

Quantification of vegetation properties plays an important role in the assessment of ecosystem functions with leaf dry mater content (LDMC) and specific leaf area (SLA) being two key functional traits. For the first time, these two leaf traits have been estimated from airborne images (HySpex) using the INFORM radiative transfer model and Continuous Wavelet Analysis (CWA). Ground truth data, were collected for 33 sample plots during a field campaign in July 2013 in the Bavarian Forest National Park, Germany, concurrent with the hyperspectral overflight. The INFORM model was used to simulate the canopy reflectance of the test site and the simulated spectra were transformed to wavelet features by applying CWA. Next, the top 1% strongly correlated wavelet features with the LDMC and SLA were used to develop predictive (regression) models. The two leaf traits were then retrieved using the CWA transformed HySpex imagery and the predictive models. The results were validated using R^2 and the RMSE of the estimated and measured variables.

Our results revealed strong correlations between six wavelet features and LDMC, as well as between four wavelet features and SLA. The wavelet features at 1741 nm (scale 5) and 2281 nm (scale 4) were the two most strongly correlated with LDMC and SLA respectively. The combination of all the identified wavelet features for LDMC yielded the most accurate prediction (R^2= 0.59 and RMSE= 4.39%). However, for SLA the most accurate prediction was obtained from the single most correlated feature: 2281 nm, scale 4 (R^2= 0.85 and RMSE= 4.90%). Our results demonstrate the applicability of Continuous Wavelet Analysis (CWA) when inverting radiative transfer models, for accurate mapping of forest leaf functional traits.

4.1 Introduction

Two key plant functional biodiversity traits are leaf dry matter content (LDMC) (which is the ratio of leaf dry mass to leaf fresh mass), and specific leaf area (SLA) (which is the ratio of leaf area to leaf dry mass). LDMC is a proxy for relative growth rate and carbon assimilation, and is an important predictor of a plant's location on an axis of resource capture, usage and availability (Wilson *et al*. 1999). SLA (also referred as leaf mass per unit area, specific leaf mass, or leaf specific mass), links plant carbon and water cycles (Pierce *et al*. 1994), provides information on spatial variation of photosynthetic capacity and leaf nitrogen content, and is indicative of plant physiological processes such as light capture, growth rates, and life strategies of plants (Pierce *et al*. 1994). A worldwide foliar dataset indicates that 82% of all variation in photosynthetic capacity can be explained by SLA and nitrogen (Wright *et al*. 2004).

The two traits are inversely correlated and are also used to estimate other traits and ecological indicators, such as leaf thickness, leaf life span (Shipley 2002, Vile *et al*. 2005, Marenco *et al*. 2009), relative growth rate (Shipley 2006), and soil fertility (Hodgson *et al*. 2011). Generally, the quantitative information and spatial distribution of LDMC and SLA improve our understanding and capacity to investigate community structure and ecosystem functioning (Mouchet *et al*. 2010, Lavorel *et al*. 2011). However; these traits are currently quantified through labour-intensive methods of field sampling. Consequently, ecological understanding of trait variation across extended spatial and temporal scales is lacking (Messier *et al*. 2010).

Remote sensing, as a relatively fast and efficient approach for estimating LDMC and SLA across a wide range of spatial and temporal scales, has so far received little attention for quantification of these traits. Only a few studies have attempted to estimate SLA using remote sensing data. Lymburner *et al*. (2000) tested vegetation indices derived from the green, red, NIR, and MIR bands of Landsat TM data and found a correlation between these bands and canopy average SLA. Vegetation indices have been developed for estimation of leaf mass per area in Fontainebleau and Fougères broadleaf forests in France by le Maire *et al*. (2008) and Feret *et al*. (2011). Until recently, however, none of the remote sensing techniques have been tested for direct estimation of LDMC. A leaf scale study using PROSPECT model inversion reported the potential of remote sensing for quantifying LDMC and SLA (Ali *et al*. 2016b). Another study by Cheng *et al*. (2014b) demonstrated the potential of wavelet analysis to retrieve leaf mass area (LMA) from sets of simulated and measured leaves reflectance however, this study was conducted at leaf scale and needs further examination when upscaling to canopy level.

A number of statistical methods have been widely applied for retrieval of biophysical and biochemical parameters of vegetation from remote sensing data (e.g. le Maire *et al*. 2008, Darvishzadeh *et al*. 2009). Nevertheless these methods have been criticized for being site-specific and lacking generalization (Darvishzadeh *et al*. 2011). Inversion of Radiative Transfer Models (RTM) has been suggested as an alternative approach for parameter retrieval from remote sensing data, but RTMs still require local information such as cover type in order to be accurately upscale (Si *et al*. 2012). RTMs allow creation of simulated training databases covering a wide range of situations and configurations to which inversion algorithms can be applied to retrieve parameters from remote sensing data. A wide variety of studies have evaluated the performance of radiative transfer model inversion techniques to estimate vegetation biophysical and biochemical parameters such as chlorophyll (Darvishzadeh *et al*. 2008, Darvishzadeh *et al*. 2012, Lv *et al*. 2014, Wang *et al*. 2014), LAI (Meroni *et al*. 2004, Dini *et al*. 2006, Darvishzadeh *et al*. 2008, Yang *et al*. 2011, Cho *et al*. 2014), biomass and others vegetation characteristics (Kazemipour *et al*. 2010, Dorigo 2012). A recent comparative analysis by (Atzberger *et al*. 2015) showed the potential and drawbacks of different retrieval methods for mapping grassland leaf area index. Their study indicated the robustness and higher accuracy of RTMs inversion approaches over statistical methods.

However, because of redundancy and multi-collinearly in hyperspectral data (Blackburn 2007a), RTM inversions are often applied on selected bands sensitive to a given vegetation variable. Although a subset of spectral bands proved to be a stable and accurate predictor for vegetation parameters (Weiss *et al*. 2000), no general criteria have been formulated for the selection of bands (Banskota *et al*. 2013b). Wavelet transformation seems to be a promising alternative technique for selecting the most informative features from hyperspectral data.

Wavelet analysis enables spectral data to be transformed into a new representation by decomposing the original spectra into various scales (frequencies). Subsequently, the correlation between the concentration of parameters and the wavelet scales can identify the most sensitive spectral feature for predicting a given parameter. Previous studies have investigated the potential of wavelet analysis for estimating leaf parameters from leaf spectra measured in the laboratory and simulated data using RTMs (Jingcheng *et al*. 2011, Cheng *et al*. 2012, Ullah *et al*. 2012, Zhang *et al*. 2012a, Cheng *et al*. 2014a). However, the applicability of wavelet analysis at canopy level using canopy spectra obtained from airborne and spaceborne hyperspectral data has received far little attention. Further study is needed to understand how wavelet analysis can be applied to airborne or spaceborne image data for retrieving vegetation parameters. This is because canopy spectral reflectance obtained

from these images is more complex than the spectral reflectance of individual leaves, due to factors such as sensor noise, soil background, shadow, canopy structural variation, non-photosynthetic vegetation, and solar and viewing geometry (Ustin *et al*. 2009, Wolf *et al*. 2010, Ollinger 2011).

There are two forms of wavelet transformation: discrete and continuous. Discrete Wavelet Analysis (DWA) has the potential to avoid redundancy; it transforms and uses the most informative part of the input data but it is difficult to assign wavelet features to a specific band because of scale variability during the transformation. Continuous wavelet analysis (CWA) is more time-consuming and has data redundancy limitations. Nevertheless, CWA has evolved as a promising tool for quantitatively analysing vegetation parameters from hyperspectral remote sensing data (e.g. Blackburn 2007b, Huang and Blackburn 2011, Cheng *et al*. 2014a). It allows band-by-band interpretation of very subtle spectral information. CWA can operate at various scales, starting from the original signal and going up to maximum scales defined by the user. Our study applied continuous wavelet transformation, because each scale component from CWA is directly comparable to the input reflectance spectrum on a band-by-band basis and the results are easily interpreted and can be related to wavelengths with minimal uncertainty (Cheng *et al*. 2011).

Banskota *et al*. (2013a and 2013b) applied DWA to estimate forest leaf area index (LAI) in temperate forests from AVIRIS (airborne visible/infrared imaging spectrometer) data using both statistical and RTM inversion techniques. In another study, CWA was found to perform well at detecting diurnal and seasonal variation in the canopy water content of nut tree orchards from airborne spectral data on the basis of canopy water content measurements in the field and concurrent imagery from the AVIRIS instrument (Cheng *et al*. (2014a).

Our study aimed at quantifying LDMC and specific leaf area (SLA) for a mountain forest using HySpex airborne hyperspectral data through the INFORM radiative transform model. The model inversion was undertaken via an optimized predictive model constructed from Continuous wavelet analysis (CWA) coefficients. We posited that there will be an optimal spectral wavelength domain for use in CWA for quantifying the two traits. Our three aims were to (1) identify spectral bands sensitive to LDMC and SLA using HySpex airborne data; (2) assess the performance of predictive models constructed from the combination of wavelet features derived from different spectral wavelength domains for LDMC and SLA retrieval, and (3) map the LDMC and SLA of the study area using HySpex imagery in conjunction with the best performing predictive models.

4.2 Methodology

4.2.1 Analytical framework

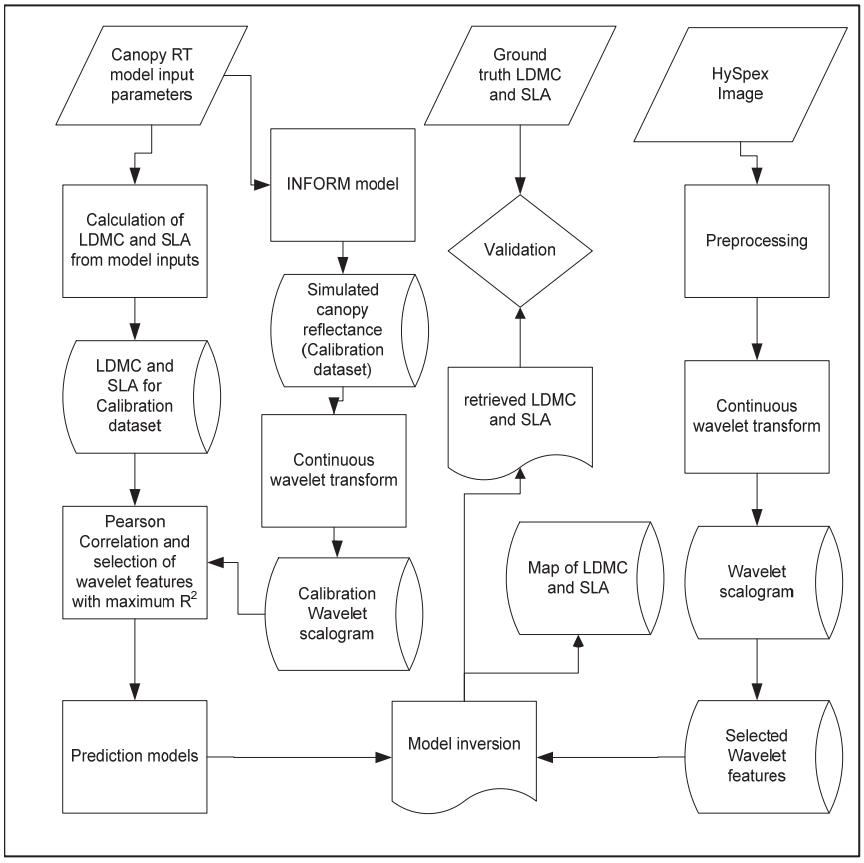

Figure 4.1: Analytical framework of the methods applied for the retrieval of LDMC and SLA from HySpex hyperspectral image.

The overall procedures followed in this study are presented in Figure 4.1. In order to retrieve and map the spatial distribution of the two leaf traits (LDMC and SLA) from HySpex imagery, three sets of data have been utilized. 1) A wide variety of simulated canopy spectra with its corresponding LDMC and SLA values (calibration dataset), 2) Ground truth data in 33 sample plots (validation dataset), which contains canopy spectra extracted from HySpex images with their corresponding LDMC and SLA values collected in the field, and 3) HySpex images of the study area. The INFORM model was parametrized and run in its forward mode to build a calibration dataset of canopy spectra with their corresponding model input parameters. The HySpex images were atmospherically corrected, mosaicked and pre-processed. Then, wavelet transformation was applied to both the INFORM simulated spectra and the

HySpex image. Spectral features strongly correlated to the two leaf traits concentration have been identified by computing and ranking the Pearson correlation calculated for the calibration dataset. The top 1% of strongly correlated wavelet features was used to develop prediction models. Next, the developed prediction models were applied on the identified wavelet features of the HySpex data to retrieve and map the spatial distribution of the two traits in the study site. Finally accuracy assessment have been conducted using the 33 sample plots spectra extracted from HySpex imagery and their corresponding ground truth LDMC and SLA values (validation dataset). The details of the methodology are presented in the following subsections.

4.2.2 Test site and field data

The test site for this study was the mixed mountain forest of the Bavarian Forest National Park. The park is located in south-eastern Germany along the border with the Czech Republic (49^0 3' 19" N, 13^0 12' 9" E) (Figure 4.2). Elevation of the test site varies from 600 m to 1,473 m above sea level. The climate of the region is temperate, with high annual precipitation (1,200 mm to 1,800 mm) and low average annual temperature (3 to 6 ^{0}C). Heavy snow cover is characteristic of the area in winter. Brown soils are the predominant soil type at lower altitude (below 900 m a.s.l) whereas at high altitude (above 900 m a.s.l) brown soils and brown podzolic soil predominate. The soils in the area are naturally acidic and poor in nutrient content (Heurich *et al*. 2010). The natural forest ecosystems of the Bavarian Forest National Park vary with altitude: there are alluvial spruce forests in the valleys, mixed mountain forests on the hillsides and mountain spruce forests in the high areas. The dominant tree species include European beech (*Fagus sylvatica*), Norway spruce (*Picea abies*) and Fir (*Abies alba*). In the mixed mountain forests Sycamore maple (*Acer pseudoplatanus L*), Mountain ash (*Sorbus aucuparia L*) and Goat willow (*Salix caprea*) are also found (Heurich and Neufanger 2005). Due to heavy disturbance by bark beetles and wind storms in recent decades the forest structure in the park is very heterogeneous (Lehnert *et al*. 2013).

A field campaign was conducted during summer 2013 to collect ground truth data from 33 plots. The test site was stratified into broadleaf, conifers and mixed forest stands. Given the heterogeneity of the forest and the time and cost constraints, we randomly selected 33 plots from the three main forest class strata resulting in 10 samples in broadleaf, nine in conifer and 14 in mixed stands. Each plot was square, with sides 30m long. In all 33 sample plots, forest structural variables such as LAI, stem density (SD), canopy closure (CC), crown diameter (CD), and stand height (SH) were measured.

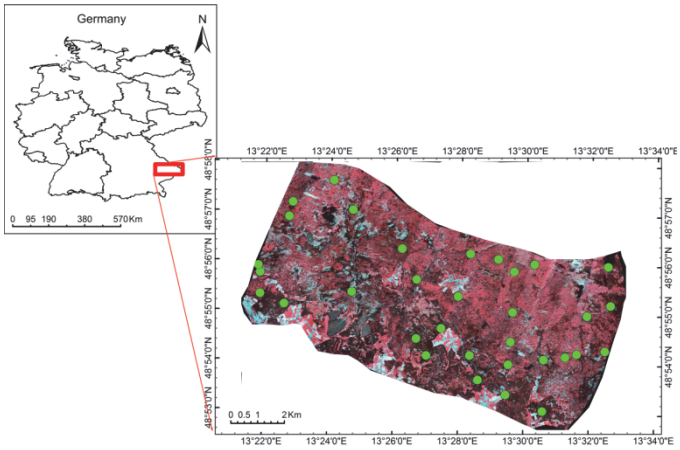

Figure 4.2: Map of the test site. The green dots show the distribution of the sample plots in the study area on a false colour composite (R=967 nm, G = 2029 nm and B=2371 nm) of the HySpex image.

The LAI of each plot was measured using an LAI_2000 canopy analyser and also computed from hemispherical photographs taken in each plot by using CIMES-FISHEYE software (Walter 2009) for validation purposes. The SD was recorded as number of trees per hectare based on the number of trees in each plot. CC was estimated by averaging five observations in a plot using a spherical crown densiometer. CD and SH were calculated from the mean crown diameter and mean height of five trees randomly selected in each plot. The CD of each tree was determined by averaging two perpendicular projected distances on the ground. The total height of each tree was estimated by using a Nikon Forestry 550 laser rangefinder.

In each plot, leaf samples were collected from mature sunlit leaves at the top of the canopy of 3 to 5 trees, using a crossbow, and their characteristics were measured (n=130). Leaf area of broadleaf leaf samples was measured using the LI-3000C portable leaf area meter (Li-Cor, Inc, Lincoln, NE, USA). The surface of sample conifer needles was scanned using an HP double lamp desktop scanner at a resolution of 1200 dpi; the needle projections were computed from the grayscale images using ImageJ image processing software (which is freely available online). For details on the leaf samples' physical variable measurements, see (Ali *et al*. 2016). The collected leaf samples were transported to the laboratory for further analysis. All samples were oven dried at 65 ^{0}C for 48 hours and then LDMC, SLA, leaf mass per leaf area (C_m) and leaf water content (C_w) were computed based on fresh and oven-dried leaf mass and leaf areas. For mixed plots, the average values for LDMC, SLA, C_m, C_w and leaf structural parameter (N) were based on crown biomass proportion of each species in a given plot.

The variables measured in the field are summarized in Table 4.1. The leaf structural parameter-N was retrieved by inverting the PROSPECT model using simulation at three wavelengths (see Ali *et al*. 2016). During the field campaign, the spectral reflectance of leaf samples and understory vegetation and ecosystem elements on the forest floor such as bark, litter, mosses and lichens was also measured by using the ASD field spectroradiometer coupled to a high intensity contact probe and integrating sphere.

Table 4.1: Summary of the measured and estimated leaf parameters and canopy structural variables of the 33 sample plots in the Bavarian Forest National Park. The measured leaf parameters were leaf mass per leaf area (C_m), leaf water content (C_w),leaf structural parameter (N) as estimated using PROSPECT model, leaf dry matter content (LDMC) and specific leaf area (SLA). The collected canopy structural variables include leaf area index (LAI), stem density (SD), canopy closure (CC), crown diameter (CD), stand height (SH) and average leaf angle (ALA).

Parameter	Minimum	Maximum	Mean	St. dev.
C_m (g/cm^2)	0.0061	0.0292	0.0147	0.0059
C_w (g/cm^2)	0.0071	0.0309	0.0178	0.0071
N	1.36	1.93	1.58	0.16
LDMC (g/g)	0.3999	0.5075	0.4534	0.0254
SLA (cm^2/g)	43.45	165.64	89.38	37.72
LAI (m^2/m^2)	2.42	6.18	4.3	0.81
SD (n/ha)	222	1722	778.4	405.5
CC (%)	38	91	75.19	5.33
CD (m)	2.91	10.55	5.67	1.56
SH (m)	12.26	27.36	20.23	4.52
ALA (deg)	40	60	50	9.96

4.2.3 Image acquisition and pre-processing

HySpex is a new airborne hyperspectral sensor developed by the Norwegian Norsk Elektro Optikk (NEO) company. It comprises two imaging spectrometers with spectral ranges of 400–1000 nm and 1000–2500 nm and up to 416 spectral channels. It is supported by a precise navigation system for georeferencing and correction of geometric errors. Both of its sensors operate in a push-broom scanning mode with an angular recording image width of 150. Its field of view can be doubled to 300 using a field expander lens. It records radiance data in contiguous bands at a spectral resolution of 3.7 nm for 400 - 992 nm spectral range (sensor 1) and 6 nm for 968 - 2498 spectral range (sensor 2). Its spatial resolution is 1.6 meters for sensor 1 and 3.4 meters for sensor 2.

The HySpex instrument was flown over the test site on board a Cessna 208B Grand Caravan at an average altitude of 3010 m above sea level on July 22 2013 between 9:00 and 11:15 local time. A total of 19 flights were made to cover the test site. The HySpex image data were supplied by the DLR team after atmospheric correction performed with the ATCOR4 model, orthorectified

and georeferenced using standard aircraft in-flight information. As only the spectral bands in the SWIR were utilized in this study, only the images from sensor 2 of HySpex were resampled and mosaicked by removing the view angle effects between the 19 flight line images using empirical view-angle correction technique proposed by Kennedy *et al*. (1997) (figure 4.2).

To prepare the HySpex data for further analysis, the image reflectance was resampled over a 9 × 9 pixel window, which most closely approximates the size of the sample plots (approximately 30 m× 30 m). Then, a Savitzky-Golay filter was applied to correct for random and systematic noise. Finally, the average reflectance of the sample plots was extracted and used for evaluation (hereafter referred as the measured or validation dataset). The noisy bands in the water absorption region (1345-1450nm and 1790–1980 nm) and bands from 2450–2498 nm were assigned zero values. This left a total of 203 bands with valid reflectance values.

4.2.4 RTM parameterization and forest reflectance simulation

To simulate the spectral property of the test site we used the Invertible Forest Reflectance model "INFORM" (Atzberger 2000, Schlerf and Atzberger 2006), which is a hybrid RTM that combines the forest light interaction model (Rosema *et al*. 1992) and SAIL (Verhoef 1984) canopy RTMs with the PROSPECT (Jacquemoud and Baret 1990) leaf RTM. In INFORM, LAI is represented by the leaf area indices of single trees. Hence, the ground truth values for LAI_s were computed from LAI and CC.

$$LAI_s = \frac{LAI}{CC} \tag{4.1}$$

And for every combination of model input parameters, LDMC and SLA were indirectly calculated from C_m and C_w as:

$$LDMC = \frac{C_m}{C_m + C_w} \tag{4.2}$$

$$SLA = \frac{1}{C_m} \tag{4.3}$$

where LAI_s is single tree leaf area index, CC is canopy closure; C_m is leaf dry mass per area and C_w is leaf water content per leaf area. See Ali *et al*. (2016b) for further details.

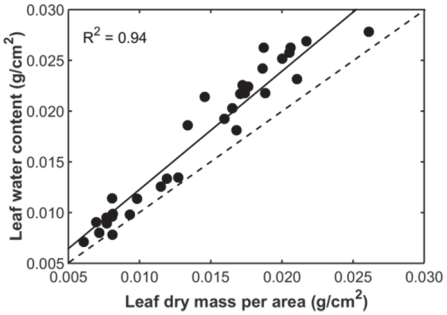

Figure 4.3: Correlation between the measured average leaf mass per area (C_m) and average leaf water content (C_w) of the 33 plots. The solid line shows the best linear correlation and the broken line indicates the 1:1 relationship.

A strong correlation (R^2 = 0.94) was observed between the model input parameters C_m and C_w (Figure 4.3). Therefore, in order to preserve the relationship between these input parameters the INFORM model was run by generating the input parameters (C_m, C_w, N, LAI_s, SD, SH, CD and ALA) using a multivariate normal distribution function based on the mean and covariance matrix of their ground truth values (Table 4.1). Leaf chlorophyll content was fixed at a value of 40µg/g, since in this study the shortwave-infrared region (SWIR) of the electromagnetic spectrum was used; a region of the electromagnetic spectrum where leaf pigments have no effect. A sensitivity study had previously reported insignificant effect of solar zenith and azimuth angles on INFORM simulated canopy reflectance (Ali *et al*. (2015). Therefore, other leaf, canopy, and external input parameters (Table 4.2) were fixed using average values based on the field data, HySpex sensor specification, and previous studies (Schlerf and Atzberger 2006, Ali *et al*. 2016). As bare soil occurred extremely rarely on the forest floor, the field spectra of understory vegetation and the forest floor elements were averaged and used as a fixed background reflectance during the simulation (Figure 4.4).

Table 4.2: Constant input parameters used during INFORM simulation based on field observation, HySpex hyperspectral sensor configuration, and previous studies.

Input variable	Symbol	Unit	value	source
Chlorophyll content	C_{ab}	µg/cm^2	40	Ali *et al.* 2016
Sun zenith angle	θ_s	Degree	32	HySpex data
Observation zenith angle	θ_0	Degree	0	HySpex data
Azimuth angle	Ψ	Degree	153	HySpex data
Fraction of diffused radiation	Sky1	fraction	0.1	Schlerf and Atzberger 2006

Next, using the INFORM model 10,000 reflectance spectra were simulated by randomly selecting leaf chemical and canopy structural properties based on the multivariate normal distributions and covariance matrix produced from the ground truth data. To avoid extreme values and unrealistic combinations, the

randomly assigned value of each variable was limited by +/-5% of the observed maximum and minimum values for that variable in the ground truth data. A random Gaussian noise value of 0.3% (Cheng *et al*. 2014b) was added to each simulated spectrum to account for model uncertainties and reduce auto-correlation between the spectrum and input variables. The simulation was performed for 256 spectral bands (1000–2500 nm) corresponding to the SWIR band settings of the HySpex system.

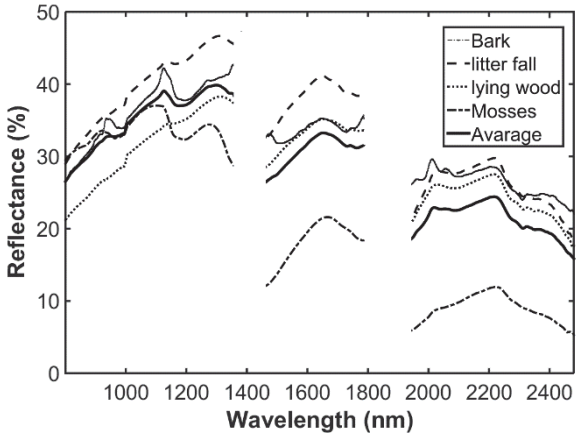

Figure 4.4: Spectral property of the Bavarian national park forest floor as measured by ASD spectroradiometer and used as representative background reflectance during INFORM simulation.

4.2.5 Continuous wavelet analysis

Signal processing, image processing, and data compression have been successfully undertaken in many fields using wavelet transformation (e.g. Tjuatja *et al*. 1993, FatemiGhomi *et al*. 1995, Roux *et al*. 2000, Lin *et al*. 2008, Jingcheng *et al*. 2011). The wavelet transform converts each one-dimensional reflectance spectrum into a two-dimensional wavelet power scalogram by using a mother wavelet function. Each element of a wavelet power scalogram is called a wavelet coefficient. The coefficients of CWA can be directly compared with the original spectra wavebands and possess information about the position and shape of the vegetation's spectral features (Blackburn and Ferwerda, 2008). The continuous wavelet analysis involves the linear transformation of a hyperspectral signal into a set of coefficients using the mother wavelet function f (λ) (where λ=1, 2, 3, …k, represent the number of wavebands). The continuous wavelet $\psi_{a,b(\lambda)}$ can be created by scaling and shifting the mother wavelet $\psi_{(\lambda)}$ (Bruce *et al*., 2001; Cheng *et al*., 2011, (Cheng *et al*. 2010));

$$\psi_{a,b}(\lambda) = \frac{1}{\sqrt{a}}\left(\frac{\lambda - b}{a}\right) \tag{4.4}$$

where a and b are positive real numbers and represent the scaling and shifting factors, respectively. The scale factor a represents the width of the wavelet and the shifting factor b denotes its position.

$$W_f(a,b) = \langle f, \psi_{a,b} \rangle = \int_{-\infty}^{+\infty} f(\lambda), \psi_{a,b}(\lambda) d\lambda \quad (4.5)$$

The continuous wavelet coefficients ($_{Wf\ (a,\ b)}$) consist of the two-dimensional scalogram (j×k matrix). The one-dimension depth of leaf spectra resulting from different amounts of LDMC and SLA can be quantified by using the wavelet coefficient (scalogram). Among mother wavelets, available in MATLAB 8.4 software, the second derivative of the Gaussian function (Mexican hat) was selected for both LDMC and SLA since it best correlated the two leaf traits with wavelet features. The Gaussian function has also been proposed as a potential mother wavelet in other remote sensing studies, because it approximates the shape of the absorption features of reflectance spectra (Cheng *et al*. 2011, Ullah *et al*. 2012, Cheng *et al*. 2014a, Cheng *et al*. 2014b).

In wavelet transform scale, values govern the degree to which the wavelet is compacted or stretched. Low scale values compress the wavelet and correlate better with high frequencies. The low scale CWA coefficients represent fine-scale features in the input signal vector. The reverse is true for high scale values. Instead of using all possible scale decompositions, the dyadic scales were used to decompose the spectra, in order to avoid intensive computation as well as to reduce the dimensions of the scalogram and the volume of data. In this study, scales for CWA were powers of 2 (2^1, 2^2, 2^3, . . .,2^{10}) and were described as power numbers (scale 1, scale 2, scale 3, . . ., scale 10), similar to the other relevant studies (e.g. Ullah *et al*. 2012, Cheng *et al*. 2014a).

Wavelet features that significantly correlated with LDMC or SLA were determined in four steps as described in Cheng *et al*. (2011), (Cheng *et al*. 2014a). First, a continuous wavelet transform was applied to both the simulated (calibration) dataset and measured (HySpex) spectra (validation) dataset, in order to represent them in the wavelet domain where the wavelet power was a function of the wavelength and the scale. Wavelet features of scales 1, 2, and 3 were excluded from the calibration and validation datasets since they have been reported as mostly capturing noise in airborne hyperspectral data. Second, a correlation scalogram was established between the calibration spectra wavelet power at each wavelength, scale location, and LDMC (or SLA) by calculating the coefficient of determination (R^2). The wavelet amplitude was correlated to log-transformed LDMC and SLA values. This resulted in a pool of wavelet features for the calibration dataset that were sensitive to LDMC or to SLA. Wavelet features with large R^2 values imply high sensitivity to LDMC or to SLA. Third, all features of a correlation scalogram were ranked in descending order of R^2 and a threshold value of 1% was applied

to delineate and define the feature regions most sensitive to LDMC or to SLA. Fourthly, features with a central wavelength within each region of the combined scalogram were selected, in order to generate a short list of predictor variables: they are described as (wavelength in nm, scale) in the following text. The selected wavelengths and scale values of the wavelet transformed validation dataset (HySpex) were taken out and put aside for validation purpose. The overall analysis process is shown schematically in Figure 4.1

4.2.6 Calibration of predictive models and inversion

The Hyspex data inversion was performed using predictive models. Predictive models were developed on the relationships between the simulated spectra wavelet features identified in section 2.5 and the INFORM model input parameters (LDMC and SLA). A wide variety of regression models such as linear, stepwise linear, multiple linear and quadratic regressions were tested for their performance. Predictive models with good fit (i.e. a high R^2 and low RMSE combination) on the calibration dataset (INFORM simulated spectra and inputs) were then used to invert the HySpex imagery wavelet features in order to retrieve LDMC and SLA.

4.2.7 Validation

The predictive performance of the inversion was assessed using LDMC and SLA values collected in 33 sample plots in the field. The accuracy of the field measured and predicted values of the two traits from HySpex imagery were evaluated using the coefficient of determination (R^2) and root mean square error in percent (RMSE %) calculated as:

$$R^2 = 1 - \frac{\sum(y_i - y_i')^2}{\sum(y_i - \bar{y}_i)^2} \quad (4.6)$$

$$RMSE\ (\%) = \sqrt{\frac{\sum(y_i - y_i')^2}{n}} / \bar{y}_i * 100 \quad (4.7)$$

Where y_i and y_i' are the actual and predicted values for sample i, and $\bar{y}$ and n are the arithmetic mean and the number of samples in the measured data, respectively.

4.2.8 Mapping the LDMC and SLA of the test site

Once the performance of the different wavelet features was investigated, the selected predictive models were applied to map the concentration of the two leaf traits in the test site. First, the non-forest areas and cloud cover in the HySpex image data were masked out using land cover maps, ground sample points and visual inspection. Next, the continuous wavelet transformation was applied and sensitive wavelet features for each pixel in the HySpex image were extracted. Then the predictive models developed in section 2.6 were applied

for pixel-by-pixel estimation of the two leaf traits in the test site. Finally, the predicted values were used to map the spatial distribution of LDMC and SLA in the Bavarian Forest National park.

4.3 Results

4.3.1 Canopy reflectance simulation and verification

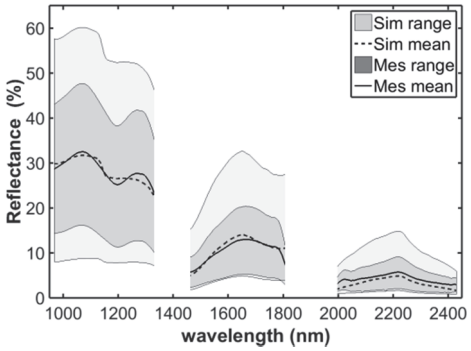

Figure 4.5: Comparison of the simulated (sim) spectra (using the INFORM model) with the sample plots' spectra (mes) extracted from HySpex hyperspectral airborne image of the study area. The solid line shows the mean of the sample plots' spectra, while the broken line indicates the mean of simulated spectra. The pale gray and dark gray shaded areas indicate the range of the simulated and measured spectra, respectively.

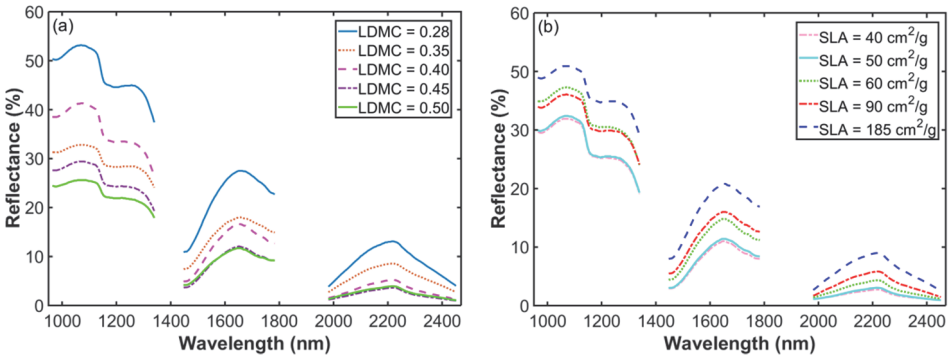

Figure 4.6: Effect of the two leaf traits on canopy reflectance in the SWIR region. INFORM simulated canopy reflectance for various concentrations of LDMC (a) and SLA (b) under specific canopy structures and sensor configurations.

The reliability of the INFORM model simulated spectra was verified by comparing their mean and range with those obtained from HySpex hyperspectral image data. As can be observed from figure 4.5, the simulated reflectance spectra showed a good match with the measured reflectance. The two leaf trait values (LDMC and SLA) had a significant effect on the canopy spectra. The INFORM simulated canopy reflectance reduced as the LDMC

increased and vice versa for SLA (Figure 4.6) across the SWIR of the electromagnetic spectrum.

4.3.2 Wavelet analysis and identification of wavelet features sensitive to LDMC and SLA

Figure 4.7 details the sensitivity of wavelet features (which are transformed from the simulated spectra) plotted for the two leaf traits. Strongly correlated wavelet features were found for both traits. More wavelet features correlate highly with SLA (Figure 4.7b) than with LDMC (Figure 4.7a). After a number of tests, the top 1 % most strongly correlated wavelet features were found to be good predictors of both traits. There were six sensitive wavelet features for LDMC and four for SLA in the top 1% strongly correlated wavelet features. The wavelet features selected for LDMC were at scales 4 and 5, whereas those selected for SLA were at scales 4, 6, and 8 (Figures 4.7b and 4.7d).

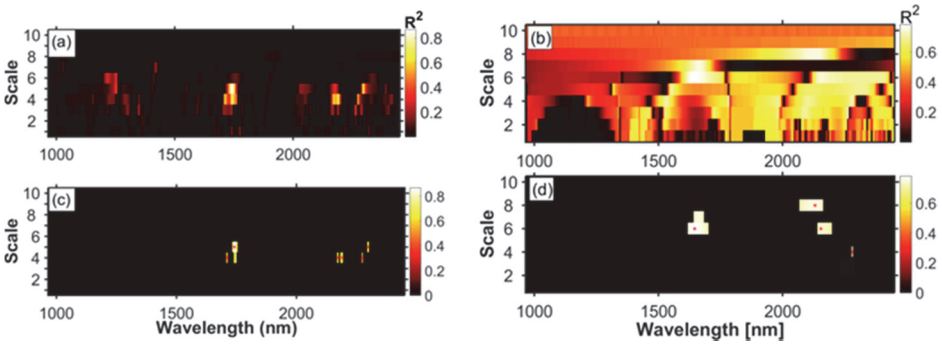

Figure 4.7: Correlation scalograms for the identification of wavelet features which significantly correlate with leaf dry matter content (LDMC) (a) and specific leaf area (SLA) (b). Scalograms are derived from continuous wavelet analysis of simulated spectra. Brightness represents the coefficient of determination (R^2) relating wavelet power to LDMC and SLA. Coloured feature regions in scalograms (c) and (d) depict the wavelet features with the top 1% greatest R^2 values for LDMC and SLA.

4.3.3 Fitting regression models to the calibration dataset

A wide variety of regression models ranging from simple linear to multiple regressions were tested and evaluated to correlate the spectral (wavelet) features with the studied leaf traits. The stepwise linear model and quadratic regression were selected for their goodness of fit to our calibration dataset. The regression models were tested for each wavelet feature separately and for different combinations of wavelet features. Figure 4.8 depicts the predictive capacity of two of the many wavelet features selected and their corresponding wavelength reflectance for the two traits estimation.

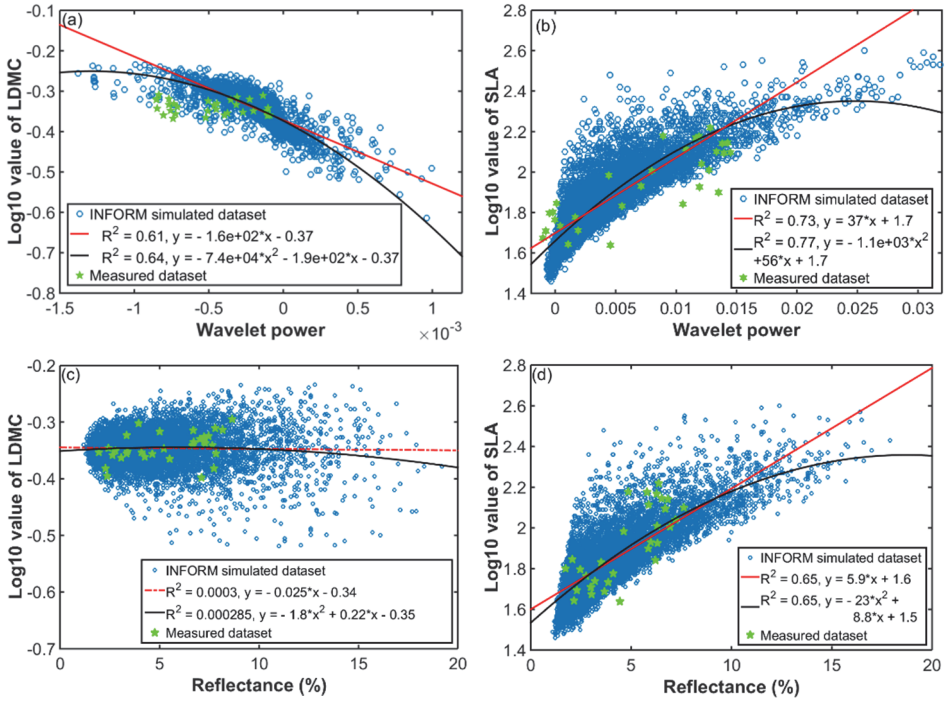

Figure 4.8: Relationships between the wavelet features and reflectance of the calibration dataset for LDMC and SLA. (a) the relationship between the logarithmic value of LDMC and the wavelet power at feature 2191 nm, scale 4, (b) the relationship between logarithmic value of SLA and wavelet power at feature 2281 nm, scale 4, (c) relationship of the simulated (INFORM) and measured spectral reflectance (HySpex data) to LDMC at 2191 nm and (d) SLA at 2281 nm. For comparison, the measured HySpex dataset (validation dataset) are shown as pentagrams.

Figures 4.8c and 4.8d demonstrate the overlaid measured spectra fall within the range of the simulated spectra. However, the relationship between the measured spectra wavelet powers and the two traits appears to be shifted toward lower values (Figure 4.8a and 4.8b). Directly correlating the two plant leaf traits with simulated spectra without any wavelet transformation performed less satisfactorily than correlating them with wavelet power. The reflectance simulated at 2191 nm turned out to be particularly insensitive to LDMC (R^2=0.0003) (Figure 4.8c) whereas the wavelet feature cantered at the same band yielded an R^2 = 0.64 of linear correlation with LDMC (Figure 4.8a). The estimated coefficients of the most accurate stepwise linear prediction equation developed by combining the selected six wavelet features for LDMC retrieval is illustrated in the appendix.

Thus, predictions made using selected wavelet features and their combination revealed high R^2 and low RMSE against the calibration data set of the two leaf traits (Table 4.3). The R^2 values range from 0.58 to 0.87 for LDMC and from 0.73 to 0.79 for SLA. The single wavelet features that showed the highest

correlation and the lowest RMSE were at 1741 nm at scale 5 for LDMC and at 1645 nm at scale 6 for SLA.

Table 4.3: Coefficients of determination (R^2) and root mean square error (RMSE %) between the logarithmic values of the two leaf traits (INFORM model input values) and predictions made using wavelet features derived from the calibration dataset.

LDMC			SLA		
Spectral (wavelet) feature	R^2	RMSE (%)	Spectral (wavelet) feature	R^2	RMSE (%)
A. Combination of All	0.92	2.41	A. combination of all	0.93	2.50
B. (1741 nm scale 5)	0.87	3.09	B. Combination of D, F & G	0.87	3.42
C. (2191 nm scale 4)	0.78	4.07	C. (combination of F & G)	0.84	3.81
D. (2173 nm scale 4)	0.72	4.62	D. (1645 nm scale 6)	0.79	4.33
E. (2299 nm scale 5)	0.66	5.08	E. (2131 nm scale 8)	0.76	4.65
F. (1711 nm scale 4)	0.63	5.32	F. (2155 nm scale 6)	0.74	4.81
G. 2275 nm scale 4	0.58	5.63	G. (2281 nm scale 4)	0.73	4.91

4.3.4 Retrieval and validation of LDMC and SLA from wavelet features

The predictive models (inversion algorithms) presented in section 3.3 were applied to the actual image dataset (HySpex airborne hyperspectral data) to estimate the two leaf traits. The predictive models were validated for each wavelet feature separately and for different combination of wavelet features. The combination of all six wavelet features gave better results than single or different combinations of wavelet features for LDMC. However, the wavelet feature cantered at 2281 nm scale 4 was most accurate for predicting SLA using the stepwise linear regression model (Table 4.4) in the validation process.

The comparison of predicted values obtained from the best combinations of wavelet features against the HySpex data after converting logarithmic values to normal values are presented in figure 4.9. As can be observed from the figure, the prediction is more precise for LDMC (RMSE = 4.39 %) than for SLA (RMSE = 4.90 %), while the inverse is true for correlation (R^2 = 0.59 and R^2 = 0.85 for LDMC and SLA respectively) when a logarithmic value is used. There is a tendency for LDMC to be overestimated, especially for higher values of LDMC. Nevertheless, the predicted values were scattered closely around the 1:1 relationship line, which indicates the sensitivity of the selected wavelet features in capturing the variation in LDMC and SLA concentrations. Furthermore, no saturation problems were observed in the predicted values.

Table 4.4: Prediction of logarithmic value of LDMC and SLA from HySpex hyperspectral airborne spectra by inversion of simulated INFORM model spectra using continuous wavelet transformation and stepwise linear regression.

LDMC			SLA		
Spectral (wavelet) feature	R^2	RMSE (%)	Spectral (wavelet) feature	R^2	RMSE (%)
A. combination of all	**0.59**	**4.39**	A. (2281 nm scale 4)	**0.85**	**4.90**
B. (1741 nm scale 5)	0.39	23.10	B. combination of all	0.85	36.44
C. (2275 nm scale 4)	0.34	24.29	C. combination of A, E & G	0.84	13.03
D. (2191 nm scale 4)	0.33	17.26	D. Combination of E & G	0.80	5.43
E. (2299 nm scale 5)	0.2	20.08	E. (2155 nm scale 6)	0.50	7.86
F. (2173 nm scale 4)	0.30	21.27	F. (2131 nm scale 8)	0.48	7.36
G. (1711 scale 4)	0.28	20.82	G. (1645 nm scale 6)	0.32	12.94

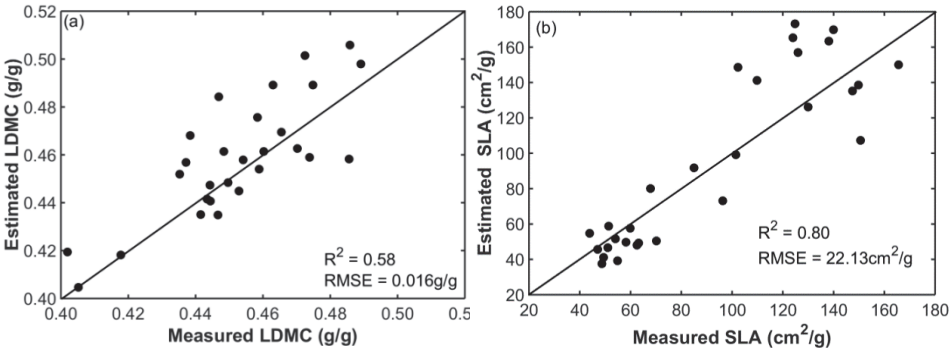

Figure 4.9: Scatter plots of measured and predicted LDMC (a) and SLA (b). Predicted values were computed by applying the models developed from the calibration dataset using six wavelet features combinations in Table 4.3 for LDMC and a wavelet feature cantered at 2281 nm scale 4) for SLA. Data points are derived from the measured (validation) dataset collected from the study site. The solid line shows the 1:1 relationship between the predicted and measured data.

4.3.5 Mapping the LDMC and SLA of the study area

The concentrations of the two leaf traits across the study area (Bavarian Forest National Park) are presented in Figures 4.10a and 4.10b. Before producing the maps, a forest mask obtained from maximum likelihood classification (MLC) was used to mask out the non-forest areas from the HySpex data, thus eliminating areas occupied by other land covers. The accuracy of the created forest mask by MLC was assessed using the existing land cover maps and the 33 sample plots data (kappa coefficient = 0.95). The masked HySpex image and the selected predictive models developed from six wavelet features for LDMC and one wavelet feature for SLA (Table 4.4) were applied to map these traits. The inverse relationship of the two leaf traits is clearly visible in the maps. Both LDMC and SLA showed perceptible variability across the study area. The means obtained for all image pixels were 0.4235 g/g for LDMC and

107cm^2/g for SLA, which are close to the means of the samples measured during the field measurements shown in Table 4.1. A comparison with a forest type map of the test site revealed that LDMC values were higher for conifer and mixed stands than for deciduous forests (Figure 4.10c).

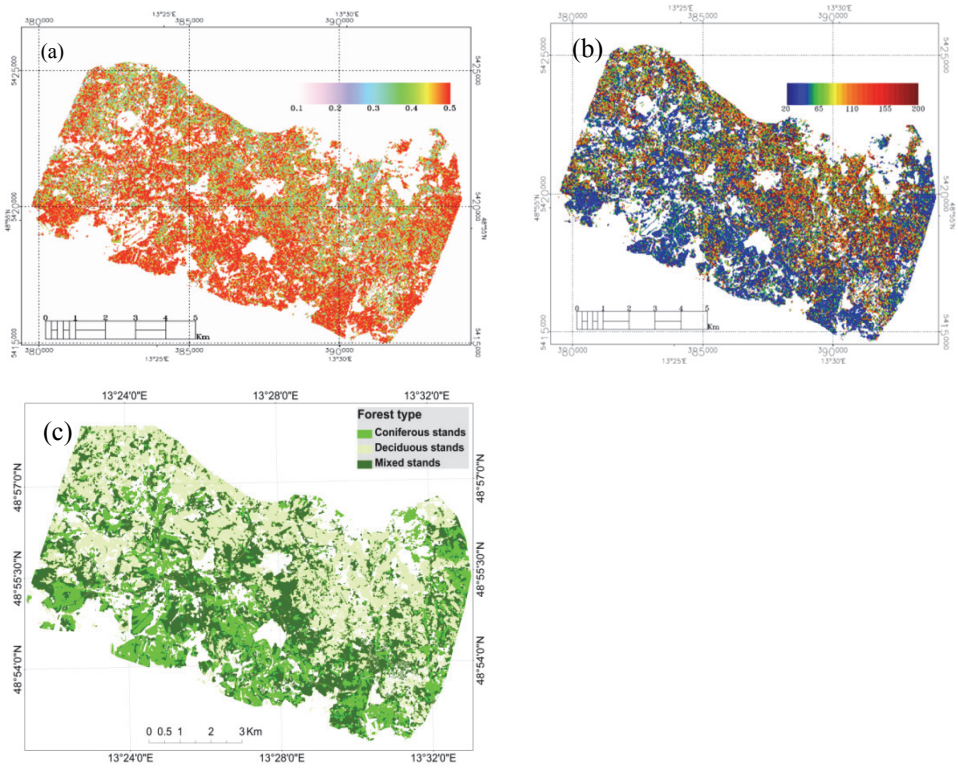

Figure 4.10: LDMC in g/g (a) and SLA in cm^2/g (b) maps derived from the HySpex imagery of July 22, 2013. The maps are based on 30 x 30 m cells retrieved using a predictive model developed on all six selected wavelet features for LDMC (Table 4.4) and one of the four selected wavelet features (2281 nm scale 4) for SLA. The forest type of the test site is shown (c) for comparison of the spatial distribution of the two leaf traits across different forest stands.

4.4 Discussion and conclusion

4.4.1 Wavelet transformation and inversion

In the last four decades, vegetation biophysical and biochemical variables have been retrieved from remote sensing data using either statistical (empirical) or physical (RTM) approaches. However, previous studies mainly focused on estimating parameters by seeking the direct correlation between remote sensing data and parameter values. The method used for retrieving variables from physical models involved the generation of a large dataset of simulated

spectra followed by inversion using approaches like look-up tables or an artificial neural network. To date, the potential for estimating vegetation variables using transformed spectra has not been investigated. Our study has for the first time successfully retrieved the two leaf traits namely, LDMC and SLA from canopy reflectance data obtained from airborne hyperspectral image by means of RTM and wavelet transformation.

4.4.2 Advantage of wavelet transformation

In this study, the CWA approach was used for the retrieval of the two functional traits from HySpex hyperspectral reflectance data. One advantage of CWA over other approaches is that it has the potential to identify the most sensitive spectral features from a large hyperspectral dataset. The second advantage of using CWA is transformation of the original spectra that resulted in stronger correlation between the variables. Decomposition of the INFORM simulated spectra and measured HySpex spectral reflectance using CWA (R^2 = 0.58 to 0.93) provided higher correlations with the two leaf traits compared with the non-transformed reflectance values (R^2 = 0.0003 to 0.65).

Our results demonstrate the robustness of CWA for estimating vegetation variables in particular leaf traits such as LDMC and SLA (Figure 4.8). After wavelet transformation, parameters which appeared uncorrelated to simulated canopy reflectance (without transformation), such as LDMC, were observed to be highly correlated (Figures 4.8a and 4.8c). This may be attributed to the effectiveness of CWA in decomposing the traits' absorption features into various scales of narrow and broad band absorption features and identifying those that correlate most with the variation in the traits' concentration. The performance of wavelet analysis compared with narrow-band indices and stepwise selection of narrow-band reflectance for retrieval of pigment concentrations in vegetation at leaf and canopy scales has also been reported by Blackburn (2007b). By comparison with narrow-band indices, wavelet analysis captures more information contained within the hyperspectral data and creates an opportunity to develop robust and extendible methods for quantifying plant traits over extended areas (Blackburn 2007a).

4.4.3 Identifying strongly correlated wavelet features

We determined six wavelet features for LDMC and four for SLA prediction in a mixed mountain forest (Table 4.4). The prediction model based on all six selected wavelet features performed with higher accuracy than any other combination of wavelet features for LDMC retrieval. However, for SLA, one unanticipated finding was that the wavelet feature at 2281 nm scale 4 provided a more accurate prediction of SLA than any other individual features and their combinations. This demonstrates the fact that application of all strongly

correlated wavelet features to calibration data sets may lead to overfitting and does not necessarily ensure the most accurate estimation.

The band position of the SLA-sensitive wavelet features found in this study agrees well with findings by Cheng *et al*. (2014b), who used simulated and measured spectra at leaf level and reported a strong correlation of LMA (inverse of SLA) with the wavelet features at (1639 nm, scale 4) and (2139 nm, scale 4). However, in our study the scale of the wavelet features has shifted to larger values. This may be due to canopy structure properties and other external factors such as sensor configuration and atmospheric effects that would influence the canopy spectral reflectance.

4.4.4 Accuracy assessment

As expected, the measured HySpex spectra overlapped exactly with the simulated spectra without transformation (Figures 4.5, 4.8c and 4.8d). However, despite the addition of 0.3% random Gaussian noise to the simulated spectra, systematic shifts to higher or lower values were observed when wavelet transformation was applied to the measured spectra (Figures 4.8a and 4.8b). This in turn led to systematic overestimation and underestimation of the two traits (Figure 4.9). Probable causes for this shift could be atmospheric effects and sensor noise on the measured spectra. These factors may cause variation in local absorption peaks on the measured spectra, and lead to higher or lower wavelet power values during the transformation.

Another possible reason could be the simplification of parameters in RTM representation. The model input parameters are based on certain input parameters and the effect of the forest heterogeneity cannot be fully estimated the stochastic processes. Therefore, strong correlations may be found between any of the input parameters and the simulated spectra or their derivatives. This is consistent with the results obtained by Cheng *et al*. (2014b), who also found wavelet power better fitted the leaf spectra simulated with the PROSPECT model than the spectra measured from leaf samples in the laboratory. They partly attributed the differences to measurement errors and simplifications intrinsic to PROSPECT. Similarly, Feret *et al*. (2011) and le Maire *et al*. (2008) reported stronger correlation between one of the model input variables and simulated spectra than between measured variables and spectra.

We found a stronger correlation between the predicted and (measured) validation values for SLA (R^2 = 0.80) than for LDMC (R^2 = 0.58). Similar outcomes have also been reported previously (Ali *et al*. 2016) for estimating the two leaf traits from the PROSPECT model inversion at leaf scale. These may be attributed to several factors. One is that LDMC is a compound variable derived from leaf water content (C_w) and leaf dry mass per unit area (C_m).

Therefore, its correlation with spectral reflectance is affected by both C_w and C_m. This would explain why many of the wavelengths did not show strong correlation to LDMC even in the simulated spectra (Figure 4.7). The relatively low R^2 value (as low as 0.58) between simulated spectral wavelet features and LDMC while that of SLA was above 0.70 (Table 4.3) also supports the contention that LDMC is less correlated with reflectance than SLA.

By contrast, the RMSE for LDMC was found to be lower than the RMSE for SLA (4.39% versus 4.90 %: Figure 4.7). The low RMSE of LDMC is partially associated with ground truth accuracy. LDMC is computed based on fresh and dry weights of samples that can be precisely and accurately obtained in the laboratory, but calculation of SLA requires measurements of leaf area that are prone to operator and instrument errors.

We did not observe significant improvements in the predictions made for deciduous, coniferous, and mixed stands separately (results not shown here). This reveals the unbiased nature of the average value weighted by the crown proportion of each species present in a mixed sample plot. However, calculating the crown volume involves extra field efforts to collect parameters such as crown diameter, crown height, total height, diameter at breast height, and other forest inventory data.

In broad terms, our findings have revealed the potential for estimating forest leaf traits from imaging spectroscopy using radiative transfer model and CWA. Here we examined the predictability of the two leaf traits in the 950-2450 nm spectral region only. The other parts of the electromagnetic spectrum should be investigated and the methods should be refined in order to address the quantification of plant traits across a wide range of spatial scales. Other traits could similarly be explored.

Chapter 5

Narrow band vegetation indices for specific leaf area retrieval at leaf and canopy scale[4]

[4] This chapter is based on:
Ali, A. M., R. Darvishzadeh, A. K. Skidmore and I. V. Duren (2016). Narrow band vegetation indices for specific leaf area retrieval at leaf and canopy scale. (In review after revision).Photogrammetric Engineering & Remote Sensing, PE&RS.

Abstract

Specific leaf area (SLA) is an important component when assessing functional diversity and plays a key role in ecosystem modelling. However, studies of SLA across relevant spatial and temporal scales are lacking. This article aims at calibrating and identifying indices for accurate estimation of SLA at leaf and canopy level. Validation of our results using field measured and simulated datasets revealed the importance of several key indices. . At leaf level, $OSAVI_{1370, 1615}$ performed strongly (R^2 = 0.93 and RMSE = 13.66cm^2/g). $NMDI_{920, 1675, 1335}$ and $VARI_{1345, 1675, 1850}$ were also among the top performing indices, with R^2 > 0.90 for all leaf level data. At canopy level, $OSAVI_{1537, 1543}$ showed that the hyperspectral data from HySpex imagery accurately estimate SLA (R^2 = 0.88 and RMSE = 13.30cm^2/g). Other canopy level indices for SLA retrieval include $RDVI_{1537, 1543}$, $SAVI_{1537, 1543}$, $TSAVI_{1537, 1543}$, and $WDVI_{1537, 1543}$. The results demonstrate the importance of vegetation indices for accurate retrieval of SLA at both leaf and canopy level.

5.1 Introduction

Specific leaf area (SLA) is one of the fundamental leaf functional traits attributed to the functional component of biodiversity (Wilson *et al.* 1999, Asner *et al.* 2011b) and is among the ten essential biodiversity variables proposed by Skidmore *et al.* (2015) to capture biodiversity change from space. SLA is defined as the leaf area per unit of dry leaf mass, usually expressed in m^2/kg. It is also commonly referred to as leaf mass per unit area, specific leaf mass, or leaf specific mass. It links plant carbon and water cycles (Pierce *et al.* 1994), and in many large-scale ecosystem models, canopy-average SLA is recognized as an important ecosystem variable. According to Pierce *et al.* (1994), SLA is indicative of plant physiological processes such as light capture and growth rates, as well as of the life strategies of plants and it therefore provides information on the spatial variation of photosynthetic capacity and leaf nitrogen content (Pierce *et al.* 1994). A worldwide foliar dataset indicated that 82% of all variation in photosynthetic capacity can be explained by SLA and nitrogen (Wright *et al.* 2004). SLA is species-specific, but significant plasticity exists within and between individual plants of the same species (Pierce *et al.* 1994, Asner *et al.* 2011b). Usually, high SLA occurs in areas with high water and nutrient availability. Plants growing at high altitude generally have a lower SLA than plants of the same species in lower elevations (Wilson *et al.* 1999).

Although remote sensing – in particular, hyperspectral imagery – has emerged as a powerful platform for measuring or estimating biochemical and biophysical vegetation parameters, few operational methods have been developed for quantifying SLA at landscape, regional or global scales from remote sensing data. Therefore, developing robust and operational algorithms that can rigorously predict plant functional traits at different scales is pivotal when assessing the biodiversity trait SLA from remotely sensed data.

Two types of approach have been developed to estimate vegetation parameters from remote sensing data or reflectance measurements: (i) empirical (such as indices and/or multiple regressions), and (ii) radiative transfer models (RTM) inversion. The most commonly used method in the empirical approach is the vegetation index (VI). Vegetation indices (VIs) constitute simple and convenient algebraic combinations of spectral reflectance to extract information from remotely sensed data, which facilitates the processing and analysis of large amounts of remotely sensed data. In other words, reflectance measurements at various spectral bands are mathematically combined to empirically correlate reflectance (or reflectance indices) to a particular vegetation parameter (such as SLA). These approaches are simple and fast to apply, but have the limitation of often being site-specific because the representativeness of the relationship is limited to the

representativeness of the database (le Maire *et al.* 2008). In addition, the effectiveness of a VI is limited to different degrees by the effect of perturbing factors such as atmospheric conditions, topography, illumination and viewing geometry, sensor calibration, soil background, and vegetative growth stage or conditions (e.g., Rascher *et al.* 2007, Somers *et al.* 2010, Zhu *et al.* 2014).

On the other hand, RTMs allow the creation of simulated training databases covering a wide range of spectral data to which inversion algorithms such as Look-Up Tables inversion and Artificial Neural Network can be applied to retrieve parameters from remote sensing data. Inversion of such models often yields a large number of different possible solutions for a specific variable. Furthermore, uncertainties in measurements and models may result in large variation in results (Combal *et al.* 2003). It is also difficult to obtain optimal parameterized solutions for radiative transfer model inversions (Atzberger *et al.* 2011), which can also lead to challenges when extrapolating models in space and time.

Despite having limitations, because of their ease of computation and capacity, VIs have been widely used to enhance the information contained in spectral reflectance data. In the past four decades, a number of researchers (e.g., Rouse *et al.* 1974, Clevers 1991, Gitelson 2004, Jensen *et al.* 2012, Wu 2014) have sought to develop spectral vegetation indices at various scales ranging from leaf to global, in order to monitor the Earth's vegetation cover and retrieve vegetation parameters such as leaf chlorophyll, leaf area index (LAI), fractional vegetation cover, biomass, canopy architecture, and photosynthetic activity from remotely sensed data. Many ecosystem researchers (Marshall and Thenkabail 2014, Wu 2014) have widely applied VIs and hyperspectral narrow bands to remote sensing data for land cover classification, biomass and net primary production (NPP) quantification, crop yield estimation, land degradation monitoring, soil mapping, and vegetation–climate interaction assessment.

Various VIs have been proposed to minimize the effects of perturbing factors and maximize accurate retrieval of vegetation parameters. For instance, soil-adjusted VIs (e.g., Huete 1988, Ren and Zhou 2014) to correct for the perturbation of soil background based on the soil line information, and atmospherically resistant VIs (e.g., Gitelson *et al.* 2002) to minimize atmospheric noise or to reduce both soil influence and atmospheric effects (e.g., Liu and Huete 1995, Huete *et al.* 1997).

Among vegetation parameters retrieved using hyperspectral data, SLA has received little attention. Few ratio-based indices have been tested for retrieval of SLA mainly by means of simulated data, either at leaf level (le Maire *et al.* 2008, Romero *et al.* 2012) or at canopy level (le Maire *et al.* 2008) Calibration

of VIs using simulated data, however, has failed to address the uncertainty and discrepancies between measured and simulated spectral datasets. In addition, the suitability of many of the index types available in the literature (other than the ratio type) has not yet been evaluated for SLA retrieval. Here we calibrated and validated the suitability of a number of vegetation indices previously proposed for retrieving various vegetation properties (see Table 5.4) for remotely estimating the SLA at leaf and canopy levels for heterogeneous mountain forest with contrasting leaf structures and canopy architectures.

5.2 Methods

5.2.1 Study site

The study site was the mixed mountain forest of the Bavarian Forest National Park, which is located in south-eastern Germany along the border with the Czech Republic (49° 3′ 19″ N, 13° 12′ 9″ E) (Figure 5.1). Elevation of the study site varies from 600m to 1473m above sea level. The climate of the region is temperate, with high annual precipitation (1200 mm to 1800 mm) and low average annual temperature (3 to 6 ^{0}C). Heavy snow cover is characteristic of the area in winter. Brown soils are the predominant soil type at lower altitude (below 900 meters a.s.l) whereas at high altitude (above 900 meters a.s.l) brown soils and brown podzolic soil predominate. The soils in the area are naturally acidic and low in nutrient content. The natural forest ecosystems of the Bavarian Forest National Park vary with altitude: there are alluvial spruce forests in the valleys, mixed mountain forests on the hillsides and mountain spruce forests in the high areas. The dominant tree species include European beech (*Fagus sylvatica*), Norway spruce (*Picea abies*) and Fir (*Abies alba*). In the mixed mountain forests Sycamore maple (*Acer pseudoplatanus L*), Mountain ash (*Sorbus aucuparia L*) and Goat willow (*Salix caprea*) are also found. Due to heavy disturbance by bark beetles and wind storms in recent decades the forest structure in the park is very heterogeneous (Lehnert *et al.* 2013).

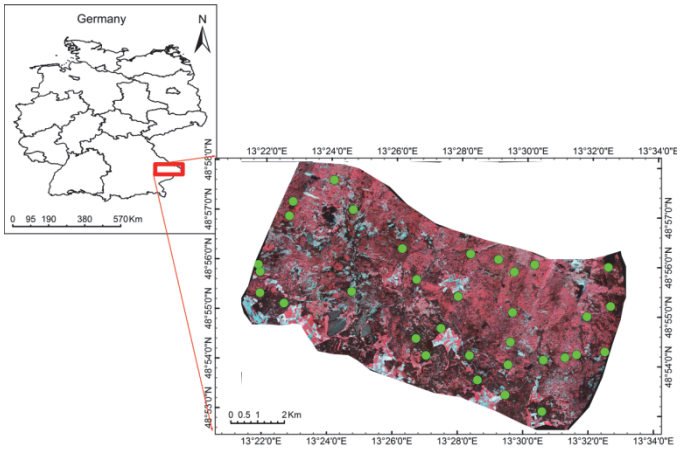

Figure 5.1: Map of the study site. The green dots show the distribution of the sample plots in the Bavarian Forest National Park on a false colour composite (R=967 nm, G = 2029 nm and B=2371 nm) of the HySpex images.

5.2.2 Analytical frame work

The procedure followed during calibration and validation of indices is illustrated in Figure 5.2. Using the measured datasets, for each VI, the highest correlation between SLA and combination of spectral bands was identified at leaf and canopy levels. At leaf level, we used spectral measurements of 137 foliar samples from six species collected across the study site and their corresponding SLA; at canopy level, we used SLA measurements from 33 sample plots and spectral datasets extracted from HySpex images of the study site. These measured datasets were used to calibrate each index in order to find the most informative sections of the electromagnetic spectrum and to search for the most accurate combination of bands for SLA retrieval. Validations of best band combinations of each VI at leaf and canopy levels were performed using the measured datasets and by applying cross-validation techniques. In addition, the robustness of the VIs for SLA retrieval was validated, using simulated leaf and canopy reflectance. For this purpose, we generated two simulated databases: one at leaf level with the PROSPECT model (Feret *et al.* 2008), and one at canopy level with the INFORM (Schlerf and Atzberger 2006) canopy radiative transfer model together with the PROSPECT leaf model.

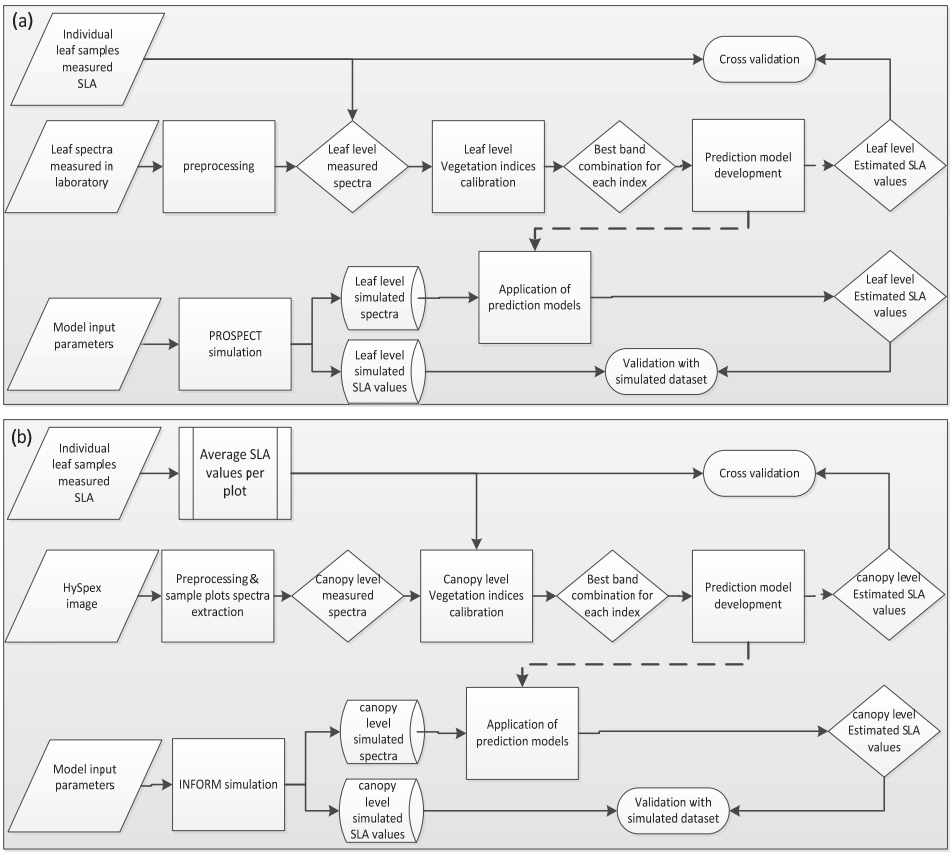

Figure 5.2: Analytical framework followed to calibrate and validate various narrow band vegetation indices for specific leaf area (SLA) estimation at leaf (a) and canopy (b) levels. The dashed lines indicate the predictive models developed from measured datasets that were applied to both measured and simulated datasets.

5.2.3 Ground data collection

A field campaign was conducted during summer 2013 to collect ground data. The study site was stratified into broadleaf, conifer and mixed forest stands. Given the nature of the forest heterogeneity and the time and cost constraints, we randomly selected 33 plots in total: 10 broadleaf, 9 conifer and 14 mixed. Each plot was square, with sides 30m long. Samples at leaf and canopy level were collected as described below.

a) Leaf level measurements

Leaf samples were collected from each tree species found in each plot (Table 5.1). As the leaf trait of interest (SLA) tends to vary (Asner and Martin 2008) as one moves downward from the top of the tree, all the samples were taken from mature sunlit leaves at the top of the canopy. A crossbow was used to shoot an arrow attached to a fishing line at a branch with sunlit leaves. Once

the fishing line had passed around the targeted branch, the fishing line was used to feed a rope over the branch and then the branch was pulled down gently until it broke off. The samples were then placed in a zip-locked plastic bag together with wet pulp paper and transported to the laboratory in a portable cooler with frozen icepacks. In the laboratory, the leaf samples were stored in a cold, dark room and processed within the day of collection.

Table 5.1: Distribution of collected leaf samples, by species.

Category	Species	No. of samples
Broadleaf trees	1. European beech	44
	2. Sycamore maple	4
	3. Mountain ash	3
	4. Goat willow	2
	Subtotal	**53**
Conifers	1. Norway spruce	63
	2. Fir	21
	Subtotal	**84**
Total No. of samples		**137**

1. Leaf biophysical and biochemical variables measurement

Table 5.2: Summary statistics of the variables measured in 137 leaf samples. The variables calculated were leaf mass per area (C_m) , which is the ratio of leaf dry mass to leaf area, specific leaf area (SLA) (i.e., $1/C_m$) and leaf water content (C_w) computed as the difference between leaf fresh mass and leaf dry mass divided by leaf area.

Basic statistics	C_m (g/cm^2)	C_w (g/cm^2)	SLA (cm^2/g)
Minimum value	0.0034	0.0063	73.48
Maximum value	0.0136	0.0156	294.09
Mean value	0.0079	0.0092	135.38
St. deviation	0.0021	0.0021	38.25

The fresh weight of each sample was determined (before the spectral measurements) by using a digital scale of high precision. Leaf area of broadleaf samples was measured using the LI-3000C portable leaf area meter (Li-Cor, Inc, Lincoln, NE, USA). In the case of the conifer needles, the surface of the sample needles was scanned using an HP double lamp desktop scanner at a resolution of 1200 dpi; the needle projections were computed from the grayscale images using ImageJ image processing software (which is freely available online). Norway spruce needles are cylindrical and therefore their total surface was first computed as a projected area multiplied by a universal conversion factor of 2.57 derived experimentally for Norway spruce needles (Waring 1983). Then, the total needle surface area was divided by two to acquire the hemispherical-surface projection of sampled spruce needles. Finally, the samples were oven-dried at 65 ^{0}C for 48 hours to obtain their dry biomass and water content. The summary statistics of all the variables measured are presented in Table 5.2.

2. Leaf Spectral measurements

Hemispherical reflectance and transmittance from 350–2500 nm with 1 nm spectral resolution were measured using a FieldSpec ®3 portable spectroradiometer equipped with an integrating sphere, manufactured by Analytical Spectral Devices, Inc. (ASD), USA. The spectral measurement for each sample was obtained by averaging the spectra on 10 randomly selected leaves in the case of broadleaf species and on 12–16 needles for conifers. Care was taken to avoid large primary and secondary veins during the spectral measurement. In order to minimize the effect of signal variance, two hundred scans were averaged in every spectral measurement to a single spectrum. A calibrated reference standard (with approximately 99% reflectance) was used to convert raw radiance to reflectance.

Whereas the spectral measurement of broadleaf material is straightforward, the spectral measurement of conifer needles is not. This is because the conifer needles are very small and do not cover the sample port of the integrating sphere, which has a port diameter of 15 mm for reflectance and 13.5 mm for transmittance. Therefore, the technique first developed by Daughtry *et al.* (1989) and later revised by (Mesarch *et al.* 1999) was applied to measure the spectral property of the conifer needles. A universal sample holder that could accommodate all lengths of conifer needles was designed, following Malenovsky *et al.* (2006). Needles were detached from each sample shoot, placed on the sample holder, and secured with scotch tape, leaving a space of approximately one needle's width between needles to avoid multiple reflectance from adjacent needles (Daughtry *et al.* 1989). The sample holder was carefully placed at the sample port of the integrating sphere, and reflectance and transmittance spectra were acquired following the port configuration procedures of the ASD integrating sphere.

A black painted paper mask with a 15 mm diameter circular aperture was precisely superimposed on the samples and photographs were taken using a 16.1 mega pixel Panasonic DCM-TZ35 camera. Then the gap fraction (GF) between illuminated needles was calculated, based on the illuminated area of the sample port, which was 9 mm diameter for both reflectance and transmittance. The illuminated areas of the samples were clipped by drawing a circle of 9 mm diameter at the centre of each picture. The proportion of pixels with gaps between needles was then determined using ImageJ software: this entailed ascertaining the total number of pixels and pixels with gaps in the 9 mm circular aperture area and then dividing the number of pixels with gaps by the total number. Then, the following equations (Eqs1 and 2) were adapted from Mesarch *et al.* (1999) for the ASD FieldSpec spectrometer, to compute the hemispherical reflectance and transmittance of the sampled needles.

$$Reflectance = \frac{\frac{\rho - Rd}{1 - Rd}.Rr}{1 - GF} \quad (5.1)$$

where ρ is measured sample reflectance, Rd is stray light (measured in reflectance mode), Rr is reference of sample reflectance and GF is the gap fraction of the sample.

Through visual inspection, spectral measurements in the ranges of 350–400 and 2351–2500 nm were found to be noisy and were removed from all spectral datasets. The Savitzky–Golay smoothing filter (Savitzky and Golay 1964) with a second order polynomial function and bandwidth of 15 nm was applied, to eliminate random noise within the reflectance spectral signatures.

b) Plot/Canopy level measurements

Table 5.3: Summary of the canopy structure variables measured in the 33 sample plots: leaf area index (LAI), stem density (SD), canopy closure (CC), crown diameter (CD), stand height (SH), and average leaf angle (ALA).

Parameter	LAI (m^2/m^2)	SD (n/ha)	CC (%)	CD (m)	SH (m)	ALA (deg)
Minimum	2.42	222	38	2.91	12.26	40
Maximum	6.18	1722	91	10.55	27.36	60
Mean	4.3	778.4	75.19	5.67	20.23	50
St. dev.	0.81	405.5	5.33	1.56	4.52	9.96

For all 33 sample plots, forest structure variables such as LAI, stem density (SD), canopy closure (CC), crown diameter (CD), stand height (SH), and average leaf angle (ALA) were measured. An overview of the canopy level variables measured is presented in Table 5.3. Average values per plot for each leaf parameter (i.e., SLA, C_m and C_w) were also computed, based on leaf samples collected from each plot. For the mixed plots, the average values for SLA, Cm and Cw were based on crown biomass proportion of each species in a given plot. The leaf structure parameter N, which is related to layers of cellular arrangements within the leaf, was retrieved by inverting the PROSPECT model using simulation at three wavelengths (see Ali *et al.* 2016b). During the field campaign, the spectral reflectance of understory vegetation and ecosystem elements on the forest floor (such as bark, litter, moss, and lichens) was also measured by using the ASD field spectroradiometer coupled to a high intensity contact probe.

5.2.4 Image acquisition and pre-processing

HySpex is a new airborne hyperspectral sensor developed by the Norwegian Norsk Elektro Optikk (NEO) company. It comprises two imaging spectrometers with spectral ranges of 400–1000 nm (sensor 1) and 1000–2500 nm (sensor 2) and up to 416 spectral channels with spatial resolution 1.6 m for sensor 1 and 3.4 m for sensor 2. It is supported by a precise navigation system for

georeferencing and correction of geometric errors. Both of its sensors operate in a push-broom scanning mode with an angular recording image width of 15°. Its field of view can be doubled to 30° using a field expander lens. It records radiance data in contiguous bands at a spectral resolution of 3.7 nm for 400–992 nm spectral range (sensor 1) and 6 nm for the 968–2498 spectral range (sensor 2).

The HySpex instrument was flown over the study site on board a Cessna 208B Grand Caravan at average altitude of 3006 m a.s.l on July 22, 2013 between 9:00 and 11:15 local time. The HySpex image data were supplied by the DLR team after atmospheric correction performed with the ATCOR4 model, orthorectified and georeferenced using standard aircraft in-flight information. As only the spectral bands in the shortwave infrared region (SWIR) were utilized in this study, only the images from sensor 2 of HySpex were mosaicked and resampled.

To prepare the HySpex data for further analysis, the image reflectance was resampled over a 9 × 9 pixel window, which most closely approximates the size of the sample plots (approximately 30 m× 30 m). Then the Savitzky–Golay filter was applied to correct for random and systematic noise. Finally, the average reflectance of the sample plots was extracted and used for further analysis. The noisy bands in the water absorption region (1345–1450nm and 1790–1980 nm) and bands from 2450–2498 nm were excluded. This left a total of 203 bands in the 33 average reflectance spectra (hereafter referred to as the measured spectral dataset at canopy level).

5.2.5 Calibration of narrow band indices

Many studies have confirmed that wavelengths in the visible and near infrared region (400–800nm) are highly sensitive to leaf pigments such as chlorophylls and carotenoids, while the SWIR region is the most sensitive region for retrieving parameters related to dry matter (Jacquemoud *et al.* 1996, Asner *et al.* 2011b, Romero *et al.* 2012). Therefore, the spectral region from 800 to 2500 nm was used to calibrate the indices used in this study.

Index types ranging from single band reflectance to more sophisticated narrow band indices (Table 5.4) were calibrated for both the leaf bidirectional hemispherical reflectance (BRF) data measured with the ASD spectroradiometer and the canopy BRF extracted from HySpex images. All possible wavelength (band) combinations between 800 nm and 2500 nm were examined for each index. The determination of the wavelength(s) for each index was based on coefficient of determination (R^2) values for the relationship between every band combination and SLA in the measured datasets.

Table 5.4: The vegetation indices tested in this study for SLA estimation at leaf and canopy level

Index	Formula	Full name	reference
DVI	$\rho\lambda_1 - \rho\lambda_2$	Difference	(Jordan 1969)
SR	$\rho\lambda_1 / \rho\lambda_2$	Simple ratio vegetation index	(Pearson *et al.* 1972)
NDVI	$(\rho\lambda_1 - \rho\lambda_2)/ (\rho\lambda_1 + \rho\lambda_2)$	Normalized difference vegetation index	(Rouse *et al.* 1974)
mND	$(\rho\lambda_1 - \rho\lambda_2)/ (\rho\lambda_1 + \rho\lambda_2 - 2* \rho\lambda_3)$	Modified normalized difference	(le Maire *et al.* 2008)
mSR	$(\rho\lambda_1 - \rho\lambda_3)/ (\rho\lambda_2 - \rho\lambda_3)$	Modified simple ratio	(le Maire *et al.* 2008)
mSR2	$\frac{\left(\frac{\rho\lambda_1}{\rho\lambda_2} - 1\right)}{\sqrt{\left(\frac{\rho\lambda_1}{\rho\lambda_2} + 1\right)}}$	Modified simple ratio2	(Chen and Cihlar 1996)
TVI	$\sqrt{\left(\frac{\rho\lambda_1 - \rho\lambda_2}{\rho\lambda_1 + \rho\lambda_2} + 0.5\right)}$	Transformed Vegetation Index	(Deering *et al.* 1975)
PVI*	$\frac{1}{\sqrt{a^2+1}}(\rho\lambda_1 - \mathrm{a}\rho\lambda_2 - b)$ where a is a weighing factor	Perpendicular Vegetation Index	(Baret and Guyot 1991)
WDVI*	$\rho\lambda_1 - \mathrm{a}\rho\lambda_2$ Where a is the slope of the soil line	Weighted Difference Vegetation Index	(Clevers 1991)
SAVI*	$\left(\frac{\rho\lambda_1 - \rho\lambda_2}{\rho\lambda_1 + \rho\lambda_2 + \mathrm{L}}\right)(1+L)$ where L is a correction factor (1, 0.5 and 0.25 for low, intermediate and high vegetation respectively)	Soil-Adjusted Vegetation Index	(Huete 1988)
TSAVI*	$\left(\frac{\mathrm{s}((\rho\lambda_1 - \mathrm{s})(\rho\lambda_2 - \mathrm{a}))}{\mathrm{a}*\rho\lambda_1 + \rho\lambda_2 - \mathrm{a}*\mathrm{s} + \mathrm{x}*(1+\mathrm{s}*\mathrm{s})}\right)$ *a* = slope of the soil line, *b* = soil line intercept, and *x* = factor to minimize soil noise	Transformed Soil-Adjusted Vegetation Index	(Baret *et al.* 1989)
SAVI2*	$\frac{\rho\lambda_1}{\rho\lambda_2 + \mathrm{b}/\mathrm{a}}$	Soil-Adjusted Vegetation Index2	(Major *et al.* 1990)
EVI	$2.5\left[\frac{\rho\lambda_1 - \rho\lambda_2}{\rho\lambda_1 + 6(\rho\lambda_2) - 7.5(\rho\lambda_3) + 1}\right]$	Enhanced Vegetation Index	(Liu and Huete 1995), (Huete *et al.* 1997)
WDRVI*	$\left(\frac{\mathrm{a}*\rho\lambda_1 - \rho\lambda_2}{\mathrm{a}*\rho\lambda_1 + \rho\lambda_2}\right)$	Wide Dynamic Range Vegetation Index	(Gitelson 2004)
OSAVI*	$(1+0.16)\,x\,\frac{\rho\lambda_1 - \rho\lambda_2}{\rho\lambda_1 + \rho\lambda_2 + 0.16}$	Optimized Soil-Adjusted Vegetation Index	(Rondeaux *et al.* 1996)
NLI	$(\rho\lambda_1{}^2 - \rho\lambda_2)/ (\rho\lambda_1{}^2 + \rho\lambda_2)$	Non-linear vegetation index	(Goel and Qin 1994)
RDVI	$\frac{(\rho\lambda_1 - \rho\lambda_2)}{\sqrt{(\rho\lambda_1 + \rho\lambda_2)}}$	Re-normalized difference vegetation index	(Roujean and Breon 1995)

MNLI	$\frac{(\rho\lambda_1{}^2 - \rho\lambda_2)(1+L)}{(\rho\lambda_1{}^2 + \rho\lambda_2 + L)}$	Modified non-linear vegetation index	(Gong *et al.* 2003)
TCARI	$3\left[(\rho\lambda_1 - \rho\lambda_2) - 0.2(\rho\lambda_1 - \rho\lambda_3)\left(\frac{\rho\lambda_1}{\rho\lambda_2}\right)\right]$	Transformed Chlorophyll Absorption in Reflectance Index	(Haboudane *et al.* 2002)
MCARI	$(\rho\lambda_1 - \rho\lambda_2) - 0.2(\rho\lambda_1 - \rho\lambda_3)\left(\frac{\rho\lambda_1}{\rho\lambda_2}\right)$	Modified Chlorophyll Absorption in Reflectance Index	(Daughtry *et al.* 2000)
VARI	$\frac{\rho\lambda_1 - \rho\lambda_2}{\rho\lambda_1 + \rho\lambda_2 - \rho\lambda_3}$	Visible Atmospherically Resistant Index	(Gitelson *et al.* 2002)
MAVI	$\frac{\rho\lambda_1 - \rho\lambda_2}{\rho\lambda_1 + \rho\lambda_2 + \rho\lambda_3}$	Moisture-adjusted vegetation index	(Zhu *et al.* 2014)
GDVI	$\frac{(\rho\lambda_1{}^2 - \rho\lambda_2{}^2)}{(\rho\lambda_1{}^2 + \rho\lambda_2{}^2)}$	Generalized difference Vegetation index	(Wu 2014)
L_SAVI	$\frac{1.5 * (1 + L + CAI) * (\rho\lambda_1 - \rho\lambda_2)}{\rho\lambda_1 + \rho\lambda_2 + 0.5 + \mathrm{L} * \mathrm{CAI}}$ $CAI = 100 * \frac{(\rho_{2000} + \rho_{2200})}{2} - \rho_{2200}$	Litter-soil-adjusted vegetation index	(Ren and Zhou 2014)
MTCI	$\frac{\rho\lambda_1 - \rho\lambda_2}{\rho\lambda_2 - \rho\lambda_3}$	MERIS Terrestrial Chlorophyll Index	(Dash and Curran 2004)
CI	$\frac{\rho\lambda_1}{\rho\lambda_2} - 1$	Chlorophyll Index	(Gitelson *et al.* 2005)
NMDI	$\frac{\rho\lambda_1 - (\rho\lambda_2 - \rho\lambda_3)}{\rho\lambda_1 + (\rho\lambda_2 - \rho\lambda_3)}$	A Normalized Multi-Band Drought Index	(Wang and Qu 2007)
DRRI	$\frac{\rho\lambda_1 - \rho\lambda_2}{\rho\lambda_3}$	Difference of Reflectance Ratio Index	Gitelson *et al*. (2004)
MCARI/ OSAVI	$\frac{(\rho\lambda_1 - \rho\lambda_2) - 0.2(\rho\lambda_1 - \rho\lambda_3)\left(\frac{\rho\lambda_1}{\rho\lambda_2}\right)}{(1+0.16)\, x\, \frac{\rho\lambda_1 - \rho\lambda_2}{\rho\lambda_1 + \rho\lambda_2 + 0.16}}$		(Haboudane *et al.* 2008)
TCARI/ OSAVI	$\frac{3\left[(\rho\lambda_1 - \rho\lambda_2) - 0.2(\rho\lambda_1 - \rho\lambda_3)\left(\frac{\rho\lambda_1}{\rho\lambda_2}\right)\right]}{(1+0.16)\, x\, \frac{\rho\lambda_1 - \rho\lambda_2}{\rho\lambda_1 + \rho\lambda_2 + 0.16}}$		(Haboudane *et al.* 2002)
GVMI	$\frac{(\rho\lambda_1 + 0.1) - (\rho\lambda_2 + 0.02)}{(\rho\lambda_1 + 0.1) + (\rho\lambda_2 + 0.02)}$	Global vegetation moisture index	(Ceccato *et al.* 2002)
mSR3	$\frac{\rho\lambda_1 - \rho\lambda_2}{\rho\lambda_1 - \rho\lambda_3}$	Modified Simple Ratio Index	(Datt 1999)
NDLI	$\frac{\left(\log(\frac{1}{\rho\lambda_1}) - \log(\frac{1}{\rho\lambda_2})\right)}{\left(\log\left(\frac{1}{\rho\lambda_1}\right) + \log(\frac{1}{\rho\lambda_2})\right)}$	Normalized difference lignin index	(Serrano *et al.* 2002)
CAI	$0.5(\rho\lambda_1 - \rho\lambda_2) - \rho\lambda_3$	Cellulose absorption index	(Nagler *et al.* 2000)
LCAI	$2\rho\lambda_1 - (\rho\lambda_2 + \rho\lambda_3)$	Ligno-Cellulose absorption index	(Daughtry *et al.* 2005)
SLAVI	$\frac{\rho\lambda_1}{\rho\lambda_2 + \rho\lambda_3}$	Specific leaf area vegetation index	(Lymburner *et al.* 2000)

* indices tested only at canopy level due to their soil/background components

At the canopy level, for the indices that contain soil parameter components, the soil line parameters were calculated from spectral measurement of understory vegetation and ecosystem elements on the forest floor such as bark, litter, moss and lichens, and bare soil, using the ASD field spectroradiometer coupled to a high intensity contact probe. It was assumed that the soil line concept, originally defined for the red-NIR feature space, could be transferred to other spectral domains (Darvishzadeh *et al.* 2008a). Hence the soil line parameters were computed for all possible band combinations between 800 nm and 2500 nm.

5.2.6 Simulated dataset

i) Leaf level simulation

The most popular RTM for estimating leaf parameters is the PROSPECT leaf optical properties model. It simulates leaf optical properties (i.e. reflectance and transmittance) parameterized by the following inputs: chlorophyll content (C_{ab}) in µg/cm^2, leaf dry mass per unit area (C_m) in mg/cm^2, leaf water mass per unit area (C_w) in mg/cm^2, and effective number of leaf layers (leaf structure-N) (Jacquemoud and Baret 1990).

In this study, the PROSPECT model was used to simulate 5000 leaf reflectance spectra by randomly selecting leaf input parameters based on the multivariate normal distributions and covariance matrix produced from the ground data (Table 5.2). Leaf chlorophyll content was fixed at an average value of 40µg/g, and the leaf structure parameter N was retrieved by inverting the PROSPECT model using simulation at three wavelengths (Ali *et al.* 2016b). For every combination of model input parameters, SLA (cm^2/mg) was computed as 1/C_m.

ii) Canopy level simulation

To simulate the canopy spectral dataset, we used the Invertible Forest Reflectance model "INFORM" (Schlerf and Atzberger 2006), which is a hybrid RTM that combines the forest light interaction model and SAIL canopy RTMs with the PROSPECT (Jacquemoud and Baret 1990) leaf RTM.

The INFORM model was used to simulate the canopy reflectance spectra by randomly selecting input parameters (C_m, C_w, N, LAI_s, SD, SH, CD and ALA) by means of a multivariate normal distribution function based on the mean and covariance matrix of their ground values (Table 5. 2 and Table 5.3). Leaf chlorophyll content was fixed at an average value of 40µg/g. A sensitivity study by (Ali *et al*. 2016a) previously reported insignificant effect of solar zenith and azimuth angles on INFORM simulated canopy reflectance. Therefore, other leaf, canopy, and external input parameters (Table 5.5) were fixed at average values based on the ground data, HySpex sensor specification, and previous studies (Schlerf and Atzberger 2006, Ali *et al.* 2016b).

Table 5.5: Constant input parameters used during INFORM simulation and based on field observation, HySpex hyperspectral sensor configuration, and previous studies.

Input variable	Symbol	Unit	Value	Source
Chlorophyll content	C_{ab}	µg/cm^2	40	Ali *et al.* 2016
Sun zenith angle	θ_s	degree	32	HySpex data
Observation zenith angle	θ_0	degree	0	HySpex data
Azimuth angle	Ψ	degree	153	HySpex data
Fraction of diffused radiation	Sky1	fraction	0.1	Schlerf and Atzberger 2006

5.2.7 Validation

All vegetation indices studied were evaluated using two sets of measured and simulated data: one of leaf-level data, the other of canopy-level data. The prediction performance of indices was evaluated using R^2 and root mean square error (RMSE %). Validation of the results was done in two steps. First the measured dataset was used in a leave-one-out cross-validation procedure in which the calibration set of n-1 samples is used to fit the predictive model and then evaluated using the sample that has been left out. Second, simulated datasets generated by PROSPECT at leaf level and INFORM at canopy level were used to assess the applicability and robustness of the indices to other datasets. The more accurate index is the one with higher R^2 and lower RMSE values.

5.3 Results

5.3.1 Leaf level SLA indices

The determination of the best wavelength(s) for each index at leaf and canopy levels was done by testing all possible combinations of wavelength for an index type, at wavelengths increasing incrementally by 5 nm. In order to show the absolute maximum, the extent of the local maximum area and local high R^2 zones, a 2-D graphical representation (matrix) of R^2 against two wavelengths ($\rho\lambda1$ and $\rho\lambda2$) was constructed. Examples of these 2D graphs for one of the best performing indices (i.e., OSAVI) are presented in Figure 5.3. A number of band combinations that correlate significantly with SLA are common to both the PROSPECT simulated and measured datasets.

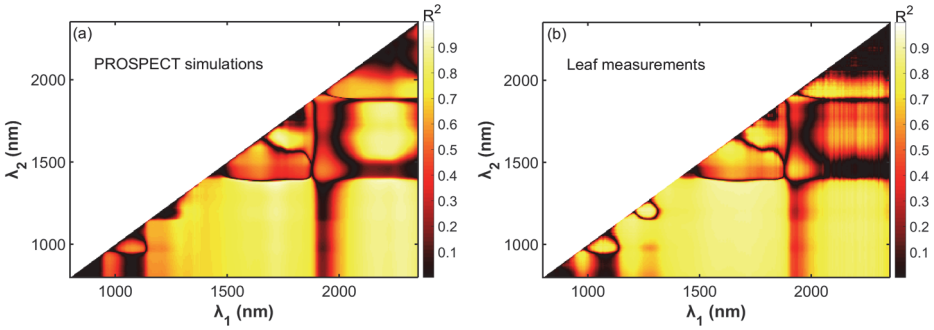

Figure 5.3: Matrices representing R^2 of specific leaf area (SLA) with different band combinations for OSAVI. Calculations are based on simulation (a) and measurement (b) datasets at leaf level.

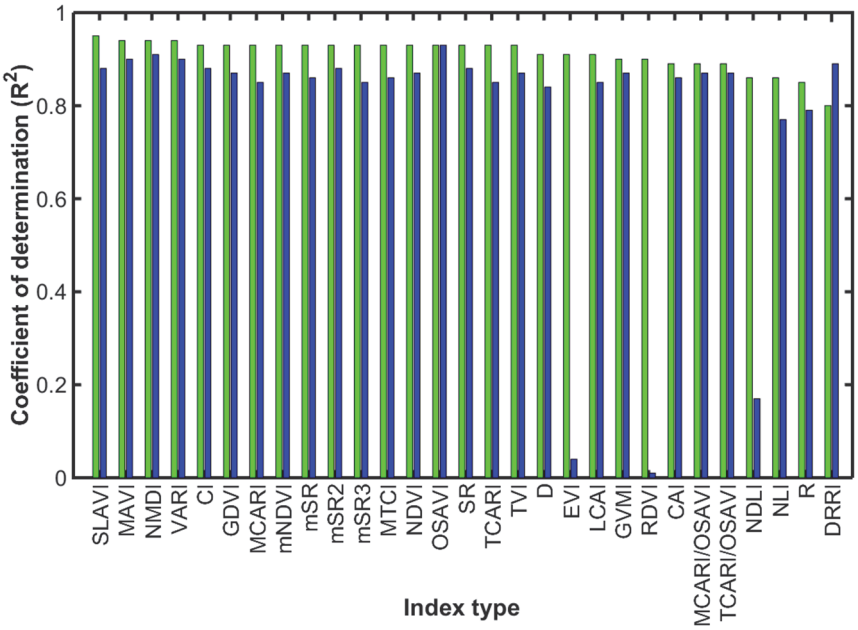

Figure 5.4: Leaf level bar graph of R^2 for SLA predictions obtained using the various indices and validation datasets. The light green bars show the indices' validation on the measured dataset; dark blue bars indicate the performance of the indices on the PROSPECT simulated dataset. The index types are arranged in descending order of their R^2 value.

Table 5.6: Leaf level SLA indices cross-validated on the measured dataset (n=137) and the PROSPECT simulated dataset (n=5000). Indices with high accuracy are show in bold

Index type	λ_1 (nm)	λ_2 (nm)	λ_3 (nm)	RMSE (%)	
				Measured dataset	PROSPECT simulation
CAI	1115	2320	1715	3.92	3.92
CI	1375	1615		3.30	3.30
D	1915	2145		3.60	3.60
DRRI	1660	1730	1345	5.46	5.46
EVI	1205	1250	1925	3.61	3.63
GDVI	1375	1615		3.20	8.23
GVMI	1315	1715		3.76	4.75
LCAI	1555	1885	1365	3.52	24.49
MAVI	1350	1675	805	2.98	19.01
MCARI	1375	1600	1930	3.34	8.61
MCARI/OSAVI				4.19	3.11
mNDVI	1600	1935	1375	3.13	15.88
mSR	1575	1920	1380	3.18	5.06
mSR2	1375	1615		3.26	10.35
mSR3	1510	1530	1335	3.19	7.65
MTCI	1575	1920	1380	3.18	9.89
NDLI	1205	1280		4.31	8.96
NDVI	1375	1615		3.21	8.27
NLI	2100	2195		4.45	11.77
NMDI	**920**	**1675**	**1335**	**2.88**	**8.96**
OSAVI	**1370**	**1615**		**3.24**	**3.12**
R	2145			4.67	8.64
RDVI	1205	1250		3.83	6.03
SLAVI	**1295**	**1680**	**1035**	**2.84**	**4.76**
SR	1375	1615		3.30	3.15
TCARI	1375	1600	1930	3.34	5.72
TCARI/OSAVI				4.19	27.41
TVI	1375	1615		3.19	8.32
VARI	**1345**	**1675**	**1850**	**3.07**	8.23

As can be seen from Figure 5.4 and Table 5.6, many of the index types tested in this study performed very well when predicting SLA. Even reflectance at a single band (2145 nm) provided high R^2 (0.85) and relatively low RMSE (4.67%). However, when the indices calibrated using the measured dataset were applied to the PROSPECT simulated dataset for SLA estimation, higher RMSEs were observed in several cases. When using both the measured and simulated datasets at leaf level, the indices that seemed to be best for SLA prediction were the multi-band indices NMDI and VARI and the two-band OSAVI index.

One of the best indices ($OSAVI_{1370,\ 1615}$) was calibrated with the measured dataset against the logarithmic value of SLA (Figure 5.5a). The index computed for both the simulated and measured datasets showed a strong association

with variation in SLA content. It is apparent from Figure 5b that the selected band combinations of $OSAVI_{1370,\ 1615}$ accurately estimated SLA at leaf level. More specifically, lower values of SLA were more precisely estimated than higher SLA values. The errors mainly originated from discrepancies in SLA values ≥ 100 cm^2/g.

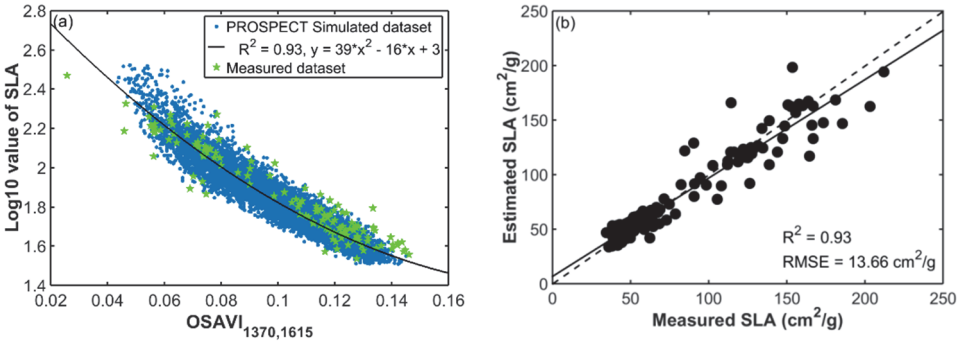

Figure 5.5: The relationship between SLA and the best narrow band index at leaf level (a). Measured and estimated SLA using the best narrow band index at leaf level (b). Solid lines show the best fit regressions; the dashed line shows the 1:1 relationship of predicted and measured values of SLA.

5.3.2 Canopy level SLA indices

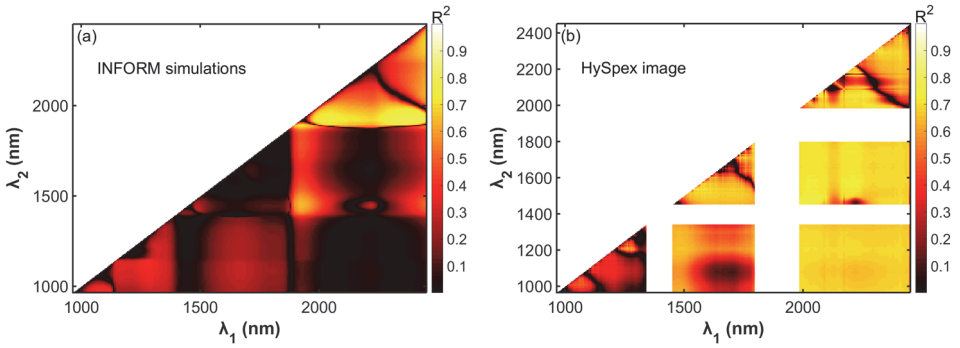

Figure 5.6: Canopy level matrices representing R^2 of specific leaf area (SLA) with different band combinations for OSAVI. Calculations were conducted on both simulation (a) and measurement (b) datasets.

Unlike at leaf level, at canopy level there were not many wavelengths strongly correlated with SLA. For the INFORM simulated spectra, only a few narrow band combination regions correlate significantly with to SLA (Figure 5.6a), and these are mostly concentrated near the water absorption region (1790–1980 nm). The matrix obtained from HySpex image at canopy level (Figure 5.6b) was similar to the leaf level R^2 matrices computed from PROSPECT simulation and leaf level measurements. The canopy level matrices obtained from the INFORM simulation and HySpex image are most similar in the top half of the 2D plots against the validation dataset. The maximum R2 and minimum RMSE

combination for both the INFORM simulated and the measured datasets was obtained with the OSAVI1537, 1543 index. Wavelengths in the two spectral regions of water absorbance (1345–1450 nm and 1790–1980 nm) were excluded, since they are not suitable for measurements under natural atmospheric conditions. Like the leaf level indices, the RMSE value of many canopy level indices was higher for the simulated dataset than for the measured dataset.

It can be seen from Figure 5.8a that the relationship between the INFORM-based $OSAVI_{1535,\ 1543}$ index and SLA is more scattered than the $OSAVI_{1535,\ 1543}$ index as calculated using the measured dataset, resulting in a higher RMSE. Nonetheless, in the measured dataset, most of the observations are close to the one-to-one relationship line. In other words, the $OSAVI_{1535,\ 1543}$ index yields satisfactory results when applied to aircraft-level hyperspectral imagery (Figure 5.8b).

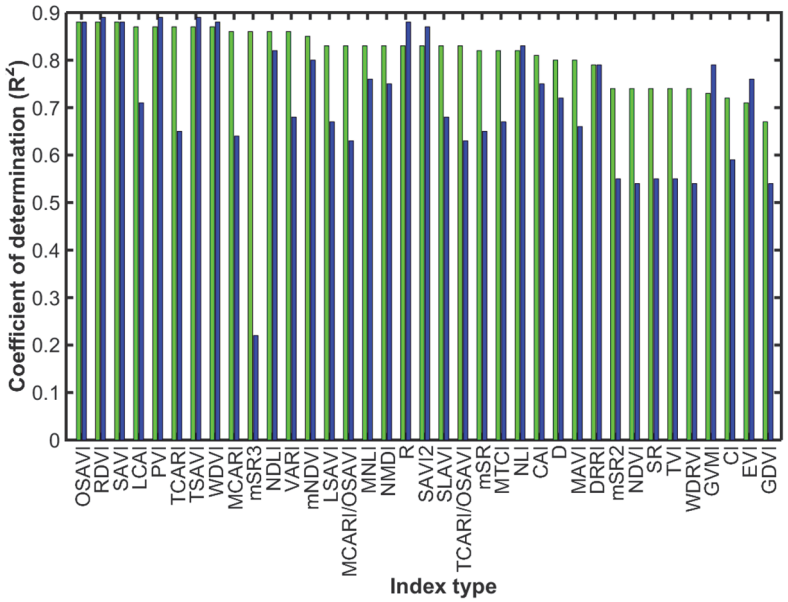

Figure 5.7: Canopy level bar graph of R^2 between SLA predictions made using the various indices and validation datasets. Light green bars show the indices' validation on the measured dataset; dark blue bars indicate the performance of the indices on the INFORM simulated dataset. The index types are arranged in descending order of their R^2 value.

The accuracy of the best canopy level index ($NDVI_{2263,\ 1489}$), which was proposed for leaf mass area (inverse of SLA) retrieval by le Maire *et al*. (2008) performed poorly (R2 = 0.09 and RMSE = 8.53 % for the measured dataset). Many of the indices calibrated and used to predict SLA in our study provided higher R2 (Figure 5.7) and lower RMSE values (Table 5.7) validated

Table 5.7: SLA indices at canopy level cross-validated on the measured dataset (n=33) and INFORM simulations (n = 10,000). Indices with higher accuracy are shown in bold

Index type	**λ1 (nm)**	**λ2 (nm)**	**λ3 (nm)**	**RMSE (%)**	
				Measured dataset	**INFORM simulation**
CAI	1573	1987	1987	4.04	5.45
CI	1214	1226		4.93	27.43
D	1567	1573		4.27	5.40
DRRI	1537	1543	1076	4.29	5.31
EVI	1537	1543	2449	5.13	6.16
GDVI	1214	1226		5.36	29.46
GVMI	2017	2299		4.89	4.70
LSAVI	2059	2281		3.98	5.30
LCAI	1573	1603	1537	3.51	6.93
MAVI	2245	2251	1741	4.25	6.54
MCARI	1537	1555	1657	3.53	8.80
MCARI/OSAVI				3.79	10.06
mNDVI	2053	2149	2083	3.59	3.17
MNLI	1208	2005		3.90	4.35
mSR	1537	1555	1657	3.80	11.71
mSR2	1214	1226		4.61	29.42
mSR3	1202	2233	1292	3.63	45.37
MTCI	1537	1657	1555	3.80	11.00
NDLI	1537	1543		3.53	4.14
NDVI	1214	1226		4.62	29.48
NLI	1609	2047		4.09	3.89
NMDI	1987	2047	2083	3.76	6.24
OSAVI	**1537**	**1543**		**3.34**	**3.12**
PVI	1537	1543		3.36	3.16
R	968			4.03	3.18
RDVI	**1537**	**1543**		**3.31**	**3.13**
SAVI	**1537**	**1543**		**3.28**	**3.18**
SAVI2	968	2089		4.01	3.20
SLAVI	1585	1657	1537	3.75	13.32
SR	1214	1226		4.62	29.48
TCARI	1537	1555	1657	3.41	8.45
TCARI/OSAVI				3.79	10.06
TSAVI	**1537**	**1543**		**3.38**	**3.16**
TVI	1214	1226		4.62	29.07
VARI	1489	1987	1519	3.53	17.20
WDRVI	1214	1226		4.62	29.48
WDVI	**1537**	**1543**		**3.38**	**3.16**

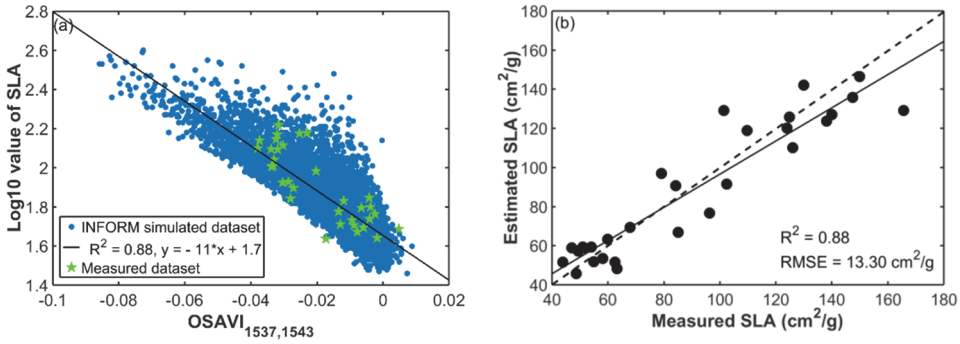

Figure 5.8: Relationship between the canopy level measured and INFORM simulated datasets for the $OSAVI_{1537,\ 1543}$ canopy level index calibrated on the measured dataset (a). Validation result of the SLA retrieved by using the index (b). Solid lines show the best fit regressions; the dashed line shows the 1:1 relationship.

5.4 Discussion

The results of this study demonstrate the applicability of key vegetation indices for accurate retrieval of SLA at both leaf and canopy levels. At both levels, wavelengths determined using the measured dataset estimated SLA efficiently.

Higher RMSE values were observed when regression equations developed using the measured dataset were applied to synthetic data. This phenomenon may be partially explained by (i) errors in the RTMs due to simplification of model input parameters and (ii) the size of the measured datasets, which was insufficient to represent the simulated datasets.

Many of the indices performed well at both leaf and canopy levels for SLA retrieval. In the measured dataset, R^2 values ranged from 0.80 to 0.94 at the leaf level (Figure 5.4) and were higher than the canopy level R^2 values of 0.67 to 0.88 (Figure 5.7). However, no significant difference in RMSE was observed for the most accurate vegetation index (OSAVI) when validated at both leaf and canopy levels using the measured dataset. The sunlit leaf SLA was obtained with an RMSE value of 13.66 cm^2/g at leaf level and 13.30 cm^2/g at canopy level. Up-scaling from leaf to canopy level was expected to decrease R^2 and increase RMSE due to effects of canopy structure, sensor noise, and other factors. However, this was not the case in our study. A possible reason may be that in the measured datasets the SLA variability at the leaf level was much greater than the variability at the forest canopy level (Tables 5.3 and 5.4). This is in agreement with earlier findings by (le Maire *et al.* 2008), who reported larger errors for LMA retrieval at leaf level than at canopy level when using vegetation indices. Similarly, the RMSEs observed in our study agree with the finding of Asner and Martin (2008) that RMSE value was 15.1 cm^2/g when SLA was retrieved from leaf spectra compared with 12.92 cm^2/g when

SLA was retrieved from simulated canopy reflectance for a humid tropical forest.

The performance of the indices calibrated using the measured datasets tended to weaken when they were applied to simulated datasets, especially at canopy level. Lower R^2 and higher RMSE combinations were observed for many vegetation indices when their predictive capacity was evaluated using a simulated dataset (Figure 5.7 and Table 5.7). A possible explanation for this is that the measurements at canopy level may not be extensive enough to fully represent the simulated dataset range (Figure 5.8a). Another reason could be an instrument bias between the HySpex spectra and INFORM simulated spectra such that the wavelengths found to be very sensitive to SLA during the indices' calibration on the measured dataset might not be among the best bands in the simulated dataset for SLA retrieval. In addition, the Gaussian noise added to the simulated datasets may have contributed to the discrepancy between simulated and measured datasets. A study by Feret *et al.* (2011) showed that more than 0.5% of noise added to simulated data degrades the correlation between LMA and normalized indices.

It is interesting to note that the PROSPECT simulated dataset and the leaf measurement dataset (Figure 5.3) were more similar than the canopy level INFORM simulation and canopy measurement datasets (Figure 5.6). This indicates that the PROSPECT model simulates leaf level spectra efficiently. The canopy level band combination difference between the INFORM simulation and corresponding measured dataset can be explained in part by model input uncertainties. Even though a more targeted simulated dataset had been created by using a priori knowledge of the measured canopy to limit the range of parameter variation, the simulated spectra from the INFORM model did not accurately match the absolute value of the reflectance of the forest canopy. Another source of uncertainty is that INFORM does not consider slope, yet slope alters canopy reflectance. It has been suggested that other RTMs such as Gastellu-Etchegorry *et al.* (2004) and Huemmrich (2001), which incorporate the effects of clumping, shadows and topographic variation as model inputs, may perform better than INFORM when simulating canopy spectra.

The method employed in this study, which uses measured spectral datasets for calibration and both simulated and measured datasets for validation, has an advantage of selecting a more generic index that can be applied for a wide variety of species and situations. At canopy level many of the indices tested in this study had excellent performance for the measured dataset but when applied to simulated dataset their accuracy dropped significantly. This observation may support the hypothesis that vegetation indices are site-specific and cannot be generalized. Nevertheless, our approach enabled us to

minimize the non-generic nature of indices by comparing indices' accuracy on a wide range of datasets (measured and simulated spectra).

In contrast to previous studies of LMA (which is the inverse of SLA) at leaf level, we found a higher correlation of SLA with leaf reflectance. Romero *et al.* (2012), who retrieved LMA from LOPEX93 using the normalized index (R_{2305} – R_{1495})/ (R_{2305} + R_{1495}), obtained R^2 = 0.63. Jacquemoud *et al.* (1996) and Riaño *et al.* (2005) reported R^2 = 0.84 for LMA estimation using dry leaf sample spectra ranging between 1100–2500 nm. Asner *et al.* (2011b) attained R^2 = 0.85 for leaf samples collected from humid tropical forests.

In our study, both at leaf and canopy level most SLA-sensitive bands occurred in the SWIR region of the electromagnetic spectrum (Tables 5.6 and 5.7): 1200–2500 nm. This reconfirms that SWIR wavelengths are the most sensitive to leaf dry matter variations, which is in accordance with the results from Jacquemoud *et al.* (1996), le Maire *et al.* (2008), Feret *et al.* (2011), Romero *et al.* (2012). By comparison with other spectral regions, the SWIR region efficiently avoids the influence of other parameters such as leaf pigments.

The wavelengths of the indices with the highest R^2 in this study were in agreement with the findings of Thenkabail *et al.* (2004), who recommended 22 bands for multi-spectral remote sensing of vegetation. In many of the indices examined in our study, bands cantered at 1537 nm and 1543 nm were the most common bands found to be sensitive to sunlit leaf SLA at canopy level. These bands are found in the SWIR (1300–1900 nm) which is very sensitive to changes (or differences) in biochemical properties such as lignin, starch, and cellulose.

However, the wavelengths we propose for SLA retrieval on the basis of our results do not fully agree with the findings of le Maire *et al.* (2008) and Feret *et al.* (2011). The most likely cause for the differences between the wavelengths we propose and those proposed in these previous studies is the type of data used in the calibration. In our case, indices were calibrated using measured leaves and HySpex spectra and direct field observations, while in the aforementioned studies, synthetic datasets were utilized. Nevertheless, applying the simple ratio and normalized indices using the wavelengths 1370 nm and1720 nm proposed by Feret *et al.* (2011) at leaf level still yielded a high accuracy (R^2 = 0.93 and RMSE = 3.29) which is similar to our wavelengths (1370 nm, 1615 nm) found suitable in OSAVI $_{1370, 1615}$ (R^2 = 0.93 and RMSE = 3.24). But the canopy level normalized index ($NDVI_{2260, 1490}$) proposed by le Maire *et al.* (2008) performed poorly when used with our measured dataset. Neither were the wavelengths of 2305 nm and 1495 nm that Romero *et al.* (2012) proposed for the normalized index among the best performing wavelengths in our study. We conclude that although there is no universally

accepted band combination for directly retrieving SLA from hyperspectral data when using vegetation indices, the wavelength region between 1300 and 1800 nm is particularly sensitive, as most of the bands selected using the wide variety of VIs were located in this region. Further study is required to validate whether a modification of VIs using land cover stratification may further increase accuracy, similar to the results obtained by (Yali *et al.* 2012).

5.5 Conclusions

The main goal of this study was to examine a number of vegetation indices in order to identify the most generic and widely applicable indices for SLA retrieval at leaf and canopy level. The best possible wavelength combinations for each index were determined by testing every possible combination in the NIR and SWIR (800–2500 nm) range of the electromagnetic spectrum by using measured spectral information. Two independent experimental datasets (i.e., synthetic and measured) were used at both leaf and canopy level for validating the calibrated indices. Our criterion for the best index was the one with the lowest RMSE and highest R^2 on both the simulated and measured datasets.

This study has found that generally a simple ratio or normalized index of two narrow bands (wavelengths) such as SR and OSAVI can be used for accurate retrieval of SLA from remotely sensed data. The best indices for SLA are $OSAVI_{1370,\ 1615}$ at leaf level and $OSAVI_{1537,\ 1543}$ at canopy level. They showed high accuracy, with an RMSE of 13.66 cm^2/ and $R^2 = 0.93$ at leaf level, and an RMSE of 13.30 cm^2/ and $R^2 = 0.88$ at canopy level.

Although only narrow band indices were examined, our findings suggest that even bands with a wider wavelength range (broad bands) can be utilized. There are continuous large areas of high R^2 values in the 2D R^2 matrices, which indicate that indices calibrated on coarser bands (bands covering a larger area of the spectrum than the bands used here) can accurately estimate SLA. This implies that remote sensing data from coarse spectral resolution sensors may suffice for SLA estimation.

The current findings add to a growing body of literature on fast and efficient retrieval of plant functional traits from remotely sensed data. However, the scope of this study was limited in terms of species composition to a mountain European forest biome. Further studies need to be carried out, using other vegetation types to validate the proposed indices.

Chapter 6

Retrieval of specific leaf area from Landsat-8 surface reflectance data using statistical and physical models [5]

[5] This chapter is based on:
Ali, A. M., R. Darvishzadeh, and A. K. Skidmore. Retrieval of specific leaf area from Landsat-8 surface reflectance data using statistical and physical models. (In Review after revision, Internation Journal of Remote Sensing)

Abstract

One of the key traits in the assessment of ecosystem functions is specific leaf area (SLA). The main aim of this study was to examine the potential of new generation satellite images such as Landsat-8 imagery for the retrieval of SLA at regional and global scales. Therefore, both statistical and radiative transfer model (RTM) inversion approaches for estimating SLA from the new Landsat-8 product were evaluated. Ground truth data were collected for 33 sample plots during a field campaign in summer 2013 in the Bavarian Forest National Park, Germany, while Landsat-8 image data concurrent with the time of field campaign were acquired. Estimates of SLA were examined using different Landsat-8 spectral bands, vegetation indices calculated from these bands, and the inversion of a canopy RTM. The RTM inversion was performed utilizing continuous wavelet analysis (CWA) and a look-up table (LUT) approach. The results were validated using R^2 and the RMSE between the estimated and measured SLA.

In general, SLA was estimated accurately by both statistical and RTM inversion approaches. The relationships between measured and estimated SLA using the enhanced vegetation index (EVI) was strong (R^2 = 0.77 and RMSE = 4.44%). Furthermore, the predictive model developed from combination of the wavelet features at 654.5 nm (scale 9) and 2200.5 nm (scale 2) correlated strongly with SLA (R^2 = 0.79 and RMSE = 7.52%). The inversion of LUT using a spectral subset consisting of bands 5, 6 and 7 of Landsat-8 (R^2 = 0.73 and RMSE = 5.33%) yielded a higher accuracy and precision than any other spectral subset. The findings of this research provide insights into the potential of the new generation of multispectral medium resolution satellite imagery such as Landsat-8 and Sentinel-2 for accurate retrieval and mapping of SLA using either statistical or RTM inversion methods.

Keywords: Landsat-8, SLA, radiative transfer model and vegetation index

6.1 Introduction

Specific leaf area (SLA) is an important indicator of plant physiological processes related to ecosystem dynamics. SLA is among the ten essential biodiversity variables proposed by Skidmore *et al.* (2015) to capture biodiversity change from space. SLA links plant carbon and water cycles, and provides information on spatial variation of photosynthetic capacity and leaf nitrogen content (Pierce *et al*. 1994). Knowledge on SLA values is important in ecosystem function assessments and for understanding plants' growth strategies, especially with respect to climate change. Accurate and regularly repeated SLA estimates at global, regional and local scales is needed when monitoring ecosystem, as well as for appropriate planning and monitoring of conservation strategies. Therefore, pinpointing affordable, timely and readily-available remote sensing data together with robust processing techniques are indispensable for fast and cost-effective SLA estimation.

The application of hyperspectral remote sensing for estimating forest variables such as SLA has not been demonstrated using satellite based remote sensing. As such, many studies have focused on high spatial and high spectral airborne imagery for the quantification of vegetation parameters in forests (e.g., Zhang *et al*. 2015; Song *et al*. 2013; Knyazikhin *et al*. 2013; Misurec *et al*. 2012; Clevers and Kooistra 2012; Wang *et al*. 2016). However, the high cost and large data volume associated with airborne data impede the use of airborne imagery for estimating vegetation variables at large spatial scales. The utilization of a new generation of satellites, which allows acquisitions of imagery at medium resolution (i.e. spectral and spatial properties), could be an alternative for accurate retrieval of forest variables including SLA at different spatial scales.

Landsat is widely available medium resolution satellite sensors providing high temporal imagery for regional, continental, and global vegetation studies. The recently launched Landsat-8 Operational Land Imager (OLI) is one of the medium spectral and spatial resolutions imagery that has global coverage and complemented by the recently launched Sentinel-2. Comparison of Landsat-8 OLI and Landsat-7 ETM+ data among different vegetation types confirmed that differences in the sensor characteristics of OLI and ETM+ have little impact on Landsat data continuity (She *et al*. 2015; Li, *et al*. 2014). Several studies have been undertaken to estimate vegetation parameters (including biomass and phenology) from Landsat-8 reflectance data by applying either statistical or physical remote sensing methods (e.g., Dube and Mutanga 2015; Ji *et al*. 2012; Robles, *et al*. 2015; Wang *et al*. 2015). A review of the literature revealed that Landsat-8 imagery has not beem to estimate SLA. Moreover, previous studies have focused mainly on the retrieval of SLA from hyperspectral (airborne) imagery. These include SLA retrieval using statistical

techniques such as narrow-band vegetation indices (Ali *et al*. 2016d) and radiative transfer model inversion through continuous wavelet analysis (Ali *et al*. 2016c). However, estimating vegetation parameters using either statistical or RTM inversion approaches has advantages and disadvantages (Darvishzadeh *et al*. 2011), and the available resources as well as expertise are often the main drivers of model selection.

In this study our aim was to explore the potential of Landsat-8 data for estimating SLA in a mountain forest. The study benefits from a comprehensive validation dataset acquired during the summer of 2013. Our specific objectives were to (1) create empirical models to relate Landsat-8 reflectance and its derived spectral indices or features to SLA measured on the ground, (2) evaluate Landsat-8 reflectance data through inversion of radiative transform model (RTM) by using continuous wavelet analysis and look-up table approaches to estimate SLA and (3) evaluate whether upscaling through Landsat-8 data would affect the SLA retrieval accuracy and models that others have investigated using airborne hyperspectral data.

6.2 Methods

6.2.1 Test site and field data

The test site for this study was the mixed mountain forest of the Bavarian Forest National Park. The park is located in south-eastern Germany along the border with the Czech Republic (49^0 3’ 19” N, 13^0 12’ 9” E). Elevation of the test site varies from 600 m to 1,473 m above sea level. The climate of the region is temperate, with high annual precipitation (1,200 mm to 1,800 mm) and low average annual temperature (3 to 6 ^{0}C). Heavy snow cover is characteristic of the area in winter. Brown soils are the predominant soil type at lower altitude (below 900 m a.s.l) whereas at high altitude (above 900 m a.s.l) brown soils and brown podzolic soil predominate. The soils in the area are naturally acidic and low in nutrient content (Heurich *et al.* 2010).

The natural forest ecosystems of the Bavarian Forest National Park vary with altitude: there are alluvial spruce forests in the valleys, mixed mountain forests on the hillsides and mountain spruce forests in the high areas. The dominant tree species include European beech (*Fagus sylvatica*), Norway spruce (*Picea abies*) and fir (*Abies alba*). In the mixed mountain forests sycamore maple (*Acer pseudoplatanus L*), mountain ash (*Sorbus aucuparia L*) and goat willow (*Salix caprea*) are also found (Heurich and Neufanger 2005). Due to heavy disturbance by bark beetle and wind storms in recent decades the forest structure in the park is very heterogeneous (Lehnert *et al.* 2013).

A field campaign was conducted during summer 2013 to collect ground truth data. The test site was stratified into broadleaf, conifer, and mixed forest stands. Given the heterogeneity of the forest and the time and cost constraints, we randomly selected 33 plots from the three main forest class strata, resulting in 10 samples in broadleaf stands, nine in conifer stands, and 14 in mixed stands. Each plot was square, with sides 30m long. In all 33 sample plots, forest structural variables such as LAI, stem density (SD), canopy closure (CC), crown diameter (CD), and stand height (SH) were measured. The LAI of each plot was measured using an LAI-2000 canopy analyser and was also computed from the hemispherical photographs taken in each plot. The SD was recorded as the number of trees per hectare based on the number of trees in each plot. CC was estimated by averaging five observations in a plot using a crown densiometer. CD and SH were calculated from the mean crown diameter and mean height of five randomly selected trees in each plot. The CD of each tree was determined by averaging two perpendicular projected distances on the ground. The total height of each tree was estimated by using a Nikon Forestry 550 laser rangefinder.

In each plot, leaf samples were collected from mature sunlit leaves at the top of the canopy of three to five trees, using a crossbow, and their characteristics were measured. Leaf area of broadleaf samples was measured using the LI-3000C portable leaf area meter (Li-Cor, Inc, Lincoln, NE, USA). The surface of sample conifer needles was scanned using an HP double lamp desktop scanner at a resolution of 1200 dpi; the needle projections were computed from the grayscale images using ImageJ image processing software (which is freely available online). For details on the leaf samples' spectral and physical variable measurements, see (Ali *et al.* 2016c). The collected leaf samples were transported to the laboratory for further analysis. All samples were oven dried at 65 ^{0}C for 48 hours and then SLA, leaf mass per leaf area (C_m), and leaf water content (C_w) were computed based on fresh and oven-dried leaf mass and corresponding leaf areas. The leaf structural parameter (N) was retrieved by inverting the PROSPECT model, using simulation at three wavelengths (see Ali *et al*. 2016c). For mixed plots, the average values for LDMC, SLA, C_m, C_w, and leaf structural parameter (N) were based on crown biomass proportion of each species in a given plot. The variables measured in the field are summarized in Table 1.

During the field campaign, the spectral reflectance of understory vegetation and ecosystem elements on the forest floor such as bark, litter, mosses and lichens was also measured by using the ASD field spectroradiometer coupled to a high intensity contact probe.

Table 6.1: Summary statistics of the measured and calculated leaf parameters and canopy structural variables of the 33 sample plots in the Bavarian Forest National Park. The measured leaf parameters were leaf mass per leaf area (C_m), leaf water content (C_w), and specific leaf area (SLA). Leaf structural parameter (N) was estimated using the PROSPECT model. The canopy structural variables measured were leaf area index (LAI), stem density (SD), canopy closure (CC), crown diameter (CD), stand height (SH), and average leaf angle (ALA).

Parameter	Minimum	Maximum	Mean	St. dev.
C_m (g/cm^2)	0.0061	0.0292	0.0147	0.0059
C_w (g/cm^2)	0.0071	0.0309	0.0178	0.0071
N	1.36	1.93	1.58	0.16
LDMC (g/g)	0.3999	0.5075	0.4534	0.0254
SLA (cm^2/g)	43.45	165.64	89.38	37.72
LAI (m^2/m^2)	2.42	6.18	4.3	0.81
SD (n/ha)	222	1722	778.4	405.5
CC (%)	38	91	75.19	5.33
CD (m)	2.91	10.55	5.67	1.56
SH (m)	12.26	27.36	20.23	4.52
ALA (deg)	40	60	50	9.96

6.2.2 Landsat-8 Imagery and pre-processing

The Landsat-8 observatory operates in a near-circular, near-polar, sun-synchronous orbit with a 705 km altitude at the equator. The observatory has a 16-day ground track repeat cycle with an equatorial crossing at 10:11 a.m. (±15 min) mean local time during the descending node. In this orbit, the Landsat-8 observatory follows a sequence of fixed ground tracks (also known as paths) defined by the second Worldwide Reference System (WRS-2). WRS-2 is a path/row coordinate system used to catalo all the science image data acquired from the Landsat 4 – 8 satellites. The Landsat-8 launch and initial orbit adjustments placed the observatory in an orbit to ensure an eight-day offset between Landsat 7 and Landsat-8 coverage of each WRS-2 path. The OLI sensor collects image data for nine shortwave spectral bands over a 190 km swath with a 30 m spatial resolution for all bands except the 15 m panchromatic band (Table 2). OLI has an uncertainty of less than 5% in terms of absolute, at-aperture spectral radiance and an uncertainty of less than 3% in terms of top-of-atmosphere spectral reflectance for each of the spectral bands (http://landsat.usgs.gov/l8handbook.php).

In order to assess the predictive accuracy of SLA from Landsat imagery, the Landsat-8 OLI image of the study area (path 192 and row 26) acquired on 08 August 2013 was utilized. The Landsat surface reflectance image was downloaded from the Global Visualization Viewer (GloVis, http://glovis.usgs.gov/) developed by the Earth Resource Observation and Science centre (EROS) of the USGS. It contains the surface reflectance data, which has been corrected for systematic radiometric and geometric errors. We ensured the overall geometric accuracy with ground control points and a digital

elevation model. Vegetation indices products were also directly downloaded and utilized for SLA estimation. The spatial resolution of Landsat-8 OLI image approximates the size of the sample plots (approximately 30 × 30 m). The reflectance values of the sample plots were extracted from the Landsat-8 scene and used for further analysis (Hereafter it is referred to as the measured reflectance).

6.2.3 SLA retrieval approaches

SLA was retrieved using two approaches: (1) developing prediction models using Landsat-8 surface reflectance including individual spectral bands and derived vegetation indices, and (2) inverting INFORM radiative transfer model through continuous wavelet analysis (CWA) and a look-up table (LUT).

a) Prediction models on Landsat bands (VIs)

Table 6.2: Bands and vegetation indices of Landsat-8 imagery examined for SLA retrieval in this study

Band/VI	Description	Wavelength (nm)/ Formulation
B1	Coastal aerosol	435-451 (443)
B2	Blue	452-512 (482)
B3	Green	533–590 (561.5)
B4	Red	636–673 (654.5)
B5	Near Infrared (NIR)	851-879 (865)
B6	Shortwave infrared (SWIR) 1	1566-1651 (1608.5)
B7	Shortwave infrared (SWIR) 2	2107-2294 (2200.5)
EVI	Enhanced vegetation index	$2.5\left[\frac{\mathrm{NIR}-\mathrm{Red}}{\mathrm{NIR}+6(\mathrm{Red})-7.5(\mathrm{blue})+1}\right]$
MSAVI	Modified soil-adjusted vegetation index	$\left(\frac{(\mathrm{NIR}-\mathrm{Red})(1+L)}{\mathrm{NIR}+\mathrm{Red}+\mathrm{L}}\right)$
NBR	Normalized Burn Ratio	(NIR- SWIR2)/ (NIR+ SWIR2)
NBR2	Normalized Burn Ratio2	
NDMI	Normalized difference moisture index	(NIR- SWIR1)/ (NIR+ SWIR1)
NDVI	Normalized difference vegetation index	(NIR- Red)/ (NIR+ Red)
SAVI	Soil-adjusted vegetation index	$\left(\frac{\mathrm{NIR}-\mathrm{Red}}{\mathrm{NIR}+\mathrm{Red}+\mathrm{L}}\right)(1+L)$

To investigate the prediction of SLA we utilized seven spectral bands of Landsat-8 located in the visible and NIR regions as well as eight vegetation index (VIs) products available directly from the USGS archive in order to predict SLA (table 2) . The performances of each spectral band and VI were evaluated using the coefficient of determination (R^2) and root mean square error (RMSE) values for the relationship between measured and estimated SLA through cross-validation. For this, a wide variety of regression models, such as linear, stepwise linear, multiple linear, and quadratic regressions, were

examined. Predictive models with good fit (i.e. a high R^2 and low RMSE combination during cross-validation) were then used to retrieve SLA.

b) Radiative transfer model inversion

i) Model parameterization and forest reflectance simulation

To simulate the spectral property of the test site we used the Invertible Forest Reflectance model "INFORM" (Atzberger 2000, Schlerf and Atzberger 2006), which is a hybrid RTM that combines the Forest Light Interaction Model (Rosema *et al.* 1992) and SAIL (Verhoef 1984) canopy RTMs with the PROSPECT (Jacquemoud and Baret 1990) leaf RTM. In INFORM, LAI is represented by the leaf area indices of single trees (LAI_s). Hence, the ground truth values for LAI_s were computed from LAI and CC.

$$\boldsymbol{LAI_s = \frac{LAI}{CC}} \quad (6.1)$$

where LAI_s is single tree leaf area index and CC is canopy closure. The model uses several canopy structural and biochemical variables and sensor configuration input parameters to generate top of forest canopy reflectance. The input parameters include leaf biochemical variables such as leaf chlorophyll content (C_{ab}), leaf dry matter content per area (C_m), leaf water content per leaf area (C_w), canopy structural parameters such as LAI_s, stand height (SH), stem density (SD), crown diameter (CD), and average leaf angle (ALA) and, geometrical parameters such as sensor zenith, azimuth, and view angles. SLA was computed as the inverse of C_m. See Ali *et al.* (2016c) for further details.

The INFORM model was run in forward mode to generate a simulated dataset for calibration of the continuous wavelet analysis. To achieve this, the input parameters (C_{ab}, C_m, C_w, N, LAI_s, SD, SH, CD, and ALA) were randomly varied 10,000 times, using a multivariate normal distribution function from the ground truth data. To avoid extreme values and unrealistic combinations, the randomly assigned value of each variable was limited to ±5% of the observed maximum and minimum values for that variable in the ground truth data. A random Gaussian noise value of 0.3% (Cheng *et al.* 2014b) was added to each simulated spectrum to account for model uncertainties as well as reduce collinearity between the spectrum and input variables. The simulation was performed for the seven spectral bands corresponding to the band settings of the Landsat-8 surface reflectance data.

A sensitivity study had previously reported an insignificant effect of solar zenith and azimuth angles on INFORM-simulated canopy reflectance (Ali *et al.* 2016a). Therefore, other canopy, and external input parameters such as understory LAI, sun zenith angle, and observation azimuth and zenith angles were fixed, using average values based on the field data and Landsat-8 OLI specifications. The fraction of diffused radiation was fixed based on previous study by Schlerf and Atzberger (2006). As bare soil occurred extremely rarely,

the field spectra of understory vegetation and the forest floor elements were averaged and used as a fixed background reflectance during the simulation. For the details on model input parameters used during INFORM parametrization see Ali *et al.* (2016c)

ii) Continuous wavelet analysis and inversion

The simulated dataset produced using the INFORM model was used for the CWA analysis.The wavelet transform converts each one-dimensional reflectance spectrum into a two-dimensional wavelet power scalogram by using a mother wavelet function. The continuous wavelet analysis involves linearly transforming a remote sensing signal into a set of coefficients by using the mother wavelet function f(λ) (where λ=1, 2, 3, …k, represent the number of wavebands). The one-dimension depth of canopy spectra resulting from different amounts of SLA can be quantified by using the wavelet coefficient (scalogram). From the mother wavelets available in MATLAB 8.4 software, the second derivative of the Gaussian function (Mexican hat) was selected, since it best correlated SLA with wavelet features. In this study, scales for CWA were powers of 2 (2^1, 2^2, 2^3, . . .,2^{10}) and were described as power numbers (scale 1, scale 2, scale 3, . . ., scale 10).

Next, wavelet features that significantly correlated with SLA were determined based on R^2 value between each wavelet feature and SLA. Wavelet features with a high correlation to SLA in the simulated dataset were then used to develop a prediction model for retrieving SLA from wavelet-transformed Landsat-8 surface reflectance data.

iii) RTM inversion using a look-up table approach

RTM inversion using look-up table (LUT) is one of the most popular and efficient methods in remote sensing (Darvishzadeh *et al.* 2008b, Dasgupta *et al.* 2009, Darvishzadeh *et al.* 2011). It involves repeated simulation of spectra, using different combinations of model input parameters constrained by reasonable ranges. An LUT of 150,000 forest canopy reflectance spectra was generated by running INFORM in forward mode for Landsat-8 bands and using the prior information on the ranges of input parameters presented in Table 1. The inversion was performed by searching for the simulated spectra in the LUT which best fit the measured spectra (Landsat-8 surface reflectance) and retrieving their corresponding SLA. The search for the best fit between simulated and measured spectra was determined by calculating and finding the lowest root mean square error of an unconstrained non-linear multivariate function (Coleman and Li 1996) as shown in Eq. 2. The search for the best fit was performed using different spectral band subsets.

$$M_N = \sqrt{\frac{\sum_\lambda [(\rho mes\text{-}\rho sim)^2]}{n}} \qquad (6.2)$$

where n is the number of wavelengths, ρmes and ρsim are measured and simulated values of reflectance respectively, and λ is wavelength.

6.2.4 Validation

The prediction performance of the three methods utilized in this study (i.e., statistical, RTM inversion using CWA and RTM inversion by LUT) was evaluated using R^2 and RMSE % between estimated and measured values of SLA. The results of the statistical methods were validated by using the measured dataset in a leave-one-out cross-validation procedure in which the calibration set of n-1 samples was used to fit the predictive model and then evaluated using the sample that had been left out. The predictive performances of the RTM inversions were assessed using SLA values collected in 33 sample plots in the field. R^2 and RMSE (%) were calculated as:

$$R^2 = 1 - \frac{\sum(y_i - y_i')^2}{\sum(y_i - \bar{y}_i)^2} \quad (6.3)$$

$$RMSE\ (\%) = \sqrt{\frac{\sum(y_i - y_i')^2}{n}} / \bar{y}_i * 100 \quad (6.4)$$

Where y_i and y_i' are the actual and predicted values for sample i, and $\bar{y}$ is the arithmetic mean of the measured data and n is the number of samples in the measured data.

6.3 Results and discussion

6.3.1 SLA retrieval using Landsat-8 vegetation indices and bands

The validation of prediction models developed with individual spectral bands as well as vegetation indices of Landsat-8 surface reflectance data revealed significant correlations with SLA (Table 6.3). Among the selected seven bands of Landsat-8, the NIR (band 5) and the SWIR (bands 6 and 7) showed stronger correlation to SLA than bands from the visible region. This is in line with previous studies that reported wavelengths in the visible region (400–800nm) being highly sensitive to leaf pigments such as chlorophylls and carotenoids, while the NIR and SWIR regions are the most sensitive regions for retrieving parameters related to dry matter, such as SLA (Jacquemoud *et al.* 1996, Asner *et al.* 2011b, Romero *et al.* 2012).

Table 6.3: Accuracy of the estimates of SLA in the Bavarian forest national park obtained using Landsat-8 bands and vegetation indices. The accuracy is assessed on the basis of the logarithmic value of SLA. The band and index with high cross- validation R^2 and low RMSE are shown in bold.

Band/VI	R^2	RMSE (%)	Linear regression equation
B1	0.33	8.41	Y = 0.0039x + 1.2434
B2	0.16	8.59	Y= 0.0041x + 1.0657
B3	0.59	6.46	Y = 0.0037x + 0.5648
B4	0.26	8.30	Y = 0.0035x + 0.9996
B5	**0.74**	**4.81**	**Y = 0.000258x + 1.1897**
B6	0.73	4.95	Y = 0.000477x + 1.3448
B7	0.71	5.26	Y = 0.0011x + 1.3325
EVI	**0.77**	**4.44**	**Y = 0.00014328x + 1.2009**
MSAVI	0.76	4.45	Y = 0.0001335x + 1.2894
NBR	0.12	8.29	Y = 0.0001851x + 3.1924
NBR2	0.60	6.02	Y = 0.0008962x + 1.6702
NDMI	0.32	7.45	Y = -0.0002417x + 2.8991
NDVI	0.73	4.68	Y = 0.0004291x + 1.6476
SAVI	0.76	4.48	Y = 0.0007401x + 1.0922

Many of the vegetation indices examined performed well in retrieving SLA from Landsat-8 imagery. In general, combinations of higher R^2 and lower RMSE values were observed at longer wavelengths and VIs, as illustrated in Figure 6.1. The highest R^2 (0.77) and the lowest RMSE (4.44%) combination was recorded for the enhanced vegetation index (EVI). This reveals the potential of EVI for fast and accurate retrieval of SLA from Landsat-8 imagery. EVI has also previously been shown to be a suitable index for other vegetation parameters (e.g., Fraga *et al*. 2014; Lin 2012).

The precision of the EVI-retrieved SLA against ground-measured SLA is illustrated in Figure 6.2. Generally the errors seem randomly distributed throughout the observation but there is a tendency to under estimate higher values of SLA. One possible explanation for this might be that compared with forest leaves with low SLA values, forest leaves with higher SLA are more transparent and therefore influenced by background material. The other cause might be model saturation. The model might become insensitive to high SLA and contribute to the under estimation of higher values.

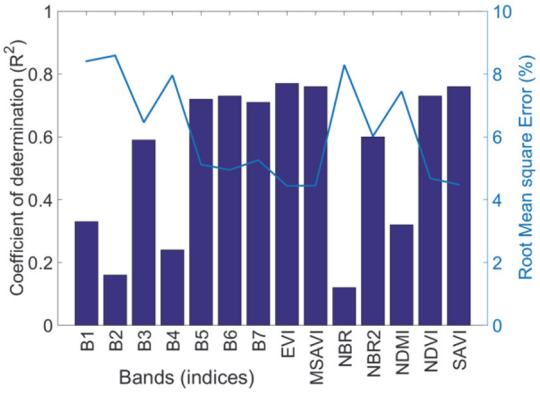

Figure 6.1: Cross-validated R^2 and RMSE combinations of the Landsat-8 bands and vegetation indices.

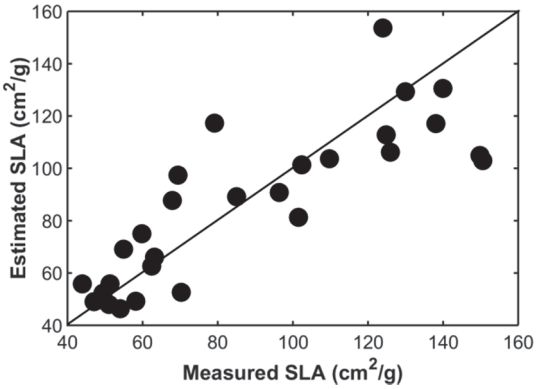

Figure 6.2: Measured SLA and SLA estimated using the Landsat-8 EVI vegetation index. The solid line shows the 1:1 relationship between predicted and measured values of SLA.

6.3.2 Inversion of radiative transfer models through wavelet analysis

In this approach SLA was retrieved from Landsat-8 data by applying predictive models developed from INFORM-simulated spectra. Figure 3a illustrates the correlation between the seven bands of Landsat-8 and SLA variation at different scales of wavelet transformation. The wavelengths centred at 561.5nm, 654.5nm and 2200.5nm showed higher correlation to SLA at scales of 10, 9 and 2 respectively (Figure 6.3b) and were selected to develop predictive models. The highest correlation is observed for the wavelet feature 561.5 nm, scale 10. The significant correlation observed between wavelet features and SLA has important implications for developing rigorous inversion algorithms using satellite imageries for fast and accurate estimation of SLA through RTM and wavelet analysis approach.

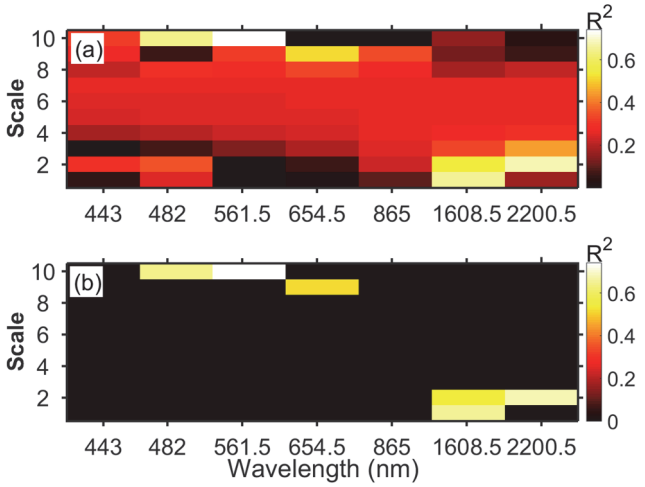

Figure 6.3: Correlation scalogram derived from continuous wavelet analysis of the simulated spectra for the identification of wavelet features which correlate significantly with specific leaf area (SLA). Brightness represents the coefficient of determination (R^2) relating wavelet power to SLA. A coloured feature region in scalogram (b) indicates the wavelet features with the top 1% highest R^2 values.

We developed and evaluated predictive models for SLA estimation using the three selected wavelet features and their possible combinations as predictor variable. The validation results for the simulated and measured Landsat-8 datasets are presented in Table 6.4. The linear prediction model developed using a combination of wavelet features 654.5 nm, scale 9 and 2200.5 nm, scale 2 showed the highest R^2 (0.79) with the Landsat-8 data (validation). The estimated coefficients of this predictive model are reported in Table 6.5. Higher R^2 and lower RMSE combinations were largely perceived in the simulated data. RMSEs were higher in the measured (Landsat-8) dataset than in the simulated dataset. This may be partly explained by mismatch between the simulated and measured datasets, which could have caused the values of the wavelet features obtained from Landsat-8 wavelet analysis to exhibit systematic shifts to higher or lower values, resulting in systematic overestimation of SLA (Figure 6.4). A study by Ali *et al.* (2016d) using hyperspectral airborne data reported a similar problem and suggested that the probable causes of this shift were atmospheric effects and sensor noise on the measured spectra. These factors may cause variation in local absorption peaks on the measured spectra, and lead to higher or lower wavelet power values during the transformation.

Table 6.4: The performance of the highly correlated wavelet features identified using INFORM-simulated spectra and validated using wavelet features from Landsat-8 data.

No.	Wavelet feature	Calibration using simulated data		Validation	
		R^2	RMSE (%)	R^2	RMSE (%)
A	561.5 nm, scale 10	0.78	3.66	0.65	5.97
B	654.5 nm, scale 9	0.52	5.43	0.69	11.73
C	2200.5 nm, scale 2	0.71	4.21	0.78	13.25
D	Combination of A & B	0.88	2.67	0.71	9.80
E	Combination of A & c	0.79	3.64	0.61	6.94
F	**Combination of B & C**	**0.78**	**3.68**	**0.79**	**7.52**
G	Combination of A, B & C	0.84	3.17	0.70	27.44

Table 6.5: Estimated coefficients of the linear regression model developed on simulated Landsat-8 spectra (by INFORM) using wavelet features 654.5 nm, scale 9 and 2200.5 nm, scale 2 as predictor variables of SLA logarithmic value.

Coefficients	Estimate	SE	tStat	pValue
Intercept	1.42	0.00616	230.49	0
654.5 nm, scale 9	6.44	0.14664	43.92	0
2200.5 nm, scale 2	4.45	0.09352	47.62	0
654.5 nm, scale 9* 2200.5 nm, scale 2	-32.79	1.88823	-17.36	0

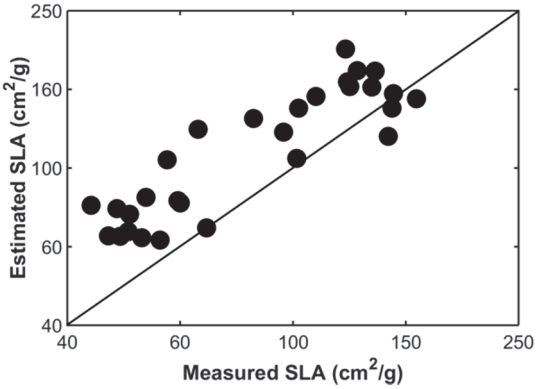

Figure 6.4: Measured and estimated SLA using a combination of the two wavelet features (654.5 nm, scale 9 and 2200.5 nm, scale 2) as predictor variables. The solid line shows the 1:1 relationship between predicted and measured values of SLA.

6.3.3 Inversion of radiative transfer model by LUT approach

Inversion of the INFORM model via a LUT, and all the Landsat-8 spectral bands yielded a high R^2 (0.84) value for SLA. However, the scatter plot of measured and estimated SLA values does not follow a one-to-one relationship line (Figure 6.5a), and the RMSE was relatively high (8.02%). This may be due to poor correlation of the VIS region bands with SLA. The latter was further investigated by performing the inversion using a spectral subset. The spectral subset was chosen from the bands that earlier (section 6.3.2) showed good

performance in the empirical method (i.e., bands 5, 6, and 7). Consequently, when inversion was performed using these bands, the relationship between measured and estimated SLA become stronger and demonstrated a lower RMSE (5.33%). This spectral subset (bands from the NIR and SWIR regions) yielded a more precise result than any other spectral subset (not shown). The estimated and measured SLA values using this subset appeared to follow a one-to-one relationship in the scatter plot (Figure 6.5b). One of the main reasons could be that there was low error (mismatch) between the simulated and measured reflectance in those spectral bands. Our results confirm those of a study by Darvishzadeh *et al*. (2008b); those authors recommended inverting RTM by LUT based on a spectral subset that has a low average absolute error between simulated and measured spectral reflectance.

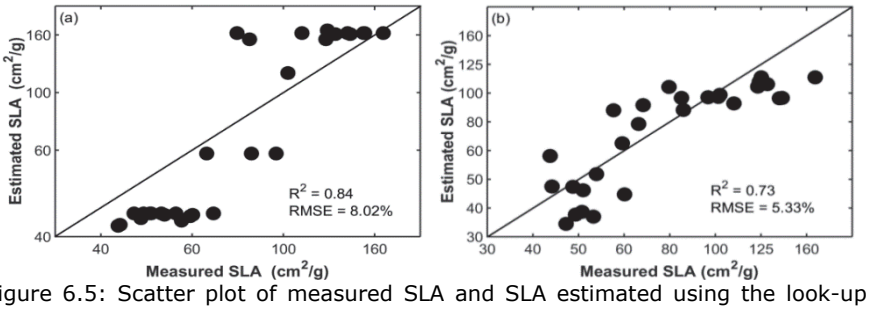

Figure 6.5: Scatter plot of measured SLA and SLA estimated using the look-up table (LUT) approach. Validation results from inversion (a) using all seven bands listed in Table 2, and validation results from inversion using bands 5, 6 and 7 (b). The solid line shows the 1:1 relationship between the predicted and measured values of SLA.

In general, validation of the two approaches (i.e., statistical and RTM inversion) showed similar accuracies for SLA retrieval. During validation, slightly higher R^2 (0.79-0.88) was recorded in the RTM inversion than in the statistical approach (maximum R^2 = 0.77). But the lowest RMSE (4.44%) was obtained in the statistical approach when using the vegetation index EVI. Our findings are in agreement with those of Lymburner *et al.* (2000), who tested several existing vegetation indices in order to estimate forest SLA from Landsat TM imagery and found a strong correlation ($R^2 \geq 0.74$) between average canopy SLA and vegetation indices of Landsat TM data such as the Soil and Atmosphere Resistant Vegetation Index (SARVI), the Normalized Difference Vegetation Index (NDVI), and the Ratio Vegetation Index (RVI). However, it is worth noting that using vegetation indices is highly site- and sensor-specific. A strong correlation between leaf mass per area and reflectance in the 750 nm to 2500 nm wavelength range has also been reported for tropical rainforest leaf samples (Asner and Martin 2008; Asner *et al.* 2011b). However, in our study, the accuracy of both statistical and RTM-based SLA retrieval from Landsat-8 data was lower than the accuracy of SLA retrieved from hyperspectral data; Ali *et al.* (2016d) reported higher accuracy (R^2 = 0.88 and RMSE =3.34 %) when retrieving SLA using OSAVI (Optimized Soil-Adjusted Vegetation Index) from

HySpex imagery. Inversion of RTM through continuous wavelet analysis on HySpex was also higher (R^2 = 0.85 and RMSE = 4.90 %) (Ali *et al.* 2016c) than in this study (R^2 =0.79 and RMSE = 7.52%). Nevertheless, the results of this study revealed the potential of multispectral satellites, in particular of the new generation of satellites, such as Landsat-8 and Sentinel-2, for retrieving SLA particularly in the NIR and SWIR regions.

6.4 Conclusions

The main goal of the current study was to evaluate the potential of Landst-8 imagery to retrieve SLA by using either statistical (empirical) or physical (RTM) approaches. In the retrieval process, both statistical and RTM approaches showed good performance. However, systematic errors were observed in the inversion of RTM through continuous wavelet analysis. Typically, the influence of upscaling to coarser remote sensing data (satellite image) on retrieval accuracy was minimal. The evidence from this study suggests that one can apply simple statistical methods such as the enhanced vegetation index for fast and reasonable mapping of SLA at local scales from spaceborne satellite imagery. However, since the vegetation index tends to be site- and sensor-specific, a more robust and vigorous approach when temporal mapping of SLA at regional and global scales is required could be RTM inversion. The study has gone some way toward enhancing our understanding of quantifying plant functional traits from remotely sensed data with coarse spectral resolution. Further research is required to assess the applicability of other vegetation index types and explore the potential of new high and medium resolution spaceborne satellite data for accurate retrieval of SLA.

Chapter 7

Synthesis: Remote sensing of forest leaf functional traits: leaf dry matter content and specific leaf area

7.1 Introduction

Accurate and up-to-date information on functional traits is critical in monitoring biodiversity. Quantifying functional traits in natural communities is pivotal to understand the spatial and temporal distribution of biodiversity, ecosystem services and plant community productivity (Cadotte *et al*. 2009, Lavorel *et al*. 2011). Since human survival relies on economic benefits and services provided by ecosystems, it is evident that ecosystem functions are a top conservation priority (Millennium Ecosystem Assessment. 2005). Scientists believe that better conservation and restoration decisions can be made by measuring and understanding functional traits (Cadotte *et al*. 2011). However, measurement of traits has traditionally been mostly limited to field observation. Due to the labour-intensive and time-consuming nature of direct field trait measurements, a general ecological understanding of trait variation across relevant spatial and temporal scales is lacking (Messier *et al*. 2010). Remotely sensed data can play a critical role in acquiring such data over broad spatial scales non-destructively and repeatedly, since it has been recognized as a reliable and practical means of characterizing various vegetation parameters (Darvishzadeh *et al*. 2009, Wang *et al*. 2010, Tong and He 2013). Hyperspectral remote sensing (often called imaging spectroscopy) has the advantage of providing more detailed and continuous spectral information, which can potentially be used for measuring plant traits. In the last three decades many studies have shown the role of remote sensing, particularly hyperspectral imagery, in quantifying vegetation biochemical and biophysical variables such as chlorophyll content, nitrogen, and leaf area index in different ecosystems (Darvishzadeh *et al*. 2008a, Vohland and Jarmer 2008, Asner and Martin 2009, Knox *et al*. 2010, Asner *et al*. 2011b, Laurent *et al*. 2011, Ramoelo *et al*. 2011, Asner and Martin 2012, Ramoelo *et al*. 2012).

Two types of methodological approaches are generally used in quantifying vegetation parameters from remotely sensed data: statistical (inductive) and physically (deductive) based models (Skidmore 2002). Inductive or statistical methods are based on empirical relationships between spectral signatures and target vegetation variables. Vegetation indices are the most commonly used products in this approach. However, when the observational scale moves from leaf to canopy or landscape scale, the relationship tends to weaken (Ustin *et al*. 2009) due to scattering from and absorption by soil, non-photosynthetic vegetation (NPV) (litter, bark, branches), and shadows (Roberts *et al*. 2004). In the second approach (physical-based models), the transfer and interaction of radiation energy is described by radiative transfer models on the basis of physical laws. Radiative transfer (RT) models provide a (somehow simplified) cause–effect relationship between scattering elements, their biochemical constituents and structure, and the reflectance. Many studies have investigated the interaction of radiation with canopy biochemical variables,

using radiative transfer models (e.g., Malenovský *et al*. 2008, Verrelst *et al*. 2010, Féret *et al*. 2011, Atzberger *et al*. 2013). But the RTM approach is computationally demanding and requires a large number of leaf and canopy model input parameters. Although much work has been done on using these two approaches to estimate biochemical and biophysical variables from remote sensing, they have rarely been used to estimate LDMC and SLA. Hardly any operational methods have been developed for quantifying these two leaf functional traits at leaf, canopy, and landscape scales from remote sensing data.

This thesis investigates the potential of remotely sensed data to quantify leaf dry matter content (LDMC) and specific leaf area (SLA) at different scales, and examines the impact of various canopy structural variables and sensor configuration on the relationship between the two leaf traits and spectral signature. Briefly, the main objectives were: (1) Investigate the potential of leaf reflectance and transmittance for indirectly estimating LDMC and SLA at leaf level, (2) Evaluate the effect of canopy structural variables such as stem density, leaf area index, crown diameter, stand height, and leaf angle distribution on spectral variation associated with LDMC and SLA variation, (3) Identify the most sensitive spectral features in order to quantify forest leaf LDMC and SLA from airborne hyperspectral data and to retrieving the two leaf functional traits at canopy level, (4) Calibrate and validate narrow-band vegetation indices for fast and accurate estimation of SLA at leaf and canopy levels from hyperspectral measurements, and (5) Investigate the potential of the new multispectral images such as Landsat-8 surface reflectance data for estimation of SLA at landscape scale. The synthesis begins by summarizing the findings at leaf level (7.2) and the effect of confounding variables in upscaling from leaf to canopy scale (7.3). The contribution of this study when upscaled to canopy (or landscape) scale is synthesized in subsection 7.4. General conclusions from the study and recommendations for future research are made in subsections 7.5 and 7.6.

7.2 Leaf level LDMC and SLA retrieval

Many leaf level studies have calibrated and validated leaf radiative transfer models (RTM) for accurate estimation of leaf biochemical contents such as chlorophyll, carotenoid, leaf water content, and leaf dry mass per area (Jacquemoud *et al.* 1996, Dawson *et al.* 1998, Malenovský *et al.* 2006, Féret *et al.* 2008, Pedros *et al.* 2010, Gerber *et al.* 2011, Ma *et al.* 2012, Romero *et al.* 2012). The most commonly used leaf RTM is PROSPECT (Jacquemoud and Baret 1990), which has been widely used for simulating leaf optical properties and retrieving vegetation parameters. However, its applicability is limited to the four model input parameters: chlorophyll content (C_{ab}), leaf mass per area (C_m), leaf water content (C_w), and the leaf structural parameter N. However,

the model's performance in characterizing other leaf parameters such as LDMC and SLA had not been tested, which is why in this study we examined the applicability of the PROSPECT model for estimating LDMC and SLA indirectly based on the model input variables. The performance of the PROSPECT model inversion for accurate retrieval of the two leaf functional traits (i.e. LDMC and SLA) was tested by generating look-up tables (LUT) for broadleaf and conifer samples separately and for pooled samples. The inversion of the generated look-up tables was run with and without prior information.

Validation of the two leaf traits estimation showed more accurate prediction though inversion of the PROSPECT model constrained by prior information. The maximum coefficient of determination (R^2) between the predicted and ground measured values was observed when the broadleaf and conifer samples were pooled (R^2 =0.83 for LDMC and R^2 = 0.89 for SLA). Lower normalized root mean square error (nRMSE) was also recorded for the inversion with prior information (nRMSE = 0.09 and 0.18 for LDMC and SLA respectively). The scatter plot of the validation result from the PROSPECT model inversion on pooled samples with prior information is illustrated in Figure 7.1.

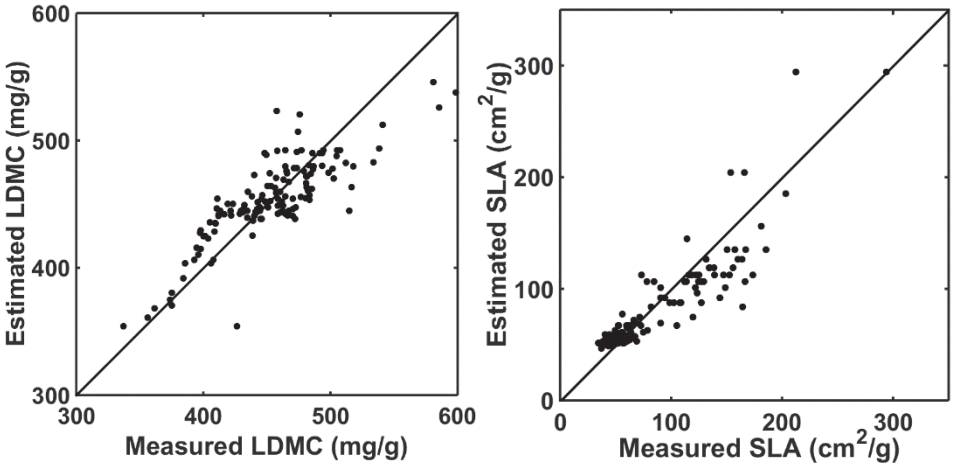

Figure 7.1: Actual vs retrieved leaf dry matter content (LDMC) and specific leaf area (SLA) of the pooled samples, using prior information. The solid line shows the1:1 relationship.

This study confirmed the accurate retrieval of two important leaf functional traits, SLA and LDMC, which are not widely addressed in the field of remote sensing. The results revealed that the PROSPECT_4 leaf model accurately simulates spectral information of samples from mixed mountain forest and can be used to retrieve the biochemical content of leaves/needles directly and indirectly through inversion over a range of vegetation types. It highlighted the fact that LDMC and SLA are quantitatively represented by leaf spectra. The results are indicative of the reliability and feasibility of using remote sensing

data for estimation of the two leaf traits. This leaf level result sheds light on extending or upscaling the application of remotely sensed data in order to accurately estimate the two functional traits at canopy or landscape scale.

7.3 Effects of canopy structural variables on LDMC and SLA retrieval

Table 7.1: R^2 and ANOVA F-test values calculated for testing HySpex single wavelengths' (bands') sensitivity for LDMC and SLA variation against the confounding variables. The R^2 column indicates the correlation between the two leaf traits and canopy spectra at the specified wavelength. The column headed LDMC provides the variations caused by LDMC against the total variance of the confounding variables tested, whereas columns $LDMC/LAI_s$, LDMC/SD, LDMC/SH, LDMC/CD and LDMC/ALA show the calculated F-test values resulting from LDMC variance against the variance caused by each factor; ditto for SLA.

Wavelength (nm)	R^2	LDMC	$LDMC/LAI_s$	LDMC/SD	LDMC/SH	LDMC/CD	LDMC/ALA
1393.44	0.538	0.3424^{ns}	131.548	5.368	46.875	0.674^{ns}	2.09^{ns}
1489.36	0.608	0.5926^{ns}	137.156	10.34	62.497	0.721^{ns}	2.897^{ns}
1519.34	0.557	0.371^{ns}	199.569	5.254	54.579	0.395^{ns}	2.005^{ns}
1921.01	0.522	1.108^{ns}	7.398	5.015	15.735	5.782^{ns}	1.195^{ns}
2262.72	0.676	2.217	76.246	81.387	72.645	2.024^{ns}	4.564^{ns}
2274.71	0.678	2.796	71.913	120.589	73.398	2.621^{ns}	4.687^{ns}
2280.71	0.685	2.935	70.36	142.354	73.98	3.008^{ns}	4.925^{ns}
2298.69	0.698	4.016	60.839	249.187	73.019	4.07^{ns}	4.631^{ns}
2382.63	0.659	8.073	35.159	56.569	57.371	17.176	5.294^{ns}
Wavelength (nm)	R^2	SLA	SLA/LAI_s	SLA/SD	SLA/SH	SLA/CD	SLA/ALA
1393.44	0.036	0.097^{ns}	64.055	2.186^{ns}	22.792	0.166^{ns}	1.005^{ns}
1489.36	0.053	0.238^{ns}	79.546	6.259	37.215	0.293^{ns}	1.389^{ns}
1519.34	0.076	0.297^{ns}	210.215	5.084	59.321	0.137^{ns}	1.291^{ns}
1921.01	0.005	0.057^{ns}	0.498^{ns}	0.312^{ns}	1.002^{ns}	0.369^{ns}	0.013^{ns}
2262.72	0.379	6.006	288.90	312.159	273.698	9.270^{ns}	19.004
2274.71	0.387	7.009	278.921	471.615	284.150	11.807^{ns}	20.356
2280.71	0.390	7.043	271.390	559.497	284.997	13.000^{ns}	19.918
2298.69	0.381	8.925	233.954	948.720	272.439	17.975	21.722
2382.63	0.204	7.061	75.659	116.277	121.914	36.976	11.995

The results described in subsection 7.2 demonstrate that LDMC and SLA can be accurately estimated from remotely sensed data at leaf level and have indicated upscaling and extension of the inversion to the canopy scale. However, before attempting to retrieve at canopy/landscape scale, it is necessary to understand the impact of confounding factors on canopy reflectance. This is a crucial first step toward accurately estimating the desired vegetation variables using remote sensing. The scattering and absorption caused by leaf traits may be confounded by soil, non-photosynthetic vegetation (litter, bark, and branches), stem characteristics, canopy structure, and shadows (Roberts *et al*. 2004, Wolf *et al*. 2010, Ollinger 2011). Indices that have originally been designed at leaf scale are particularly likely to suffer from

these additional heterogeneity factors when used at canopy (i.e., larger) scale (Asner *et al*. 1998, Ustin *et al*. 2009, Ollinger 2011). As no previous study had examined the impact of canopy structural variables on the estimation accuracy of LDMC and SLA from remotely sensed data, this study aimed at investigating the influence of key canopy structural variables such as single tree LAI (LAI_s), stem density (SD), stand height (SH), crown diameter (CD,) and average leaf angle (ALA) on LDMC and SLA retrieval.

The study confirmed that canopy-scale spectral variation due to LDMC and SLA in the presence of canopy-confounding factors is statistically significant. A substantial influence on spectral variation originated from the structural variables SD, CD, and ALA, and the least disturbing effect came from LAI_s and SH. The F-test result indicated that the confounding factors are more influential at shorter wavelengths than at longer wavelengths (Table 7.1). Among the tested vegetation indices (VI), the modified normalized difference (mND) (R2274.71-R1921.01)/ (R2274.71+R1921.01-2*R1519.34) and the modified simple ratio (mSR) (R2274.71-R1519.34)/ (R1921.01-R1519.34) indices performed better in removing many of the confounding variables' effects on the relationship between the two leaf traits and canopy reflectance (Figure 7.2).

In addition, the slope of the relationship between the leaf traits and the mND index was used as a measure of detectability, to examine how varying two confounding variables at a time affects the accuracy of LDMC and SLA retrieval. Based on the principle that the greater the slope, the higher is the detectability of the two leaf traits, the mND index and structural information derived from the broadleaf, conifer and mixed stands of the test site showed nearly optimal conditions for retrieving canopy LDMC and SLA in terms of LAI_s and SH. However, the broadleaf and mixed stands (particularly some of the broadleaf stands) had very low SD values, which could significantly weaken the relationship between the traits and spectral variation at canopy scale.

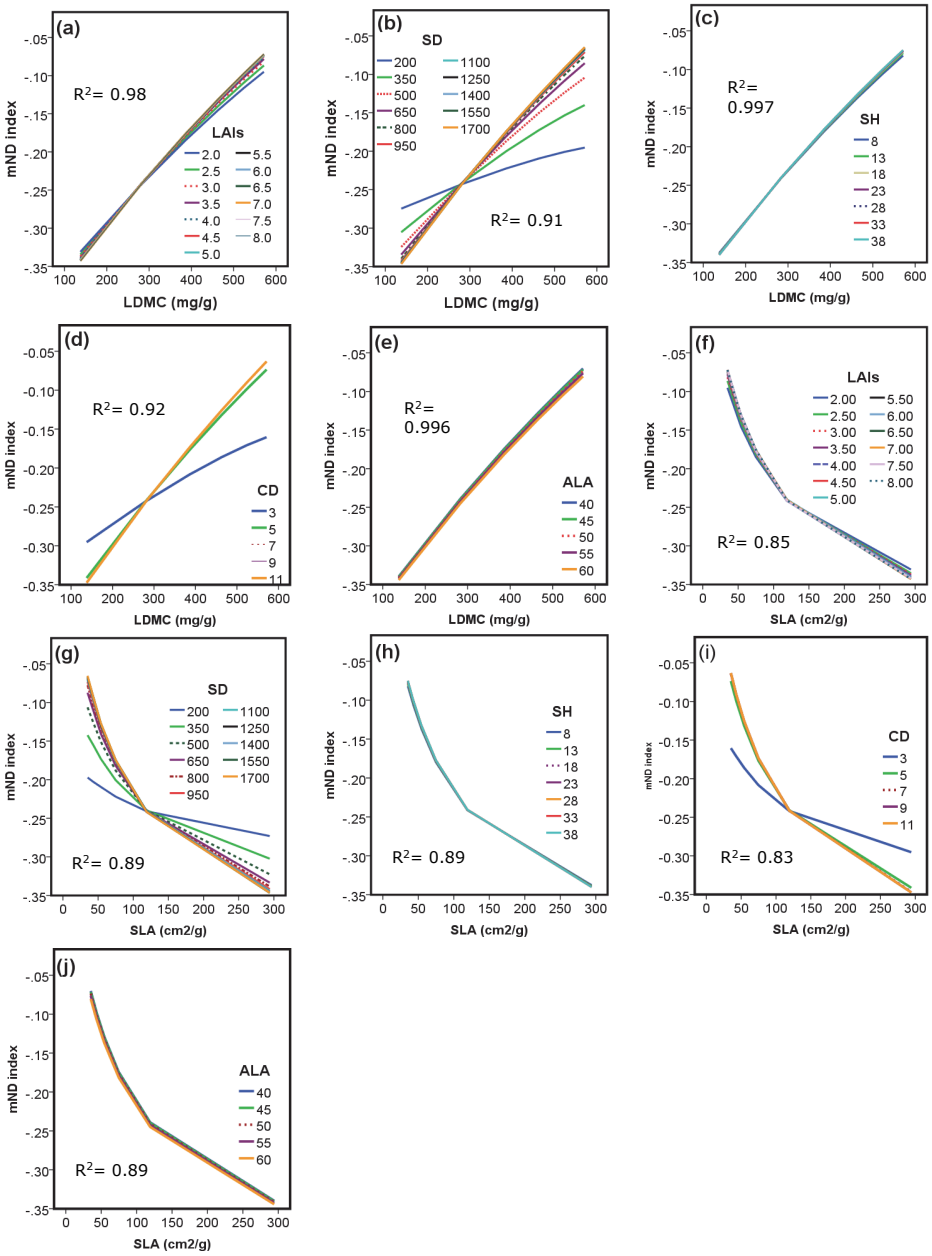

Figure 7.2: Relationship between LDMC, SLA, and the modified normalized index (mND) for a range of single tree LAI (a, f), stem density (b, g), stand height (c, h), crown diameter (d, i), and average leaf angle (e, j) with fixed values set to LAI_s= 5.5; SD = 800 trees/ha, SH = 23m, CD =5.4m, ALA = 50^0, θ_s = 32^0 and Ψ =153.

In general, this local sensitivity study on INFORM-simulated canopy reflectance in the NIR and SWIR spectral ranges addressed the relative importance of each structural variable on the retrieval of LDMC and SLA from canopy reflectance. Although spectral variation at canopy level is suppressed by structural variables, the study confirmed the presence of significant spectral variation that could be used to estimate the two leaf traits. It indicated that longer wavelengths were more suitable than shorter wavelengths for assessing both LDMC and SLA at canopy scale. Of the five structural variables (LAI_s, SD, SH, CD, and ALA) examined in this study, greatest influence was observed for SD and CD, followed by ALA. The mND vegetation index was able to avoid much of the influence of all the five structural variables, except in a few cases of low SD and CD conditions. Post hoc testing confirmed that higher values of LAI_s (≥ 5) and SH (≥ 13m) have no impact and can be ignored in parametrizing RTM. Nevertheless, the correlation between the two leaf traits and canopy reflectance may decline or vanish as long as the forest is sparse (SD<400 trees/ha) with trees of medium or small tree crown diameter. The promising sensitivity analysis results of detectability of LDMC and SLA of the test site encouraged us to look for discovering spectral features and VIs that are specifically sensitive to LDMC and SLA, so that they can be accurately retrieved and mapped using remotely sensed data.

7.4 Canopy/landscape level retrieval and mapping

Hardly any statistical or physical models have been tested to estimate LDMC and SLA from remotely sensed data. Unlike other biophysical and biochemical variables such as chlorophyll and Leaf area index, there are no well-developed methods for fast and accurate retrieval of LDMC and SLA at canopy or larger scales. Hence, both the statistical and physical approaches to vegetation parameter retrieval were investigated to map the two leaf traits in a mixed mountain forest, using the hyperspectral HySpex airborne images and the multispectral Landsat-8 Operational Land Imager (OLI) data. Ground measurements of LDMC and SLA were collected in a field campaign during the time of image acquisition. We evaluated the performance of the INFORM radiative transfer model inversion through wavelet transformation and also calibrated and validated a wide range of vegetation index types.

7.4.1 Retrieval of forest leaf functional traits from hyperspectral data using radiative transfer models and continuous wavelet analysis

Previous studies had shown the potential of wavelet analysis for estimating leaf parameters from leaf spectra measured in the laboratory and data simulated using RTMs (Jingcheng *et al*. 2011, Cheng *et al*. 2012, Ullah *et al*. 2012, Zhang *et al*. 2012a, Cheng *et al*. 2014a). However, the applicability of wavelet analysis at canopy level using canopy spectra obtained from airborne and

spaceborne hyperspectral data had not been investigated. Therefore, the effectiveness of hyperspectral remote sensing in estimating LDMC and SLA in a mixed forest by means of radiative transfer model and continuous wavelet analysis was examined. We identified spectral features that have high correlation with LDMC and SLA by applying a continuous wavelet analysis to INFORM-simulated canopy spectra. Predictive models were developed, which use the identified spectral features to estimate the two leaf traits (LDMC and SLA) from HySpex airborne images.

The application of continuous wavelet analysis resulted in six sensitive wavelet features for LDMC and four for SLA being in the top 1% strongly correlated wavelet features. The correlation strength of wavelet features of the INFORM-simulated spectra and position of the significantly correlated features to the two leaf traits are illustrated in Figure 7.3. The top 1% strongly correlated wavelet features are generally located at longer wavelengths. This confirmed our earlier result during the sensitivity analysis of canopy structural variables, which suggested the sensitivity of longer wavelengths to LDMC and SLA variation. The single wavelet features that showed the highest correlation and the lowest NRMSE were at 1741 nm at scale 5 for LDMC and at 1645 nm at scale 6 for SLA. The band position of the SLA-sensitive wavelet features found in this study agreed well with findings by Cheng *et al*. (2014b), who used simulated and measured spectra at leaf level and reported a strong correlation of LMA (inverse of SLA) with the wavelet features at (1639 nm, scale 4) and (2139 nm, scale 4). However, in our study the scale of the wavelet features shifted to larger values. This may be due to canopy structure properties and other external factors such as sensor configuration and atmospheric effects that may influence the canopy spectral reflectance.

Using the predictive models developed on the identified wavelet features, we found a stronger correlation between the predicted and (measured) validation values for SLA (R^2 = 0.80) than for LDMC (R^2 = 0.58), which is in agreement with our result for estimating the two leaf traits from the PROSPECT model inversion at leaf scale. These may be attributed to several factors. One is that LDMC is a compound variable derived from leaf water content (C_w) and leaf dry mass per unit area (C_m). Therefore, its correlation with spectral reflectance is affected by both C_w and C_m. This would explain why many of the wavelengths did not show high correlation to LDMC, even in the simulated spectra (Figure 7.3). By contrast, the RMSE for LDMC was found to be lower than the RMSE for SLA (4.39% versus 4.90 %). The low RMSE of LDMC is partially associated with ground truth accuracy. LDMC is computed based on fresh and dry weights of samples that can be precisely and accurately obtained in the laboratory, but calculation of SLA requires measurements of leaf area that are prone to operator and instrument errors.

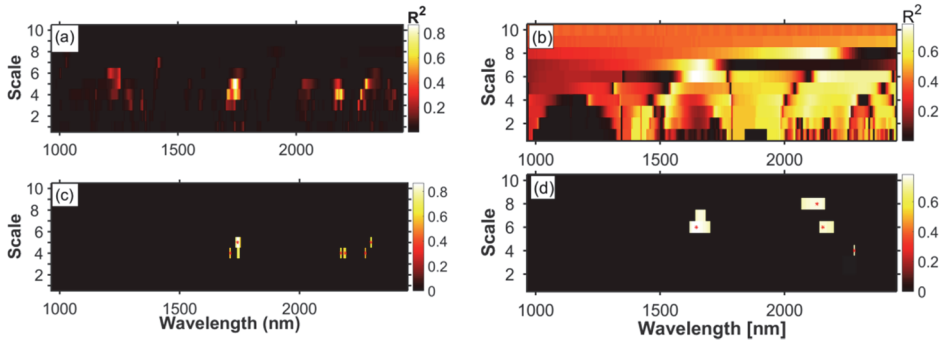

Figure 7.3: Correlation scalograms for the identification of wavelet features which significantly correlate with leaf dry matter content (LDMC) (a) and specific leaf area (SLA) (b). Scalograms are derived from continuous wavelet analysis of simulated spectra. Brightness represents the coefficient of determination (R^2) relating wavelet power to LDMC and SLA. Coloured feature regions in scalograms (c) and (d) depict the wavelet features with the top 1% greatest R^2 values for LDMC and SLA.

Our findings confirmed the potential of wavelet-transformed spectra for estimating vegetation parameters, thereby indicating the capability of the wavelet transformation to identify the most sensitive spectral features from a large hyperspectral dataset and the robustness of wavelet transformation in creating higher correlation of wavelet features to vegetation variables compared to non-transformed original spectra. This may be attributed to the effectiveness of wavelet analysis in decomposing the trait's absorption features into various scales of narrow and broad band absorption features and identifying those that correlate best with the variation in the traits' concentration. The performance of wavelet analysis compared with narrow-band indices and stepwise selection of narrow-band reflectance for retrieval of pigment concentrations in vegetation at leaf and canopy scales has also been reported by Blackburn (2007b). In comparison with narrow-band indices, wavelet analysis captures more information contained within the hyperspectral data and creates an opportunity to develop robust and extendible methods for quantifying plant traits over large areas (Blackburn 2007a).

7.4.2 Calibration and validation of narrow-band indices for estimation of SLA from hyperspectral data

Vegetation indices (VIs) constitute simple and convenient algebraic combinations of spectral reflectance to extract information from remotely sensed data, which facilitates the processing and analysis of large amounts of remotely sensed data. In the past four decades, a number of researchers (e.g., Rouse *et al.* 1974, Clevers 1991, Gitelson 2004, Jensen *et al.* 2012, Wu 2014) have attempted to develop spectral vegetation indices at various scales to monitor the Earth's vegetation cover and retrieve vegetation parameters such as leaf chlorophyll, leaf area index (LAI), fractional vegetation cover, biomass,

canopy architecture, and photosynthetic activity from remotely sensed data. Among vegetation parameters retrieved using hyperspectral data, SLA has received little attention. The suitability of many of the index types available in the literature had not yet been evaluated for SLA retrieval and therefore we calibrated and validated the suitability of a number of vegetation indices previously proposed for retrieving various vegetation properties for remotely estimating the SLA at leaf and canopy levels for heterogeneous mountain forest. Ground measurements of SLA with laboratory spectroscopy measurement and HySpex imagery were used to calibrate indices. The performance of each index was cross-validated using PROSPECT and INFORM simulated datasets in addition to ground-measured datasets.

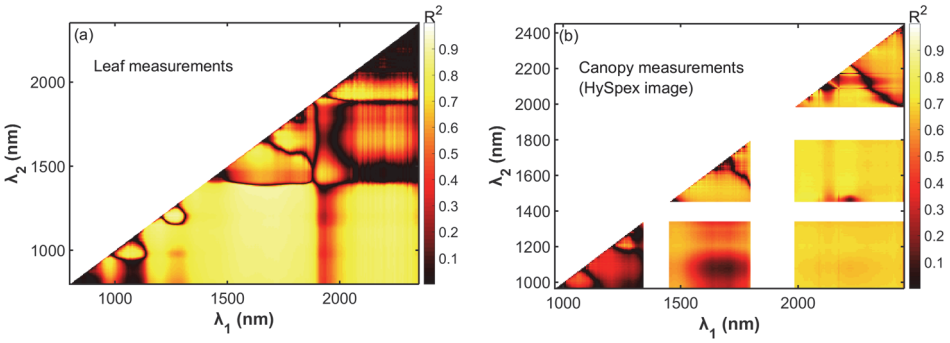

Figure 7.4: Matrices representing R^2 of specific leaf area (SLA) with different band combinations for OSAVI based on leaf level measurements (a) and canopy level measurement (b).

The determination of the best wavelength(s) for each index at leaf and canopy levels by testing all possible combinations of wavelength in the NIR and SWIR region of the measured dataset revealed the presence of many band combinations that correlate significantly with SLA (Figure 7.4). However, the correlation tended to be lower at canopy level and many of band combinations that showed high correlation to SLA at leaf level became insensitive at canopy scale. Although only narrow-band indices were examined, our findings suggest that even bands with a wider wavelength range (broad bands) can be utilized. The large continuous areas of high R^2 values in the 2D R^2 matrices indicate that indices calibrated on coarser bands (bands covering a larger area of the spectrum than the bands used here) can accurately estimate SLA. This implies that remote sensing data from coarse spectral resolution sensors may suffice for SLA estimation.

Table 7.2: Leaf level SLA indices cross-validated on the measured dataset (n=137) and the PROSPECT simulated dataset (n=5000).

Index type	λ_1 (nm)	λ_2 (nm)	λ_3 (nm)	Measured dataset		PROSPECT simulation	
				R^2	RMSE (%)	R^2	RMSE (%)
CAI	1115	2320	1715	0.89	3.92	0.86	3.63
D	1915	2145		0.91	3.60	0.84	4.75
GVMI	1315	1715		0.90	3.76	0.87	3.11
NMDI	**920**	**1675**	**1335**	**0.94**	**2.88**	**0.91**	**4.76**
OSAVI	**1370**	**1615**		**0.93**	**3.24**	**0.93**	**3.15**
R	2145			0.85	4.67	0.79	5.72
VARI	**1345**	**1675**	**1850**	**0.94**	**3.07**	**0.90**	**4.35**

Many of the indices calibrated and used to predict SLA in our study provided higher R^2 and lower RMSE values (Table 7.2 and Table 7.3) at both leaf and canopy levels. In the measured dataset, R^2 values ranged from 0.80 to 0.94 at the leaf level and were higher than the canopy level R^2 values of 0.67 to 0.88. The multi-band indices NMDI and VARI and the two-band OSAVI index (Table 7.2) were among the best indices for SLA prediction at leaf level. $OSAVI_{1370, 1615}$ showed a strong association with variation in SLA content for both the simulated and measured datasets and could be a first choice for accurate estimation of SLA at leaf level. At canopy scale, the maximum R^2 and minimum RMSE combination was obtained with the $OSAVI_{1537, 1543}$ index and was proposed for SLA retrieval from aircraft-level hyperspectral imagery.

Table 7.3: SLA indices at canopy level cross-validated on the measured dataset (n=33) and INFORM simulations (n = 10,000).

Index type	λ_1 (nm)	λ_2 (nm)	λ_3 (nm)	Measured dataset		INFORM simulation	
				R^2	RMSE (%)	R^2	RMSE (%)
GVMI	2017	2299		0.73	4.89	0.79	4.70
mNDVI	2053	2149	2083	0.85	3.59	0.80	3.17
MNLI	1208	2005		0.83	3.90	0.76	4.35
NDLI	1537	1543		0.86	3.53	0.82	4.14
NLI	1609	2047		0.82	4.09	0.83	3.89
OSAVI	**1537**	**1543**		**0.88**	**3.34**	**0.88**	**3.12**
PVI	1537	1543		0.87	3.36	0.89	3.16
R	968			0.83	4.03	0.88	3.18
RDVI	**1537**	**1543**		**0.88**	**3.31**	**0.89**	**3.13**
SAVI	**1537**	**1543**		**0.88**	**3.28**	**0.88**	**3.18**
SAVI2	968	2089		0.83	4.01	0.87	3.20
TSAVI	**1537**	**1543**		**0.87**	**3.38**	**0.89**	**3.16**
WDVI	**1537**	**1543**		**0.87**	**3.38**	**0.88**	**3.16**

However, when the indices calibrated using the measured dataset were applied to the PROSPECT and INFORM simulated datasets for SLA estimation, higher RMSEs were observed in several cases. This phenomenon may be partially

explained by errors in the RTMs resulting from simplification of model input parameters. Due to discrepancies between the simulated and measured datasets, the wavelengths found to be very sensitive to SLA during the indices' calibration (using the measured dataset) might not be among the best bands in the simulated dataset for SLA retrieval. Another reason could be that the measured datasets may not be extensive enough to fully represent the range of the simulated datasets. This observation may support the hypothesis that vegetation indices are site-specific and cannot be generalized. Nevertheless, our approach enabled us to minimize the non-generic nature of indices by comparing indices' accuracy on a wide range of datasets (measured and simulated spectra).

7.4.3 Upscaling and assessment of the multispectral Landsat imagery for SLA estimation

Satellite images have rarely been used for characterizing forest leaf biochemical and biophysical variables. Therefore, the potential of the new generation of satellite images to predict SLA for a mixed mountain forest was examined. It was evaluated whether the methods earlier studied at field and canopy scale using hyperspectral field and airborne data can be utilized at lager scale using medium resolution satellite data. Therefore, SLA was retrieved from the recently launched Landsat-8 imagery by means of empirical methods (individual bands and vegetation indices) and the inversion of INFORM radiative transfer model through wavelet transformation and look-up table approaches.

Both the statistical and INFORM inversion predicted SLA with satisfactory accuracy. Of the seven bands and seven vegetation indices investigated, the enhanced vegetation index (EVI) yielded the highest accuracy (R^2 = 0.77 and RMSE = 4.44%). Validation of the INFORM inversion through continuous wavelet analysis resulted in R^2 = 0.79 and RMSE = 7.52%. INFORM inversion by means of a spectral subset using bands 5, 6, and 7 of Landsat-8 provided R^2 = 0.73 and RMSE = 5.33%. The relatively high RMSE value observed in the INFORM model inversion reaffirmed the reasons stated in section 7.4.2 that simplification of model input parameters and sensor noise result in disparity between simulated and measured datasets, which might lead to systematic errors. Further upscaling has implications for the retrieval accuracy and will increase the retrieval error. Generally, the findings are in agreement with our results in section 7.4.2, which suggested indices calibrated on coarser bands (bands covering a larger area of the spectrum) can accurately estimate SLA. This indicated that the multispectral Landsat-8 data provides sufficient spectral information for a successful estimation of SLA at landscape and other larger scales.

7.5 Conclusions

The main objective of the thesis was to explore the potential of remote sensing for estimating forest leaf functional traits such as leaf dry matter content (LDMC) and specific leaf area (SLA) at leaf, canopy, and landscape levels by means of statistical and radiative transfer model (RTM) inversion approaches. We also examined the influence of canopy structural variables (i.e., leaf area index, stem density, stand height, crown diameter, and leaf angle distribution) on the retrieval accuracy of the leaf functional traits from spectral information. The research findings confirmed that the spectral variability in both hyperspectral and the new multispectral remote sensing data such as Landsat-8 provide the means to estimate leaf functional traits with satisfactory accuracy.

The results suggested that the shortwave infrared (SWIR) region of the electromagnetic spectrum contributed plentiful spectral information for assessment of leaf functional traits related to the dry matter content of leaves. In both statistical and radiative transfer model inversion techniques, many of the bands selected for estimation of the LDMC and SLA were from SWIR. Therefore it is imperative to exploit the bands of this region in an endeavour to retrieve LDMC and SLA from hyperspectral and multispectral remote sensing data.

This work indicated the role of canopy structural variables on spectral data. It has been inferred that stem density and crown diameter, which constitute canopy closure, are the two most important structural factors that affect the estimation of LDMC and SLA from remote sensing data. Regardless of the retrieval approach implemented, prior knowledge about understory materials and soil background is pivotal, particularly in remote sensing of sparse forests. Since vegetation indices were able to easily remove the effect of stand height and leaf angle distribution on canopy reflectance, accurate estimations of LDMC and SLA could be performed without prior information on these two canopy structure variables.

The research further demonstrated the potential of wavelet transformation to enhance the correlation between forest canopy variables and canopy reflectance, and to identify the most informative spectral features for quantifying leaf traits. This justifies further use of such techniques in quantifying vegetation characteristics from remote sensing measurements.

The calibration and validation of a wide variety of existing vegetation indices for SLA estimation has shown that many indices may be used for accurate estimation of SLA. This implies that vegetation indices, which are simple and fast, might be preferred over physical model inversion techniques, which are computationally demanding and need a large number of input parameters. A

compromise should be made between the accuracy and need for reproducibility of the outputs generated.

The comparable prediction accuracy obtained from using multispectral Landsat-8 satellite images with those from imaging spectroscopy, applying either a statistical or a physical model approach for the retrieval of SLA showed that the new generation of satellite imagery has potential for the retrieval of forest leaf functional traits such as SLA at regional and global scales.

To sum up, this work contributes to applied research on the remote sensing of vegetation. The findings and methods of this work have the potential to produce useful information from hyperspectral and multispectral remote sensing data about leaf functional traits at local, regional, and global scales. The results further confirmed the applicability of remote sensing to elucidate variation in general ecological leaf functional traits across relevant spatial and temporal scales. This will facilitate regular monitoring of biodiversity, particularly natural or anthropogenic changes in ecosystem functioning.

7.6 Future work and recommendations

In this study, quantification and validation of leaf functional traits particularly at leaf and canopy scale were investigated using spectral data mainly in the NIR and SWIR regions (800-2500 nm). The other parts of the electromagnetic spectrum may be explored for their potential to address the quantification of plant traits across a wide range of spatial scales.

The number of plant traits needed in biodiversity studies and monitoring is immense and ranges from the whole-plant traits such as growth form and height to leaf traits such as specific leaf area and leaf phenology, from stem and below-ground traits (e.g. stem specific density and specific root length) to regenerative traits (e.g. seed mass and dispersal mode). However, in this study only two leaf traits (SLA and LDMC) have been studied. Other traits could be similarly explored.

This study has demonstrated the applicability of remote sensing for estimating and mapping LDMC and SLA in a mixed mountain forest. The forest area is mainly dominated by three tree species: European beech (*Fagus sylvatica*), Norway spruce (*Picea abies*) and Fir (*Abies alba*). Therefore, the application of the developed methods to other structurally different vegetation types and heterogeneous areas with high species variability and vegetation communities needs to be evaluated using both hyperspectral and multispectral remote sensing data.

In this thesis, the data collected in the field were used to parameterize radiative transfer models. To improve parameter retrieval in forest canopy from remote

sensing data by using radiative transfer model inversion, it is necessary to model the surface bidirectional reflectance distribution function that takes into account canopy structure (e.g. crown shape, forest stand density, and canopy heterogeneity) and background, particularly in sparse canopies. For this, alternative methods should be developed to acquire the vast model input parameters. One possible option to overcome this can be to use LiDAR (light detection and ranging) data, which provides direct measurement of canopy architectural variables and background information. Therefore further research is needed to integrate radiative transfer modeling and LiDAR structural information to improve the efficiency and accuracy of leaf functional traits estimation.

Appendix:

The best Linear regression model formula for LDMC retrieval developed from 6 predictors (wavelet features) with 19 terms. Each predictor represent wavelet feature value at the given wavelength and scale: a = (1711 nm scale 4), b = (1741 nm scale 5), c = (2173 nm scale 4), d = (2191 nm scale 4), e = (2275 nm scale 4) and f = (2299 nm scale 5).

Estimated Coefficients:

	Estimate	**SE**	**tStat**	**pValue**
Intercept	-0.37	0.001	-280.06	0
(1711 nm scale 4)	2.78	1.243	2.239	0.0252
(1741 nm scale 5)	-25.96	0.548	-47.375	0
(2173 nm scale 4)	19.19	6.016	3.190	0.001
(2191 nm scale 4)	68.51	5.672	12.079	0
(2275 nm scale 4)	-12.45	2.870	-4.337	0
(2299 nm scale 5)	-12.68	0.938	13.516	0
(1711 nm scale 4)* (1741 nm scale 5)	4523.7	286.98	15.763	0
(1711 nm scale 4)* (2173 nm scale 4)	-13529	3078.8	4.394	0
(1711 nm scale 4)* (2191 nm scale 4)	-24490	3605.1	6.793	0
(1711 nm scale 4)* (2299 nm scale 5)	2761.4	476.57	5.794	0
(1741 nm scale 5)* (2173 nm scale 4)	5873.5	1114.4	5.271	0
(1741 nm scale 5)* (2191 nm scale 4)	6822.1	954.03	7.151	0
(1741 nm scale 5)* (2275 nm scale 4)	-8598.3	1026.2	-8.379	0
(1741 nm scale 5)* (2299 nm scale 5)	-1838.9	264.17	-6.961	0
(2173 nm scale 4)* (2275 nm scale 4)	32559	7925	4.108	0
(2173 nm scale 4) * (2299 nm scale 5	-11629	3037.2	-3.829	0
(2191 nm scale 4)* (2275 nm scale 4)	37772	6081.3	6.211	0
(2191 nm scale 4) * (2299 nm scale 5	-6341.8	1042.3	-6.084	0

Bibliography

Albert, C. H., W. Thuiller, N. G. Yoccoz, A. Soudant, F. Boucher, P. Saccone and S. Lavorel, 2010. Intraspecific functional variability: extent, structure and sources of variation*,Journal of Ecology* 98(3): 604-613.

Ali, A. M., R. Darvishzadeh, A. K. Skidmore and I. V. Duren, 2016a. Effects of Canopy Structural Variables on Retrieval of Leaf Dry Matter Content and Specific Leaf Area from Remotely Sensed Data*,Ieee Journal of Selected Topics in Applied Earth Observations and Remote Sensing* 9(2): 898-909.

Ali, A. M., R. Darvishzadeh, A. K. Skidmore, I. v. Duren, U. Heiden and M. Heurich, 2016b. Estimating leaf functional traits by inversion of PROSPECT: Assessing leaf dry matter content and specific leaf area in mixed mountainous forest*,International Journal of Applied Earth Observation and Geoinformation* 45, Part A: 66-76.

Ali, A. M., A. K. Skidmore, R. Darvishzadeh, I. V. Duren, S. Holzwarthc and J. Muellerd, 2016c. Retrieval of Forest Leaf Functional Traits from HySpex Imagery Using Radiative Transfer Models and Continuous Wavelet Analysis*,photogrammetry and remote sensing.* under review.

Ali, A. M., R. Darvishzadeh, A. K. Skidmore and I. V. Duren, 2016d. Narrow band vegetation indices for specific leaf area retrieval at leaf and canopy scale*,ASPRS PE&RS Journal.* under review.

Asner, G. P., 1998. Biophysical and biochemical sources of variability in canopy reflectance*,Remote Sensing of Environment* 64(3): 234-253.

Asner, G. P. and R. E. Martin, 2008. Spectral and chemical analysis of tropical forests: Scaling from leaf to canopy levels*,Remote Sensing of Environment* 112(10): 3958-3970.

Asner, G. P. and R. E. Martin, 2009. Airborne spectranomics: Mapping canopy chemical and taxonomic diversity in tropical forests*,Frontiers in Ecology and the Environment* 7(5): 269-276.

Asner, G. P. and R. E. Martin, 2012. Contrasting leaf chemical traits in tropical lianas and trees: implications for future forest composition*,Ecology Letters* 15(9): 1001-1007.

Asner, G. P., R. E. Martin, A. J. Ford, D. J. Metcalfe and M. J. Liddell, 2009. Leaf chemical and spectral diversity in Australian tropical forests*,Ecological Applications* 19(1): 236-253.

Asner, G. P., R. E. Martin, D. E. Knapp, R. Tupayachi, C. Anderson, L. Carranza, P. Martinez*, et al.*, 2011a. Spectroscopy of canopy chemicals in humid tropical forests*,Remote Sensing of Environment* 115(12): 3587-3598.

Asner, G. P., R. E. Martin, R. Tupayachi, R. Emerson, P. Martinez, F. Sinca, G. V. N. Powell, S. J. Wright and A. E. Lugo, 2011b. Taxonomy and remote sensing of leaf mass per area (LMA) in humid tropical forests*,Ecological Applications* 21(1): 85-98.

Asner, G. P., C. A. Wessman, D. S. Schimel and S. Archer, 1998. Variability in leaf and litter optical properties: Implications for BRDF model inversions using AVHRR, MODIS, and MISR*,Remote Sensing of Environment* 63(3): 243-257.

Atzberger, C., 2000. Development of an invertible forest reflectance model:The INFOR-Model*,In Buchroithner (Ed.), A decade of trans-European remote sensing cooperation*: Proceedings of the 20th EARSeL Symposium Dresden, Germany, 14- 16. June 2000 (pp. 2039- 2044).

Atzberger, C., R. Darvishzadeh, M. Immitzer, M. Schlerf, A. Skidmore and G. le Maire, 2015. Comparative analysis of different retrieval methods for mapping grassland leaf area index using airborne imaging spectroscopy*,International Journal of Applied Earth Observation and Geoinformation* 43: 19-31.

Atzberger, C., R. Darvishzadeh, M. Schlerf and G. Le Maire, 2013. Suitability and adaptation of PROSAIL radiative transfer model for hyperspectral grassland studies*,Remote Sensing Letters* 4(1): 56-65.

Atzberger, C., K. Richter, F. Vuolo, R. Darvishzadeh and M. Schlerf, 2011. Why confining to vegetation indices? Exploiting the potential of improved spectral observations using radiative transfer models*,Remote Sensing for Agriculture, Ecosystems, and Hydrology Xiii* 8174.

Bach, H. and W. Verhoef, 2003. Sensitivity studies on the effect of surface soil moisture on canopy reflectance using the radiative transfer model GeoSAIL*,Igarss 2003: Ieee International Geoscience and Remote Sensing Symposium, Vols I - Vii, Proceedings*: 1679-1681.

Bannari, A., K. Staenz, D. Haboudane and K. S. Khurshid, 2006. Sensitivity Analysis of Chlorophyll Indices to Soil Optical Properties Using Ground-Reflectance Data*,2006 Ieee International Geoscience and Remote Sensing Symposium, Vols 1-8*: 120-123.

Banskota, A., R. H. Wynne, S. P. Serbin, N. Kayastha, V. A. Thomas and P. A. Townsend, 2013a. Utility of the Wavelet Transform for LAI Estimation Using Hyperspectral Data*,Photogrammetric Engineering and Remote Sensing* 79(7): 653-662.

Banskota, A., R. H. Wynne, V. A. Thomas, S. P. Serbin, N. Kayastha, J. P. Gastellu-Etchegorry and P. A. Townsend, 2013b. Investigating the Utility of Wavelet Transforms for Inverting a 3-D Radiative Transfer Model Using Hyperspectral Data to Retrieve Forest LAI*,Remote Sensing* 5(6): 2639-2659.

Baret, F. and G. Guyot, 1991. Potentials and Limits of Vegetation Indexes for Lai and Apar Assessment*,Remote Sensing of Environment* 35(2-3): 161-173.

Baret, F., G. Guyot and D. J. Major, 1989. TSAVI: A vegetation index which minimizes soil brightness effects on LAI and APAR estimation. Digest - International Geoscience and Remote Sensing Symposium (IGARSS).

Barton, C. V. M. and P. R. J. North, 2001. Remote sensing of canopy light use efficiency using the photochemical reflectance index: Model and sensitivity analysis*,Remote Sensing of Environment* 78(3): 264-273.

Baumgartner, A., P. Gege, C. Kohler, K. Lenhard and T. Schwarzmaier, 2012. Characterisation methods for the hyperspectral sensor HySpex at DLR's calibration home base*,Sensors, Systems, and Next-Generation Satellites Xvi* 8533.

Benomar, L., A. DesRochers and G. R. Larocque, 2011. Changes in specific leaf area and photosynthetic nitrogen-use efficiency associated with physiological acclimation of two hybrid poplar clones to intraclonal competition*,Canadian Journal of Forest Research-Revue Canadienne De Recherche Forestiere* 41(7): 1465-1476.

Bernhardt-Römermann, M., C. Römermann, R. Nuske, A. Parth, S. Klotz, W. Schmidt and J. Stadler, 2008. On the identification of the most suitable traits for plant functional trait analyses*,Oikos* 117(10): 1533-1541.

Blackburn, G. A., 2007a. Hyperspectral remote sensing of plant pigments*,Journal of Experimental Botany* 58(4): 855-867.

Blackburn, G. A., 2007b. Wavelet decomposition of hyperspectral data: A novel approach to quantifying pigment concentrations in vegetation*, International Journal of Remote Sensing* 28(12): 2831-2855.

Bowyer, P., F. M. Danson and N. M. Trodd, 2003. Methods of sensitivity analysis in remote sensing: Implications for canopy reflectance model inversion*,Igarss 2003: Ieee International Geoscience and Remote Sensing Symposium, Vols I - Vii, Proceedings*: 3839-3841.

Broge, N. H. and J. V. Mortensen, 2002. Deriving green crop area index and canopy chlorophyll density of winter wheat from spectral reflectance data*,Remote Sensing of Environment* 81(1): 45-57.

Cadotte, M. W., K. Carscadden and N. Mirotchnick, 2011. Beyond species: Functional diversity and the maintenance of ecological processes and services*,Journal of Applied Ecology* 48(5): 1079-1087.

Cadotte, M. W., J. Cavender-Bares, D. Tilman and T. H. Oakley, 2009. Using Phylogenetic, Functional and Trait Diversity to Understand Patterns of Plant Community Productivity*,Plos One* 4(5): e5695.

Carlson, K. M., G. P. Asner, R. F. Hughes, R. Ostertag and R. E. Martin, 2007. Hyperspectral remote sensing of canopy biodiversity in Hawaiian lowland rainforests*,Ecosystems* 10(4): 536-549.

Ceccato, P., N. Gobron, S. Flasse, B. Pinty and S. Tarantola, 2002. Designing a spectral index to estimate vegetation water content from remote sensing data: Part 2. Validation and applications*,Remote Sensing of Environment* 82(2-3): 198-207.

Chen, J. M. and J. Cihlar, 1996. Retrieving leaf area index of boreal conifer forests using landsat TM images*,Remote Sensing of Environment* 55(2): 153-162.

Cheng, T., D. Riano and S. L. Ustin, 2014a. Detecting diurnal and seasonal variation in canopy water content of nut tree orchards from airborne imaging spectroscopy data using continuous wavelet analysis*,Remote Sensing of Environment* 143: 39-53.

Cheng, T., B. Rivard and A. Sánchez-Azofeifa, 2011. Spectroscopic determination of leaf water content using continuous wavelet analysis*,Remote Sensing of Environment* 115(2): 659-670.

Cheng, T., B. Rivard, A. G. Sánchez-Azofeifa, J.-B. Féret, S. Jacquemoud and S. L. Ustin, 2014b. Deriving leaf mass per area (LMA) from foliar reflectance across a variety of plant species using continuous wavelet analysis*,Isprs Journal of Photogrammetry and Remote Sensing* 87(0): 28-38.

Cheng, T., B. Rivard, A. G. Sánchez-Azofeifa, J. B. Féret, S. Jacquemoud and S. L. Ustin, 2012. Predicting leaf gravimetric water content from foliar reflectance across a range of plant species using continuous wavelet analysis*,Journal of Plant Physiology* 169(12): 1134-1142.

Cheng, T., B. Rivard and G. A. Sánchez-Azofeifa, 2010. Spectroscopic determination of leaf water content using continuous wavelet analysis.

Cho, M. A., A. Ramoelo and R. Mathieu, 2014. Estimation of Leaf Area Index (Lai) of South Africa from Modis Imagery by Inversion of Prosail Radiative Transfer Model*,2014 Ieee International Geoscience and Remote Sensing Symposium (Igarss)*: 2590-2593.

Clevers, J. G. P. W., 1991. Application of the Wdvi in Estimating Lai at the Generative Stage of Barley*,Isprs Journal of Photogrammetry and Remote Sensing* 46(1): 37-47.

Clevers, J. G. P. W. and L. Kooistra, 2012. Using Hyperspectral Remote Sensing Data for Retrieving Canopy Chlorophyll and Nitrogen Content*,Ieee Journal of Selected Topics in Applied Earth Observations and Remote Sensing* 5(2): 574-583.

Coleman, T. F. and Y. Y. Li, 1996. An interior trust region approach for nonlinear minimization subject to bounds*,Siam Journal on Optimization* 6(2): 418-445.

Combal, B., F. Baret, M. Weiss, A. Trubuil, D. Mace, A. Pragnere, R. Myneni, Y. Knyazikhin and L. Wang, 2003. Retrieval of canopy biophysical variables from bidirectional reflectance - Using prior information to solve the ill-posed inverse problem*,Remote Sensing of Environment* 84(1): 1-15.

Cornelissen, J. H. C., S. Lavorel, E. Garnier, S. Diaz, N. Buchmann, D. E. Gurvich, P. B. Reich*, et al.*, 2003. A handbook of protocols for standardised and easy measurement of plant functional traits worldwide*,Australian Journal of Botany* 51(4): 335-380.

Darvishzadeh, R., C. Atzberger, A. Skidmore and M. Schlerf, 2011. Mapping grassland leaf area index with airborne hyperspectral imagery: A comparison study of statistical approaches and inversion of radiative

transfer models*,Isprs Journal of Photogrammetry and Remote Sensing* 66(6): 894-906.

Darvishzadeh, R., C. Atzberger, A. K. Skidmore and A. A. Abkar, 2009. Leaf Area Index derivation from hyperspectral vegetation indices and the red edge position*,International Journal of Remote Sensing* 30(23): 6199-6218.

Darvishzadeh, R., A. A. Matkan and A. D. Ahangar, 2012. Inversion of a Radiative Transfer Model for Estimation of Rice Canopy Chlorophyll Content Using a Lookup-Table Approach*,Ieee Journal of Selected Topics in Applied Earth Observations and Remote Sensing* 5(4): 1222-1230.

Darvishzadeh, R., A. Skidmore, C. Atzberger and S. van Wieren, 2008a. Estimation of vegetation LAI from hyperspectral reflectance data: Effects of soil type and plant architecture*,International Journal of Applied Earth Observation and Geoinformation* 10(3): 358-373.

Darvishzadeh, R., A. Skidmore, M. Schlerf and C. Atzberger, 2008b. Inversion of a radiative transfer model for estimating vegetation LAI and chlorophyll in a heterogeneous grassland*,Remote Sensing of Environment* 112(5): 2592-2604.

Darvishzadeh, R., A. Skidmore, M. Schlerf, C. Atzberger, F. Corsi and M. Cho, 2008c. LAI and chlorophyll estimation for a heterogeneous grassland using hyperspectral measurements*,Isprs Journal of Photogrammetry and Remote Sensing* 63(4): 409-426.

Dasgupta, S., J. J. Qu and S. Bhoi, 2009. Constrained radiative transfer inversions for vegetation moisture retrievals in grasslands*,Journal of Applied Remote Sensing* 3.

Dash, J. and P. J. Curran, 2004. The MERIS terrestrial chlorophyll index*,International Journal of Remote Sensing* 25(23): 5403-5413.

Datt, B., 1999. Remote sensing of water content in Eucalyptus leaves*,Australian Journal of Botany* 47(6): 909-923.

Daughtry, C. S. T., L. L. Biehl and K. J. Ranson, 1989. A new technique to measure the spectral properties of conifer needles*,Remote Sensing of Environment* 27(1): 81-91.

Daughtry, C. S. T., E. R. Hunt Jr, P. C. Doraiswamy and J. E. McMurtrey Iii, 2005. Remote sensing the spatial distribution of crop residues*,Agronomy Journal* 97(3): 864-871.

Daughtry, C. S. T., C. L. Walthall, M. S. Kim, E. B. de Colstoun and J. E. McMurtrey, 2000. Estimating corn leaf chlorophyll concentration from leaf and canopy reflectance*,Remote Sensing of Environment* 74(2): 229-239.

Dawson, T. P., P. J. Curran and S. E. Plummer, 1998. LIBERTY - Modeling the effects of Leaf Biochemical Concentration on Reflectance Spectra*,Remote Sensing of Environment* 65(1): 50-60.

Deering, D. W., J. W. Rouse Jr, R. H. Haas and J. A. Schell, 1975. MEASURING "FORAGE PRODUCTION" OF GRAZING UNITS FROM LANDSAT MSS DATA*,* 2: 1169-1178.

Demarez, V., J. P. Gastellu-Etchegorry, E. Mougin, G. Marty, C. Proisy, E. Dufrene and V. Le Dantec, 1999. Seasonal variation of leaf chlorophyll content of a temperate forest. Inversion of the PROSPECT model*,International Journal of Remote Sensing* 20(5): 879-894.

Díaz, S. and M. Cabido, 2001. Vive la différence: Plant functional diversity matters to ecosystem processes*,Trends in Ecology and Evolution* 16(11): 646-655.

Dini, L., F. Vuolo and L. Randazzo, 2006. Leaf Area Index retrieval from SPARC data: Assessment of radiative transfer model inversion.*,Earth Observation for Vegetation Monitoring and Water Management* 852: 219-226.

Dominguez, M. T., C. Aponte, I. M. Perez-Ramos, L. V. Garcia, R. Villar and T. Maranon, 2012. Relationships between leaf morphological traits, nutrient concentrations and isotopic signatures for Mediterranean woody plant species and communities*,Plant and Soil* 357(1-2): 407-424.

Dorigo, W. A., 2012. Improving the Robustness of Cotton Status Characterisation by Radiative Transfer Model Inversion of Multi-Angular CHRIS/PROBA Data*,Ieee Journal of Selected Topics in Applied Earth Observations and Remote Sensing* 5(1): 18-29.

Dube, T. and O. Mutanga, 2015. Investigating the robustness of the new Landsat-8 Operational Land Imager derived texture metrics in estimating plantation forest aboveground biomass in resource constrained areas*,Isprs Journal of Photogrammetry and Remote Sensing* 108: 12-32.

Duro, D. C., N. C. Coops, M. A. Wulder and T. Han, 2007. Development of a large area biodiversity monitoring system driven by remote sensing*,Progress in Physical Geography* 31(3): 235-260.

Duru, M., R. A. H. Khaled, C. Ducourtieux, J. P. Theau, F. L. F. de Quadros and P. Cruz, 2009. Do plant functional types based on leaf dry matter content allow characterizing native grass species and grasslands for herbage growth pattern?*,Plant Ecology* 201(2): 421-433.

Fan, W., J. M. Chen, W. Ju and G. Zhu, 2014. GOST: A geometric-optical model for sloping terrains*,Ieee Transactions on Geoscience and Remote Sensing* 52(9): 5469-5482.

FatemiGhomi, N., M. Petrou and P. L. Palmer, 1995. Wavelet texture analysis for remote sensing*,Image and Signal Processing for Remote Sensing Ii* 2579: 329-340.

Feng, Y. L., G. L. Fu and Y. L. Zheng, 2008. Specific leaf area relates to the differences in leaf construction cost, photosynthesis, nitrogen

allocation, and use efficiencies between invasive and noninvasive alien congeners*,Planta* 228(3): 383-390.

Féret, J.-B. and G. P. Asner, 2014. Mapping tropical forest canopy diversity using high-fidelity imaging spectroscopy*,Ecological Applications*.

Féret, J. B. and G. P. Asner, 2011. Spectroscopic classification of tropical forest species using radiative transfer modeling*,Remote Sensing of Environment* 115(9): 2415-2422.

Feret, J. B., C. Francois, G. P. Asner, A. A. Gitelson, R. E. Martin, L. P. R. Bidel, S. L. Ustin, G. le Maire and S. Jacquemoud, 2008. PROSPECT-4 and 5: Advances in the leaf optical properties model separating photosynthetic pigments*,Remote Sensing of Environment* 112(6): 3030-3043.

Feret, J. B., C. Francois, A. Gitelson, G. P. Asner, K. M. Barry, C. Panigada, A. D. Richardson and S. Jacquemoud, 2011. Optimizing spectral indices and chemometric analysis of leaf chemical properties using radiative transfer modeling*,Remote Sensing of Environment* 115(10): 2742-2750.

Fraga, H., M. Amraoui, A. C. Malheiro, J. Moutinho-Pereira, J. Eiras-Dias, J. Silvestre, and J. A. Santos. 2014. Examining the relationship between the Enhanced Vegetation Index and grapevine phenology. European Journal of Remote Sensing 47:753-71. doi: Doi 10.5721/Eujrs20144743.

Fu, Z., A. Robles-Kelly, T. Caelli and R. T. Tan, 2007. On automatic absorption detection for imaging spectroscopy: A comparative study*,Ieee Transactions on Geoscience and Remote Sensing* 45(11): 3827-3844.

Gastellu-Etchegorry, J. P., E. Martin and F. Gascon, 2004. DART: a 3D model for simulating satellite images and studying surface radiation budget*,International Journal of Remote Sensing* 25(1): 73-96.

Gerber, F., R. Marion, A. Olioso, S. Jacquemoud, B. R. da Luz and S. Fabre, 2011. Modeling directional-hemispherical reflectance and transmittance of fresh and dry leaves from 0.4 mu m to 5.7 mu m with the PROSPECT-VISIR model*,Remote Sensing of Environment* 115(2): 404-414.

Gitelson, A. A., 2004. Wide Dynamic Range Vegetation Index for Remote Quantification of Biophysical Characteristics of Vegetation*,Journal of Plant Physiology* 161(2): 165-173.

Gitelson, A. A., Y. J. Kaufman, R. Stark and D. Rundquist, 2002. Novel algorithms for remote estimation of vegetation fraction*,Remote Sensing of Environment* 80(1): 76-87.

Gitelson, A. A., A. Vina, V. Ciganda, D. C. Rundquist and T. J. Arkebauer, 2005. Remote estimation of canopy chlorophyll content in crops*,Geophysical Research Letters* 32(8).

Goel, N. S. and W. Qin, 1994. Influences of canopy architecture on relationships between various vegetation indices and LAI and FPAR: a computer simulation*,Remote Sensing Reviews* 10(4): 309-347.

Gong, P., R. L. Pu, G. S. Biging and M. R. Larrieu, 2003. Estimation of forest leaf area index using vegetation indices derived from Hyperion hyperspectral data*,Ieee Transactions on Geoscience and Remote Sensing* 41(6): 1355-1362.

Gould, W., 2000. Remote sensing of vegetation, plant species richness, and regional biodiversity hotspots*,Ecological Applications* 10(6): 1861-1870.

Gregory, A., 2008. Hyperspectral Remote Sensing of Canopy Chemistry, Physiology, and Biodiversity in Tropical Rainforests. *Hyperspectral Remote Sensing of Tropical and Sub-Tropical Forests*, CRC Press**:** 261-296.

Haboudane, D., J. R. Miller, N. Tremblay, P. J. Zarco-Tejada and L. Dextraze, 2002. Integrated narrow-band vegetation indices for prediction of crop chlorophyll content for application to precision agriculture*,Remote Sensing of Environment* 81(2-3): 416-426.

Haboudane, D., N. Tremblay, J. R. Miller and P. Vigneault, 2008. Estimation of plant chlorophyll using hyperspectral observations and radiative transfer models: Spectral indices sensitivity and crop-type effects. International Geoscience and Remote Sensing Symposium (IGARSS).

He, C., Z. K. Feng, J. J. Yuan, J. Wang, Y. X. Gong and Z. H. Dong, 2012. Advances in the research on hyperspectral remote sensing in biodiversity and conservation*,Guang Pu Xue Yu Guang Pu Fen Xi/Spectroscopy and Spectral Analysis* 32(6): 1628-1632.

Heurich, M., B. Beudert, H. Rall and Z. Krenova, 2010. National Parks as model regions for interdisciplinary long-term ecological research. *Long-term Ecological Research. Between Theory and Application*. F. Müller, C. Baessler, H. Schubert and S. Klotz. Netherlands, Springer**:** 327-344.

Heurich, M. and M. Neufanger, 2005. *Die Wälder des Nationalparks Bayerischer Wald. Ergebnisse der Waldinventur 2002/2003 im geschichtlichen und waldökologischen Kontext.* . Grafenau, 178 S.

Hodgson, J. G., G. Montserrat-Marti, M. Charles, G. Jones, P. Wilson, B. Shipley, M. Sharafi*, et al.*, 2011. Is leaf dry matter content a better predictor of soil fertility than specific leaf area?*,Annals of Botany* 108(7): 1337-1345.

Homolova, L., P. Lukes, Z. Malenovsky, Z. Lhotakova, V. Kaplan and J. Hanus, 2013. Measurement methods and variability assessment of the Norway spruce total leaf area: implications for remote sensing*,Trees-Structure and Function* 27(1): 111-121.

Houborg, R., H. Soegaard and E. Boegh, 2007. Combining vegetation index and model inversion methods for the extraction of key vegetation

biophysical parameters using Terra and Aqua MODIS reflectance data*,Remote Sensing of Environment* 106(1): 39-58.

Huemmrich, K. F., 2001. The GeoSail model: a simple addition to the SAIL model to describe discontinuous canopy reflectance*,Remote Sensing of Environment* 75(3): 423-431.

Huete, A. R., 1988. A Soil-Adjusted Vegetation Index (Savi)*,Remote Sensing of Environment* 25(3): 295-309.

Huete, A. R., H. Q. Liu, K. Batchily and W. vanLeeuwen, 1997. A comparison of vegetation indices global set of TM images for EOS-MODIS*,Remote Sensing of Environment* 59(3): 440-451.

Jacquemoud, S. and F. Baret, 1990. Prospect - a Model of Leaf Optical-Properties Spectra*,Remote Sensing of Environment* 34(2): 75-91.

Jacquemoud, S., S. L. Ustin, J. Verdebout, G. Schmuck, G. Andreoli and B. Hosgood, 1996. Estimating leaf biochemistry using the PROSPECT leaf optical properties model*,Remote Sensing of Environment* 56(3): 194-202.

Jacquemoud, S., W. Verhoef, F. Baret, C. Bacour, P. J. Zarco-Tejada, G. P. Asner, C. Francois and S. L. Ustin, 2009. PROSPECT plus SAIL models: A review of use for vegetation characterization*,Remote Sensing of Environment* 113: S56-S66.

Jensen, R. R., P. J. Hardin and A. J. Hardin, 2012. Estimating Urban Leaf Area Index (LAI) of Individual Trees with Hyperspectral Data*,Photogrammetric Engineering & Remote Sensing* 78(5): 495-504.

Ji, L., B. K. Wylie, D. R. Nossov, B. Peterson, M. P. Waldrop, J. W. McFarland, J. Rover and T. N. Hollingsworth, 2012. Estimating aboveground biomass in interior Alaska with Landsat data and field measurements*,International Journal of Applied Earth Observation and Geoinformation* 18(1): 451-461.

Jingcheng, Z., L. Juhua, H. Wenjiang and W. Jihua, 2011. Continuous wavelet analysis based spectral feature selection for winter wheat yellow rust detection*,Intelligent Automation and Soft Computing* 17(5): 531-540.

Jordan, C. F., 1969. Derivation of Leaf-Area Index from Quality of Light on the Forest Floor*,Ecology* 50(4): 663-666.

Kampe, T. U., G. P. Asner, R. O. Green, M. Eastwood, B. R. Johnson and M. Kuester, 2010. Advances in Airborne Remote Sensing of Ecosystem Processes and Properties - Toward High-Quality Measurement on a Global Scale*,Remote Sensing and Modeling of Ecosystems for Sustainability Vii* 7809.

Kattge, J., S. Díaz, S. Lavorel, I. C. Prentice, P. Leadley, G. Bönisch, E. Garnier*, et al.*, 2011. TRY - a global database of plant traits*,Global Change Biology* 17(9): 2905-2935.

Kazemipour, F., P. Launeau and V. Meleder, 2010. A New Approach for Microphytobenthos Biomass Mapping by Inversion of Simple Radiative Transfer Model: Application to Hyspex Images of Bourgneuf Bay*,2010*

Ieee International Geoscience and Remote Sensing Symposium: 433-436.

Kennedy, R. E., W. B. Cohen and G. Takao, 1997. Empirical methods to compensate for a view-angle-dependent brightness gradient in AVIRIS imagery*,Remote Sensing of Environment* 62(3): 277-291.

Kleyer, M., R. M. Bekker, I. C. Knevel, J. P. Bakker, K. Thompson, M. Sonnenschein, P. Poschlod*, et al.*, 2008. The LEDA Traitbase: A database of life-history traits of the Northwest European flora*,Journal of Ecology* 96(6): 1266-1274.

Knox, N. M., A. K. Skidmore, M. Schlerf, W. F. de Boer, S. E. van Wieren, C. van der Waal, H. H. T. Prins and R. Slotow, 2010. Nitrogen prediction in grasses: effect of bandwidth and plant material state on absorption feature selection*,International Journal of Remote Sensing* 31(3): 691-704.

Knyazikhin, Y., M. A. Schull, P. Stenberg, M. Mottus, M. Rautiainen, Y. Yang, A. Marshak*, et al.*, 2013. Hyperspectral remote sensing of foliar nitrogen content*,Proceedings of the National Academy of Sciences of the United States of America* 110(3): E185-E192.

Kokaly, R. F., G. P. Asner, S. V. Ollinger, M. E. Martin and C. A. Wessman, 2009. Characterizing canopy biochemistry from imaging spectroscopy and its application to ecosystem studies*,Remote Sensing of Environment* 113(SUPPL. 1): S78-S91.

Laurent, V. C. E., W. Verhoef, J. G. P. W. Clevers and M. E. Schaepman, 2011. Estimating forest variables from top-of-atmosphere radiance satellite measurements using coupled radiative transfer models*,Remote Sensing of Environment* 115(4): 1043-1052.

Lauver, C. L., 1997. Mapping species diversity patterns in the Kansas shortgrass region by integrating remote sensing and vegetation analysis*,Journal of Vegetation Science* 8(3): 387-394.

Lauvernet, C., F. Baret, L. Hascoet, S. Buis and F. X. Le Dimet, 2008. Multitemporal-patch ensemble inversion of coupled surface-atmosphere radiative transfer models for land surface characterization*,Remote Sensing of Environment* 112(3): 851-861.

Lavorel, S., S. Díaz, J. H. C. Cornelissen, E. Garnier, S. P. Harrison, s. McIntyre, J. G. Pausas*, et al.*, 2007. Plant Functional Types: Are We Getting Any Closer to the Holy Grail? *Terrestrial Ecosystems in a Chenging World*.

Lavorel, S., K. Grigulis, P. Lamarque, M. Colace, D. Garden, J. Girel, G. Pellet and R. Douzet, 2011. Using plant functional traits to understand the landscape distribution of multiple ecosystem services*,Journal of Ecology* 99(1): 135-147.

Lavorel, S., K. Grigulis, S. McIntyre, N. S. G. Williams, D. Garden, J. Dorrough, S. Berman*, et al.*, 2008. Assessing functional diversity in the field - Methodology matters!*,Functional Ecology* 22(1): 134-147.

le Maire, G., C. Francois, K. Soudani, D. Berveiller, J. Y. Pontailler, N. Breda, H. Genet, H. Davi and E. Dufrene, 2008. Calibration and validation of hyperspectral indices for the estimation of broadleaved forest leaf chlorophyll content, leaf mass per area, leaf area index and leaf canopy biomass*,Remote Sensing of Environment* 112(10): 3846-3864.

Lehnert, L. W., C. Bässler, R. Brandl, P. J. Burton and J. Müller, 2013. Conservation value of forests attacked by bark beetles: Highest number of indicator species is found in early successional stages*,Journal for Nature Conservation* 21(2): 97-104.

Li, P., L. G. Jiang and Z. M. Feng, 2014. Cross-Comparison of Vegetation Indices Derived from Landsat-7 Enhanced Thematic Mapper Plus (ETM plus) and Landsat-8 Operational Land Imager (OLI) Sensors*,Remote Sensing* 6(1): 310-329.

Lin, Q. H. 2012. Enhanced Vegetation Index Using Moderate Resolution Imaging Spectroradiometers. 2012 5th International Congress on Image and Signal Processing (Cisp):1043-6.

Lin, Y. B., Y. P. Lin, D. P. Deng and K. W. Chen, 2008. Integrating remote sensing data with directional two-dimensional wavelet analysis and open geospatial techniques for efficient disaster monitoring and management*,Sensors* 8(2): 1070-1089.

Liu, H. Q. and A. Huete, 1995. A Feedback Based Modification of the Ndvi to Minimize Canopy Background and Atmospheric Noise*,Ieee Transactions on Geoscience and Remote Sensing* 33(2): 457-465.

Lv, J., Z. G. Yan and J. Y. Wei, 2014. Inversion of a radiative transfer model for estimation of rice chlorophyll content using support vector machine*,Land Surface Remote Sensing Ii* 9260.

Lymburner, L., P. J. Beggs and C. R. Jacobson, 2000. Estimation of canopy-average surface-specific leaf area using Landsat TM data*,Photogrammetric Engineering and Remote Sensing* 66(2): 183-191.

Ma, Z. G., X. Chen, Q. Wang, P. H. Li and G. Jiapaerl, 2012. Retrieval of leaf biochemical properties by inversed PROSPECT model and hyperspectral indices: an application to Populus euphratica polymorphic leaves*,Journal of Arid Land* 4(1): 52-62.

Major, D. J., F. Baret and G. Guyot, 1990. A Ratio Vegetation Index Adjusted for Soil Brightness*,International Journal of Remote Sensing* 11(5): 727-740.

Malenovsky, Z., J. Albrechtova, Z. Lhotakova, R. Zurita-Milla, J. G. P. W. Clevers, M. E. Schaepman and P. Cudlin, 2006. Applicability of the PROSPECT model for Norway spruce needles*,International Journal of Remote Sensing* 27(23-24): 5315-5340.

Malenovský, Z., E. Martin, L. Homolová, J.-P. Gastellu-Etchegorry, R. Zurita-Milla, M. E. Schaepman, R. Pokorný, J. G. P. W. Clevers and P. Cudlín, 2008. Influence of woody elements of a Norway spruce canopy on nadir

reflectance simulated by the DART model at very high spatial resolution*,Remote Sensing of Environment* 112(1): 1-18.

Marenco, R. A., S. A. Antezana-Vera and H. C. S. Nascimento, 2009. Relationship between specific leaf area, leaf thickness, leaf water content and SPAD-502 readings in six Amazonian tree species*,Photosynthetica* 47(2): 184-190.

Marshall, M. and P. Thenkabail, 2014. Biomass Modeling of Four Leading World Crops Using Hyperspectral Narrowbands in Support of HyspIRI Mission*,Photogrammetric Engineering & Remote Sensing* 80(8): 757-772.

Meer, F., Jong, Steven M. de, and NetLibrary, Inc. (2002). Imaging spectrometry basic principles and prospective applications (Remote sensing and digital image processing ; v. 4 (NL-LeOCL)33217011X). Dordrecht ; Boston: Kluwer Academic.

Meroni, M., R. Colombo and C. Panigada, 2004. Inversion of a radiative transfer model with hyperspectral observations for LAI mapping in poplar plantations*,Remote Sensing of Environment* 92(2): 195-206.

Mesarch, M. A., E. A. Walter-Shea, G. P. Asner, E. M. Middleton and S. S. Chan, 1999. A revised measurement methodology for conifer needles spectral optical properties: Evaluating the influence of gaps between elements*,Remote Sensing of Environment* 68(2): 177-192.

Messier, J., B. J. McGill and M. J. Lechowicz, 2010. How do traits vary across ecological scales? A case for trait-based ecology*,Ecology Letters* 13(7): 838-848.

Millennium Ecosystem Assessment., 2005. *Our human planet : summary for decision makers*. Washington, Island Press.

Misurec, J., V. Kopackova, Z. Lhotakova, J. Hanus, J. Weyermann, P. Entcheva-Campbell and J. Albrechtova, 2012. Utilization of hyperspectral image optical indices to assess the Norway spruce forest health status*,Journal of Applied Remote Sensing* 6.

Morris, R. D., A. Kottas, M. Taddy, R. Furfaro and B. D. Ganapol, 2008. A Statistical Framework for the Sensitivity Analysis of Radiative Transfer Models*,Ieee Transactions on Geoscience and Remote Sensing* 46(12): 4062-4074.

Morsdorf, F., C. Nichol, T. Malthus and I. H. Woodhouse, 2009. Assessing forest structural and physiological information content of multi-spectral LiDAR waveforms by radiative transfer modelling*,Remote Sensing of Environment* 113(10): 2152-2163.

Mouchet, M. A., S. Villéger, N. W. H. Mason and D. Mouillot, 2010. Functional diversity measures: An overview of their redundancy and their ability to discriminate community assembly rules*,Functional Ecology* 24(4): 867-876.

Nagler, P. L., C. S. T. Daughtry and S. N. Goward, 2000. Plant litter and soil reflectance*,Remote Sensing of Environment* 71(2): 207-215.

Okin, G. S., D. A. Roberts, B. Murray and W. J. Okin, 2001. Practical limits on hyperspectral vegetation discrimination in arid and semiarid environments*,Remote Sensing of Environment* 77(2): 212-225.

Ollinger, S. V., 2011. Sources of variability in canopy reflectance and the convergent properties of plants*,New Phytologist* 189(2): 375-394.

Osnas, J. L. D., J. W. Lichstein, P. B. Reich and S. W. Pacala, 2013. Global Leaf Trait Relationships: Mass, Area, and the Leaf Economics Spectrum*,Science* 340(6133): 741-744.

Papeş, M., R. Tupayachi, P. Martínez, A. T. Peterson and G. V. N. Powell, 2010. Using hyperspectral satellite imagery for regional inventories: A test with tropical emergent trees in the Amazon Basin*,Journal of Vegetation Science* 21(2): 342-354.

Pearson, R. L., L. D. Miller, U. S. I. B. Program and E. International Symposium on Remote Sensing of, 1972. *Remote mapping of standing crop biomass for estimation of the productivity of the shortgrass prairie, Pawnee National Grasslands, Colorado*. Fort Collins, Colo., Dept. of Watershed Sciences, College of Forestry and Natural Resources, Colorado State University.

Pedros, R., Y. Goulas, S. Jacquemoud, J. Louis and I. Moya, 2010. FluorMODleaf: A new leaf fluorescence emission model based on the PROSPECT model*,Remote Sensing of Environment* 114(1): 155-167.

Petchey, O. L. and K. J. Gaston, 2006. Functional diversity: Back to basics and looking forward*,Ecology Letters* 9(6): 741-758.

Pierce, L. L., S. W. Running and J. Walker, 1994. Regional-Scale Relationships of Leaf-Area Index to Specific Leaf-Area and Leaf Nitrogen-Content*,Ecological Applications* 4(2): 313-321.

Ramoelo, A., A. K. Skidmore, M. A. Cho, M. Schlerf, R. Mathieu and I. M. A. Heitkonig, 2012. Regional estimation of savanna grass nitrogen using the red-edge band of the spaceborne RapidEye sensor*,International Journal of Applied Earth Observation and Geoinformation* 19: 151-162.

Ramoelo, A., A. K. Skidmore, M. Schlerf, R. Mathieu and I. M. A. Heitkonig, 2011. Water-removed spectra increase the retrieval accuracy when estimating savanna grass nitrogen and phosphorus concentrations*,Isprs Journal of Photogrammetry and Remote Sensing* 66(4): 408-417.

Rascher, U., C. J. Nichol, C. Small and L. Hendricks, 2007. Monitoring Spatio-temporal Dynamics of Photosynthesis with a Portable Hyperspectral Imaging System*,Photogrammetric Engineering & Remote Sensing* 73(1): 45-56.

Ren, H. R. and G. S. Zhou, 2014. Determination of green aboveground biomass in desert steppe using litter-soil-adjusted vegetation index*,European Journal of Remote Sensing* 47: 611-625.

Riou, R. and F. Seyler, 1995. The Effect of Soil on Rain-Forest Canopy Nir Reflectance on Spot Oblique Imagery*,Comptes Rendus De L Academie Des Sciences Serie Ii* 320(11): 1079-1086.

Rivera, J. P., J. Verrelst, G. Leonenko and J. Moreno, 2013. Multiple Cost Functions and Regularization Options for Improved Retrieval of Leaf Chlorophyll Content and LAI through Inversion of the PROSAIL Model*,Remote Sensing* 5(7): 3280-3304.

Roberts, D. A., S. L. Ustin, S. Ogunjemiyo, J. Greenberg, S. Z. Dobrowski, J. Q. Chen and T. M. Hinckley, 2004. Spectral and structural measures of northwest forest vegetation at leaf to landscape scales*,Ecosystems* 7(5): 545-562.

Robles, W., J. D. Madsen and R. M. Wersal, 2015. Estimating the Biomass of Waterhyacinth (Eichhornia crassipes) Using the Normalized Difference Vegetation Index Derived from Simulated Landsat 5 TM*,Invasive Plant Science and Management* 8(2): 203-211.

Romero, A., I. Aguado and M. Yebra, 2012. Estimation of dry matter content in leaves using normalized indexes and PROSPECT model inversion*,International Journal of Remote Sensing* 33(2): 396-414.

Rondeaux, G., M. Steven and F. Baret, 1996. Optimization of soil-adjusted vegetation indices*,Remote Sensing of Environment* 55(2): 95-107.

Rosema, A., W. Verhoef, H. Noorbergen and J. J. Borgesius, 1992. A New Forest Light Interaction-Model in Support of Forest Monitoring*,Remote Sensing of Environment* 42(1): 23-41.

Ross, Y. K., A. A. Golinis, T. A. Nilson and K. Y. Ross, 1990. Effect of Liming on Soil Reflectance*,Soviet Journal of Remote Sensing* 6(6): 1003-1011.

Roujean, J. L. and F. M. Breon, 1995. Estimating Par Absorbed by Vegetation from Bidirectional Reflectance Measurements*,Remote Sensing of Environment* 51(3): 375-384.

Rouse, J. W., Jr., R. H. Haas, J. A. Schell and D. W. Deering (1974). Monitoring Vegetation Systems in the Great Plains with Erts. In: Fraden S.C., Marcanti E.P. & Becker M.A. (eds),. Third ERTS-1 symposium, 10-14 Dec. 1973, NASA SP-351, . Washington D.C., NASA. I**:** 309-3017.

Roux, S. G., A. Arneodo and N. Decoster, 2000. A wavelet-based method for multifractal image analysis. III. Applications to high-resolution satellite images of cloud structure*,European Physical Journal B* 15(4): 765-786.

Ruiliang, P., 2011. Detecting and Mapping Invasive Plant Species by Using Hyperspectral Data. *Hyperspectral Remote Sensing of Vegetation*, CRC Press**:** 447-466.

Saatchi, S., W. Buermann, H. Ter Steege, S. Mori and T. B. Smith, 2008. Modeling distribution of Amazonian tree species and diversity using remote sensing measurements*,Remote Sensing of Environment* 112(5): 2000-2017.

Schlerf, M. and C. Atzberger, 2006. Inversion of a forest reflectance model to estimate structural canopy variables from hyperspectral remote sensing data*,Remote Sensing of Environment* 100(3): 281-294.

Serrano, L., J. Peñuelas and S. L. Ustin, 2002. Remote sensing of nitrogen and lignin in Mediterranean vegetation from AVIRIS data: Decomposing biochemical from structural signals*,Remote Sensing of Environment* 81(2-3): 355-364.

She, X. J., L. F. Zhang, Y. Cen, T. X. Wu, C. P. Huang and M. H. A. Baig, 2015. Comparison of the Continuity of Vegetation Indices Derived from Landsat-8 OLI and Landsat 7 ETM+ Data among Different Vegetation Types*,Remote Sensing* 7(10): 13485-13506.

Shi, R. H., D. F. Zhuang and Z. Niu, 2006. Simulated hyperspectral data analysis using continuum removal: Case study on leaf chlorophyll prediction*,2006 8th International Conference on Signal Processing, Vols 1-4*: 2503-2505.

Shipley, B., 2002. Trade-offs between net assimilation rate and specific leaf area in determining relative growth rate: relationship with daily irradiance*,Functional Ecology* 16(5): 682-689.

Shipley, B., 2006. Net assimilation rate, specific leaf area and leaf mass ratio: which is most closely correlated with relative growth rate? A meta-analysis*,Functional Ecology* 20(4): 565-574.

Si, Y., M. Schlerf, R. Zurita-Milla, A. Skidmore and T. Wang, 2012. Mapping spatio-temporal variation of grassland quantity and quality using MERIS data and the PROSAIL model*,Remote Sensing of Environment* 121: 415-425.

Skidmore, A., 2002. *Environmental Modelling with GIs and Remote Sensing*. London, by Taylor & Francis.

Skidmore, A. K., J. G. Ferwerda, O. Mutanga, S. E. Van Wieren, M. Peel, R. C. Grant, H. H. T. Prins, F. B. Balcik and V. Venus, 2010. Forage quality of savannas - Simultaneously mapping foliar protein and polyphenols for trees and grass using hyperspectral imagery*,Remote Sensing of Environment* 114(1): 64-72.

Skidmore, A. K., N. Pettorelli, N. C. Coops, G. N. Geller, M. Hansen, R. Lucas, C. A. Mücher*, et al.*, 2015. Environmental science: Agree on biodiversity metrics to track from space*,Nature* 523(7561): 403-405.

Smith, T. M., H. H. Shugart and F. I. Woodward, 1997. *Plant functional types : their relevance to ecosystem properties and global change*. Cambridge ; New York, Cambridge University Press.

Somers, B., S. Delalieux, W. W. Verstraeten, A. V. Eynde, G. H. Barry and P. Coppin, 2010. The Contribution of the Fruit Component to the Hyperspectral Citrus Canopy Signal*,Photogrammetric Engineering & Remote Sensing* 76(1): 37-47.

Song, X. N., J. W. Ma, X. T. Li, P. Leng, F. C. Zhou and S. Li, 2013. Estimation of Vegetation Canopy Water Content Using Hyperion Hyperspectral Data*,Spectroscopy and Spectral Analysis* 33(10): 2833-2837.

Staenz, K., A. Mueller and U. Heiden, 2013. Overview of terrestrial imaging spectroscopy missions. 2013 IEEE International Geoscience and Remote Sensing Symposium - IGARSS.

Thenkabail, P. S., E. A. Enclona, M. S. Ashton and B. Van der Meer, 2004. Accuracy assessments of hyperspectral waveband performance for vegetation analysis applications*,Remote Sensing of Environment* 91(3-4): 354-376.

Tilman, D., 2001. Functional Diversity. *Encyclopedia of Biodiversity*. A. L. Editor-in-Chief: Simon. New York, Elsevier**:** 109-120.

Tilman, D., J. Knops, D. Wedin, P. Reich, M. Ritchie and E. Siemann, 1997. The influence of functional diversity and composition on ecosystem processes*,Science* 277(5330): 1300-1302.

Tjuatja, S., A. K. Fung and J. W. Bredow, 1993. Optical Remote-Sensing of Air Pollutant - an Analysis Using Wavelet Representation*,Igarss'93: Better Understanding of Earth Environment, Vols I-Iv*: 1953-1955.

Tong, A. and Y. H. He, 2013. Comparative analysis of SPOT, Landsat, MODIS, and AVHRR normalized difference vegetation index data on the estimation of leaf area index in a mixed grassland ecosystem*,Journal of Applied Remote Sensing* 7.

Tucker, C. J., 1980. A Critical-Review of Remote-Sensing and Other Methods for Nondestructive Estimation of Standing Crop Biomass*,Grass and Forage Science* 35(3): 177-182.

Turner, W., S. Spector, N. Gardiner, M. Fladeland, E. Sterling and M. Steininger, 2003. Remote sensing for biodiversity science and conservation*,Trends in Ecology and Evolution* 18(6): 306-314.

Ullah, S., A. K. Skidmore, M. Naeem and M. Schlerf, 2012. An accurate retrieval of leaf water content from mid to thermal infrared spectra using continuous wavelet analysis*,Science of the Total Environment* 437: 145-152.

Ustin, S. L., A. A. Gitelson, S. Jacquemoud, M. Schaepman, G. P. Asner, J. A. Gamon and P. Zarco-Tejada, 2009. Retrieval of foliar information about plant pigment systems from high resolution spectroscopy*,Remote Sensing of Environment* 113: S67-S77.

Verhoef, W., 1984. Light-Scattering by Leaf Layers with Application to Canopy Reflectance Modeling - the Sail Model*,Remote Sensing of Environment* 16(2): 125-141.

Verrelst, J., M. E. Schaepman, Z. Malenovský and J. G. P. W. Clevers, 2010. Effects of woody elements on simulated canopy reflectance: Implications for forest chlorophyll content retrieval*,Remote Sensing of Environment* 114(3): 647-656.

Vile, D., É. Garnier, B. Shipley, G. Laurent, M.-L. Navas, C. Roumet, S. Lavorel*, et al.*, 2005. Specific Leaf Area and Dry Matter Content Estimate Thickness in Laminar Leaves*,Annals of Botany* 96(6): 1129-1136.

Vile, D., B. Shipley and E. Garnier, 2006. Ecosystem productivity can be predicted from potential relative growth rate and species abundance*,Ecology Letters* 9(9): 1061-1067.

Violle, C., M. L. Navas, D. Vile, E. Kazakou, C. Fortunel, I. Hummel and E. Garnier, 2007. Let the concept of trait be functional!*,Oikos* 116(5): 882-892.

Vohland, M. and T. Jarmer, 2008. Estimating structural and biochemical parameters for grassland from spectroradiometer data by radiative transfer modelling (PROSPECT plus SAIL)*,International Journal of Remote Sensing* 29(1): 191-209.

Vygodskaya, N. N. and I. I. Gorshkova, 1986. Analysis of Canopy-Soil Optical Reflectance Behavior Using Goudriaans Model .2. Effect of Illumination Conditions on Reflectance*,Soviet Journal of Remote Sensing* 4(6): 991-1004.

Walter, J.-M. N. (2009). "CIMES-FISHEYE. Hemispherical photography of forest canopies. A package of programs for the assessment of canopy geometry and solar radiation regimes through hemispherical photographs [online]. ." Retrieved 11-03, 2014, from http://equinoxe.u-strasbg.fr/cimes

Wang, J., J. F. Huang, X. Z. Wang, M. T. Jin, Z. Zhou, Q. Y. Guo, Z. W. Zhao*, et al.*, 2015. Estimation of rice phenology date using integrated HJ-1 CCD and Landsat-8 OLI vegetation indices time-series images*,Journal of Zhejiang University-Science B* 16(10): 832-844.

Wang, K., S. E. Franklin, X. L. Guo and M. Cattet, 2010. Remote Sensing of Ecology, Biodiversity and Conservation: A Review from the Perspective of Remote Sensing Specialists*,Sensors* 10(11): 9647-9667.

Wang, L. L. and J. J. Qu, 2007. NMDI: A normalized multi-band drought index for monitoring soil and vegetation moisture with satellite remote sensing*,Geophysical Research Letters* 34(20).

Wang, M. C., X. F. Niu, S. B. Chen, P. J. Guo, Q. Yang and Z. J. Wang, 2014. Inversion of chlorophyll contents by use of hyperspectral CHRIS data based on radiative transfer model*,35th International Symposium on Remote Sensing of Environment (Isrse35)* 17.

Wang, Z., T. Wang, R. Darvishzadeh, A. K. Skidmore, S. Jones, L. Suarez, W. Woodgate, U. Heiden, M. Heurich, and J. Hearne. 2016. Vegetation indices for mapping canopy foliar nitrogen in a mixed temperate forest. Remote Sensing 8 (6). doi: 10.3390/rs8060491.

Waring, R. H., 1983. Estimating Forest Growth and Efficiency in Relation to Canopy Leaf-Area*,Advances in Ecological Research* 13: 327-354.

Weiss, M., F. Baret, R. B. Myneni, A. Pragnere and Y. Knyazikhin, 2000. Investigation of a model inversion technique to estimate canopy

biophysical variables from spectral and directional reflectance data*,Agronomie* 20(1): 3-22.

Widlowski, J. L., B. Pinty, M. Lopatka, C. Atzberger, D. Buzica, M. Chelle, M. Disney*, et al.*, 2013. The fourth radiation transfer model intercomparison (RAMI-IV): Proficiency testing of canopy reflectance models with ISO-13528*,Journal of Geophysical Research-Atmospheres* 118(13): 6869-6890.

Wilson, P. J., K. E. N. Thompson and J. G. Hodgson, 1999. Specific leaf area and leaf dry matter content as alternative predictors of plant strategies*,New Phytologist* 143(1): 155-162.

Wolf, A., J. A. Berry and G. P. Asner, 2010. Allometric constraints on sources of variability in multi-angle reflectance measurements*,Remote Sensing of Environment* 114(6): 1205-1219.

Wright, I. J., P. B. Reich, M. Westoby, D. D. Ackerly, Z. Baruch, F. Bongers, J. Cavender-Bares*, et al.*, 2004. The worldwide leaf economics spectrum*,Nature* 428(6985): 821-827.

Wu, W. C., 2014. The Generalized Difference Vegetation Index (GDVI) for Dryland Characterization*,Remote Sensing* 6(2): 1211-1233.

Xiao, Y. F., W. J. Zhao, D. M. Zhou and H. L. Gong, 2014. Sensitivity Analysis of Vegetation Reflectance to Biochemical and Biophysical Variables at Leaf, Canopy, and Regional Scales*,Ieee Transactions on Geoscience and Remote Sensing* 52(7): 4014-4024.

Xiaowen, L. and A. H. Strahler, 1992. Geometric-optical bidirectional reflectance modeling of the discrete crown vegetation canopy: effect of crown shape and mutual shadowing*,Geoscience and Remote Sensing, IEEE Transactions on* 30(2): 276-292.

Yali, M. P., J. Razmjou, M. Khanjani, A. Golizadeh and M. Hassanpour, 2012. Life history traits of Tetranycopsis horridus (Canestrini and Fanzago) (Acari: Tetranychidae) at three constant temperatures*,International Journal of Acarology* 38(3): 251-256.

Yanez-Rausell, L., Z. Malenovsky, J. G. P. W. Clevers and M. E. Schaepman, 2014. Minimizing measurement uncertainties of coniferous needle-leaf optical properties. Part II: Experimental setup and error analysis*,Ieee Journal of Selected Topics in Applied Earth Observations and Remote Sensing* 7(2): 406-420.

Yang, G. J., C. J. Zhao, Q. Liu, W. J. Huang and J. H. Wang, 2011. Inversion of a Radiative Transfer Model for Estimating Forest LAI From Multisource and Multiangular Optical Remote Sensing Data*,Ieee Transactions on Geoscience and Remote Sensing* 49(3): 988-1000.

Yoder, B. J. and R. H. Waring, 1994. The Normalized Difference Vegetation Index of Small Douglas-Fir Canopies with Varying Chlorophyll Concentrations*,Remote Sensing of Environment* 49(1): 81-91.

Zhang, C. F., Z. Y. Pan, H. Dong, F. J. He and X. B. Hu, 2015. Remote Estimation of Leaf Water Content Using Spectral Index Derived From

Hyperspectral Data*,Proceedings of the First International Conference on Information Science and Electronic Technology* 3: 20-23.

Zhang, J. C., L. Yuan, J. H. Wang, W. J. Huang, L. P. Chen and D. Y. Zhang, 2012a. Spectroscopic Leaf Level Detection of Powdery Mildew for Winter Wheat Using Continuous Wavelet Analysis*,Journal of Integrative Agriculture* 11(9): 1474-1484.

Zhang, J. T., L. Fan and M. Li, 2012b. Functional diversity in plant communities: Theory and analysis methods*,African Journal of Biotechnology* 11(5): 1014-1022.

Zhang, Y. Q., J. M. Chen, J. R. Miller and T. L. Noland, 2008. Retrieving chlorophyll content in conifer needles from hyperspectral measurements*, Canadian Journal of Remote Sensing* 34(3): 296-310.

Zhu, G. L., W. M. Ju, J. M. Chen and Y. B. Liu, 2014. A Novel Moisture Adjusted Vegetation Index (MAVI) to Reduce Background Reflectance and Topographical Effects on LAI Retrieval*,Plos One* 9(7).

Summary

Assessment and monitoring of biodiversity is still based on measuring biodiversity variables by traditional techniques which are labor-intensive and spatially constrained. The task of measuring (estimating) biodiversity variables, particularly those related to biochemical and biophysical characteristics of vegetation, can be readily assessed by using remote sensing data. The rapidly growing technology in developing new sensors and the launch of a new generation of satellite systems over the past four decades have made remote sensing approaches more reliable and a practical means for efficient and regular measurement of biodiversity variables at any spatial scale.

This thesis presents research on the potential of hyperspectral and multi-spectral remote sensing data to quantify two leaf functional traits: leaf dry matter content (LDMC), and specific leaf area (SLA) at laboratory (leaf), canopy and landscape levels. The research investigated the applicability of both statistical (empirical) and physical model approaches to estimate and map the LDMC and SLA of a heterogeneous mountain forest (Bavarian Forest National Park, Germany) from leaf spectroscopy, and airborne and spaceborne remote sensing measurements.

The laboratory research demonstrated the presence of significant variation in leaf/needle spectral signature values that can be utilized to quantify LDMC and SLA from remotely sensed data. It was concluded that at leaf level, LDMC and SLA of mixed mountain forest leaf samples can be successfully estimated through inversion of the leaf radiative transfer model, PROSPECT, irrespective of samples' species composition. The findings confirmed the imperative role of wavelengths (bands) in the near infrared (NIR) and shortwave infrared (SWIR) regions of the electromagnetic spectrum for spectral variation detection due to the two leaf traits.

The results from analysis of the influence of canopy structural variables on the relationship between the two leaf traits and canopy reflectance revealed that stem density and crown diameter, which constitute canopy closure are the factors most influencing the canopy reflectance. Nevertheless, most of the influence of canopy structural factors can be minimized by using vegetation indices, as long as canopy closure is above 50%. Thus, the understory and background soil information is fundamental, particularly when retrieving vegetation variables in sparse forests.

Likewise, the findings of the study in chapters 4, 5 and 6 highlighted the significance of statistical and radiative transfer model (RTM) inversion techniques to estimate and map the leaf functional traits (LDMC and SLA) in the study area from hyperspectral airborne and multispectral spaceborne

satellite images. Inversion of canopy RTM through continuous wavelet analysis (CWA) revealed the unbiased power of CWA to identify the most sensitive spectral subset (wavelet features) for accurate quantification of these vegetation traits. The results of the study also showed the excellent performance of many narrow-band vegetation indices to retrieve SLA at leaf and canopy levels using laboratory and airborne spectroscopy measurements. The outcomes of estimating SLA from multispectral satellite data were very promising, with accuracy comparable to predictions made from hyperspectral data.

In general, this study extends existing knowledge of applied research in remote sensing of vegetation. The findings and methods of this work have demonstrated the potential of hyperspectral and multispectral remote sensing data to produce useful information about leaf functional traits at local, regional, and global scales. The results further confirm the applicability of remote sensing to understand general ecological leaf functional traits variation across relevant spatial and temporal scales. This will facilitate regular monitoring of biodiversity, particularly of changes to ecosystem functioning.

Samenvatting

Biodiversiteit wordt nog steeds beoordeeld door biodiversiteits variabelen te meten met behulp van traditionele methoden, die zowel tijdrovend zijn als ruimtelijke beperkingen ondervinden. Voor het meten (schatten) van biodiversiteits variabelen, vooral die gerelateerd zijn aan biochemische en biophysische eigenschappen van vegetatie, kunnen remote sensing data eenvoudig worden ingezet. De zich snel ontwikkelende technologie met betrekking tot nieuwe sensoren en de lancering van een hele nieuwe generatie sateliet systemen in de afgelopen vier decennia, heeft het gebruik van remote sensing betrouwbaarder gemaakt en praktisch voor efficiënte en met regelmaat herhaalde beoordeling van biodiversiteits variabelen op elk gewenste ruimtelijke schaal.

Dit proefschrift presenteert onderzoek aangaande de mogelijkheden van het gebruik van hyperspectrale en multispectrale remote sensing data om twee functionele eigenschappen van bladeren te kwantificeren, namelijk: de hoeveelheid droog materiaal in blad (LDMC) en het specifieke blad oppervlak (SLA), zowel op laboratorium- (blad-), kroonlaag-, als landschappelijk niveau. Het onderzoek richtte zich op de toepasbaarheid van zowel statistische (proefondervindelijke), als concrete model benaderingen om de LDMC en SLA in te schatten en in kaart te brengen van een heterogeen bergwoud (National park Bayerischer Wald, Duitsland), door middel van blad spectroscopie en remote sensing data, gemeten vanuit zowel de lucht als de ruimte.

Het laboratorium onderzoek bracht significante variatie in de waarden van de spectrale handtekening van blad en naald aan het licht, wat vervolgens gebruikt kan worden om LDMC en SLA uit remote sensing data te kwantificeren. De conclusie was dat, op blad niveau, LDMC en SLA van gemengde bergbos bladmonsters succesvol kunnen worden geraamd door omzetting van het 'leaf radiative transfer' model, PROSPECT, onafhankelijk van de soorten samenstelling van de monsters. De bevindingen bevestigen de noodzakelijke rol van nabije infrarode (NIR) en korte golf infrarode (SWIR) golflengte gebieden van het electromagnetische spectrum voor het bespeuren van spectrale variatie als gevolg van de twee blad karakteristieken.

De resultaten van de analyse aangaande de invloed van structurele variabelen van de kroonlaag op de relatie tussen de twee blad karakteristieken en kroonlaag reflectie brachten aan het licht dat stam dichtheid en kroon diameter, die de kroonlaag dichtheid bepalen, de grootste invloed uitoefenen op de kroonlaag reflectie. Desalniettemin kan de grootste invloed van structurele factoren van de kroon geminimaliseerd worden door vegetatie indicatoren te gebruiken, zolang de kroonlaag dichtheid boven de 50% is. Derhalve is informatie over de lagere vegetatielagen en de onderliggende

bodem van essentieel belang, zeker wanneer gegevens van vegetatie variabelen uit open bossen worden verkregen.

Ook de bevindingen van het onderzoek in de hoofstukken 4, 5 en 6 geven het belang aan van inversie technieken van statistische en 'radiative transfer' modellen (RTM) om LDMC en SLA in het studiegebied in te kunnen schatten en in kaart te kunnen brengen op basis van hyperspectrale beelden vanuit de lucht en multispectrale satelietbeelden vanuit de ruimte. Inversie van de kroonlaag RTM met behulp van 'continuous wavelet analysis' (CWA) toonde onbevooroordeeld de waarde van CWA aan bij het identificeren van de meest gevoelige spectrale deelgroep ('wavelet features') voor het nauwkeurig kwantificeren van deze vegetatie kenmerken. De resultaten van het onderzoek lieten ook de uitstekende prestaties zien van veel 'narrow-band' vegetatie indicatoren in het openbaren van SLA op blad- en kroonlaagniveua met behulp van laboratorium en 'airborne spectroscopy' metingen. De uitkomsten van het ramen van SLA door middel van multiprectrale sateliet gegevens was veelbelovend en van een nauwkeurigheid vergelijkbaar met voorspellingen gedaan met behulp van hyperspectrale gegevens.

Algemeen beschouwd, draagt deze studie bij aan het uitbreiden van kennis aangaande toegepast onderzoek in remote sensing van vegetatie. De bevindingen en methodes demonstreren het vermogen van hyperspectrale en multispectrale remote sensing gegevens om nuttige informatie te produceren over functionele blad kenmerken op lokale, regionale en globale schaal. De resultaten bevestigen verder de toepasbaarheid van remote sensing voor het begrijpen van variaties in algemene ecologische funktionele blad kenmerken op relevante ruimtelijke en temporale schaal. Dit zal helpen bij het in de gaten houden van biodiversiteit, en vooral van veranderingen in het functioneren van een ecosysteem.

Author's Biography

Abebe Mohammed Ali was born on 23 February 1973 in Wollo, Ethiopia. He attended primary education in Genete elementary school between 1978 and 1984. He joined Borena junior high school in 1984 and obtained junior secondary school certificate in 1986. From 1986-1989 he followed his high school education in Borena senior secondary school. Later in 1991 he acquired Ethiopian schools leaving certificate examination (ESLCE) from Woizero Sihin comprehensive high school. In the same year (1991), he joined Wondo Genete College of forestry, Shashemene, Ethiopia and obtained diploma in forestry in 1993. Due to his avid interest in furthering his academic level, he pursued undergraduate study from 1999 to 2002 and received Bachler degree in forestry from the same college on July 06, 2002. In 2004 he enrolled in Wageningen University and research centre and earned his master in Geo Information science on January 18, 2007.

He has spent most of his career working for Ethiopian government institutes starting as a junior wildlife expert in 1993 at Ethiopian wildlife development and conservation organization, then as a GIS and remote sensing analyst in the finance and economic development bureau of Amhara national regional state, Bahir Dar, Ethiopia, and as a GIS/RS lecturer since 2009 in the geography and environmental studies department of Wollo University in Ethiopia. In 2012, he received the Netherlands fellowship program for his doctoral research and moved to University of Twente-ITC, Enschede, Netherlands to start his PhD research project which resulted in this thesis and the following publications.

ISI journal articles

Ali, A. M., R. Darvishzadeh, A. K. Skidmore, I. v. Duren, U. Heiden and M. Heurich, 2016b. Estimating leaf functional traits by inversion of PROSPECT: Assessing leaf dry matter content and specific leaf area in mixed mountainous forest*,International Journal of Applied Earth Observation and Geoinformation* 45, Part A: 66-76.

Ali, **A**. **M**., R. Darvishzadeh, A. K. Skidmore and I. V. Duren, 2016. Effects of Canopy Structural Variables on Retrieval of Leaf Dry Matter Content and Specific Leaf Area from Remotely Sensed Data, Ieee Journal of Selected Topics in Applied Earth Observations and Remote Sensing 9(2): 898-909.

(Under review)

Ali, **A**. **M**., A. K. Skidmore, R. Darvishzadeh, I. V. Duren, S. Holzwarthc and J. Müller, Retrieval of Forest Leaf Functional Traits from HySpex Imagery Using Radiative Transfer Models and Continuous Wavelet Analysis, In Review (after second revision). ISPRS Journal of Photogrammetry and Remote Sensing.

Ali, **A**. **M**., R. Darvishzadeh, A. K. Skidmore and I. V. Duren. Narrow band vegetation indices for specific leaf area retrieval at leaf and canopy scale. In Review, ASPRS PE&RS Journal.

Ali, **A**. **M**., R. Darvishzadeh, A. K. Skidmore. Fast and accurate retrieval of forest specific leaf area from Landsat-8 surface reflectance data. (In Review, International Journal of Remote Sensing).

Conference Proceedings (Full paper)

Ali, A. M., R. Darvishzadeh, A. K. Skidmore, I. Van Duren, U. Heiden and M. Heurich, 2015. Prospect inversion for indirect estimation of leaf dry matter content and specific leaf area. International Archives of the Photogrammetry, Remote Sensing and Spatial Information Sciences - ISPRS Archives.

Ali, A.M., A.K. Skidmore, R. Darvishzadeh, I.C. van Duren, S. Holzwarth and J. Müller, 2016. Mapping forest leaf dry matter content from hyperspectral data. In: Proceedings of ASPRS 2016 annual conference: IGTF 2016: imaging & geospatial technology forum, 11-15 April 2016, Fort Worth, United States of America. Fort Worth: ASPRS, 2016. 14 p.

ITC Dissertation List

http://www.itc.nl/research/phd/phd_graduates.aspx